Engineering of Functional, Striated Muscle Tissues with Controllable 3D Architectures Using a Novel, Thermoresponsive, Nanofabricated Substratum

Alex Jiao

A doctoral dissertation

submitted in partial fulfillment of the

requirements for the degree of

Doctor of Philosophy

University of Washington

2016

Reading Committee:

Deok-Ho Kim, Chair

Charles E. Murry

William M. Mahoney

Program Authorized to Offer Degree:

Bioengineering

ABSTRACT

Engineering of Functional, Striated Muscle Tissues with Controllable 3D Architectures Using a Novel, Thermoresponsive, Nanofabricated Substratum

Alex Jiao
Chair of the Supervisory Committee:
Deok-Ho Kim, Department of Bioengineering

Most tissues in the human body demonstrate multiscale organization, from extracellular matrix (ECM) structure, to cell morphologies, to overall tissue architecture. Further, in the cases of cardiac and skeletal muscle, tissue structure is critical to appropriate tissue function. However, current tissue engineering methods lack the ability to properly recreate scaffold-free, cell dense tissues with physiological structures. A platform which could engineer 3D tissues with controllable architectures could thus enable the study of more complex biological phenomenon, such as the effect of tissue structure on skeletal muscle development and engineered cardiac tissue function. For this reason, we developed a simple, yet versatile platform combining a thermoresponsive nanofabricated substratum (TNFS) incorporating nanotopographical cues and a gel casting method for the fabrication of scaffold-free 3D tissues with controllable architectures. The developed TNFS could be engineered with a variety of nanotopographies and thus cell monolayer structures which can be spontaneously detached via a change in culture temperature. The detached, nanoengineered cell sheets can then be stacked using our gel casting method to engineer specifically structured, 3D tissues. To this end, we first used the developed TNFS to engineer organized myoblast tissues with specific tissue architectures to demonstrate proof of concept engineering of 3D tissues with layer-by-layer architectural control. We found that using the gel casting method and TNFS, individual aligned myoblast sheets can be stacked into trilayer tissues and maintain individual layer alignment and stacked layer angles without reorganization between the individual sheets, whereas unpatterned controls demonstrated reorganization and

layer mixing. We then utilized our developed platform to analyze the effects of engineered myoblast tissue structures on myoblast fusion and subsequent myotube morphology and alignment. We found that parallel-aligned myoblast bilayers could differentiate into aligned myotube sheets in a single layer, however orthogonally-oriented myoblast bilayers lost structural organization during differentiation. Additionally, transferred ECM and tissue structure from the TNFS could provide sufficient alignment cues to allow for the formation of aligned muscle tissue in a 3D microenvironment similar to that of the myofiber niche. Finally, we utilized our developed platform to engineer multilayered human cardiac tissues. We first found that by incorporating a vascular cell population capable of producing ECM, aligned human induced Pluripotent Stem (iPS) cell-derived cardiac sheets could be detached and stacked together. We then engineered 4-layer, aligned and helical cardiac tissues as microscale models of physiologically-structured myocardium. Aligned and helical 3D tissues demonstrated different contractile profiles, such as linear and spiraling, and also demonstrated improved contractile function over unpatterned controls, with aligned 3D cardiac tissues demonstrating the largest contractile magnitudes and velocities. These findings highlight the importance of tissue structure on cardiac function, and can be utilized in future works to engineer structured cardiac organoids for eventual *in vitro* whole-organ experiments. Taken together, these works present a novel platform which can be utilized for a variety of studies to engineer complex cell microenvironments and tissue architectures.

ACKNOWLEDGMENTS

I would first like to thank my advisor, Dr. Deok-Ho Kim, for providing me guidance and support during my studies. Dr. Kim not only placed great trust in me and my abilities and allowed me to pursue a project of my own inspiration, but also continued to push me as a student and a scientist to further improve myself and my work. I would also to thank Dr. Charles Murry for his continued support, especially as a co-sponsor and advocate on my training grants and fellowships, as well as the individual efforts he has put forth in assisting and developing this project. Finally, I would also like to thank committee members Dr. Michael Regnier, Dr. Michael Laflamme, and Dr. William Mahoney for their support, input, and flexibility during my training as a graduate student.

I would also like to thank the many members and alumni of the Kim and Murry lab who have shared their expertise, advice, questions, and time and energy, with me. In no particular order, Dr. Hyun Jung Lee, Dr. Hee Seok Yang, Daniel Carson, Nicole Trosper, Jinsung Kim, Jesse Macadangdang, Jonathan Tsui, Dr. Kajohnkiart Janebodin, Peter Kim, Dr. Alec Smith, Nisa Penland, Mikael Perla, Dr. Eunpyo Choi, Travis Moerk and Emil Jahng have all assisted me in some way towards the successful completion of my degree. Additionally, members of the Murry lab, past and present, have been invaluable with advice and guidance as well, specifically Dr. Lil Pabon, Dr. Hans Reinecke, Dr. Nathan Palpant and Dr. Daniel Yang.

Before graduate school, my love of academic research and development as a scientist was fostered by Dr. Jan Stegemann, who took a chance hiring an inexperienced undergraduate as his first hire in his new lab, Dr. Karen Lapidos, who patiently trained me not only in scientific skills but also in my critical thinking and hypothesis development, and Dr. Guillermo Ameer, my undergraduate academic advisor who allowed me to pursue and experience undergraduate research while at Northwestern.

Finally, support for this work was generously provided by the National Institutes of Health (F31 HL126445-01, T32 EB001650-07, T32 HL007312-35) and the American Heart Association (AHA Predoctoral Fellowship).

DEDICATION

I would like to dedicate this work to my mom and dad, who have sacrificed so much in providing for me. Without their hard work, love, and unceasing belief in me, I would never have had the privilege of being in the position I am in today. I would like to also dedicate this work to my best friend, advocate, and girlfriend, Taylor, whose love and support over the past four years have helped steady the oft tumultuous path towards graduation.

TABLE OF CONTENTS

LIST OF TABLES

LIST OF FIGURES

CHAPTER 1. Introduction

1.1 Overview and Specific Aims

The goal of this proposal is to develop a platform which can engineer tissues with controllable 3D architectures, and to use this platform to study the effects of 3D muscle structure on tissue function. Current tissue engineering strategies are unable to precisely control 3D tissue architecture in cell-dense tissues *in vitro,* preventing the study of tissue structure-function relationships and hindering engineered tissue function. Thus, we aim to engineer novel 3D tissues with controllable structures by utilizing biomimetic nanotopography and thermoresponsive cell sheet engineering. We hypothesize that engineered 3D tissue scan provide a physiological microenvironments which can enhance certain cell functions, such as myoblast fusion, as well as improve engineered tissue function, such as enhanced cardiac contractile function. Such work could lead to new clinical therapies to treat heart disease, improve platforms for drug screening and disease modeling, and provide insights into stem cell biology. Towards this, we propose the following specific aims:

Aim 1. Develop a platform to engineer cell dense tissues with controllable 3D architecture. Our laboratory has previously utilized bioinspired nanotopographical cues to align monolayers of cells, such as cardiomyocytes. In order to engineer 3D tissues, we hypothesize that the thermoresponsive polymer, poly(N-isopropylacrylamide) (PNIPAm) can be grafted to these nanofabricated scaffolds to promote temperature-dependent detachment of intact anisotropic cell sheets. Further, such sheets could then be stacked together to engineer multilayered, 3D tissues with layer-by-layer control. For this aim, we will optimize PNIPAm grafting to our nanofabricated scaffolds to allow for thermoresponsive detachment of anisotropic

cell sheets, as well as a method to manipulate and stack detached cell sheets to engineer tissues. We will validate our platform and method through cytoskeletal and live/dead staining.

Aim 2. Engineer 3D skeletal muscle microenvironments with specific structures to augment myoblast fusion. Skeletal muscle is comprised of aligned myofibers encased in an extracellular matrix sheath or lamina, which also house satellite cells, which migrate to the site of injury to dedifferentiate into myoblasts and fuse with myofibers to regenerate muscle tissue. We hypothesize that the structure of skeletal muscle tissue in both 2D and 3D can affect the organization and morphology of differentiating myoblasts and formed myotubes. Using our TNFS platform developed in Aim 1, we will engineer multilayered myoblast tissues and analyze the effects of tissue architecture on myoblast fusion and myotube morphology alignment. We will assess myotube formation through immunofluorescent staining and imaging.

Aim 3. Assess the physiological structure-function relationship of engineered cardiac tissue with varying 3D architectures. To achieve physiological ejection fractions, muscle fibers in the heart must be organized in a complex, helical 3D structure. Although promising, current engineered cardiac tissues are restricted to randomly organized and uniaxially aligned structures, possibly inhibiting overall contractile function. We hypothesize that fabricated 3D cardiac tissues with a helical structure will demonstrate improved overall tissue function when compared to randomly organized or simply aligned 3D cardiac tissue. To test this, we will use our developed platform to fabricate 4-layer 3D cardiac tissues with helical (physiological), aligned and randomly organized structures and assess contractile function using Correlation-based Contraction Quantification pixel tracking of cardiac tissue contraction.

1.2 Background

1.2.1 Motivation

Heart disease remains the leading cause of death both in the United States and in the developing world. Clinical events such as myocardial infarction cause substantial necrosis in the myocardium during a single incident [1], chronic conditions such as hypertension slowly compound cardiomyocyte death over many years [2] and even aging is associated with cardiomyocyte death and cardiomyopathy [3]. Unfortunately, the heart lacks robust regenerative capability, demonstrating only 1% cardiomyocyte renewal per year under the most optimal conditions [4]. Current treatments of heart disease are unable to fully restore lost heart function without mechanical assistance, and therapies such as injection of hematopoietic or mesenchymal stem cells have shown inconsistent results and ultimately are unable to regenerate heart tissue [5]. Pluripotent stem cells offer a promising alternative to current treatments, as they can be reliably differentiated into cardiomyocytes [6] and thus are a renewable cell source for the treatment of heart disease. Additionally, as cardiac safety concerns accounted for 45% of all drug withdrawals in the US in spite of stringent FDA requirements for cardiotoxicity screening [7], pluripotent stem cell technology could have a large impact outside the clinic for drug development and disease modeling.

However, several challenges face stem cell-based technology for the treatment of heart disease or development of physiological heart models. First, pluripotent stem cell-derived cardiomyocytes are phenotypically immature and lack the structure, electrical properties and contractility of adult cardiomyocytes [8, 9]. For clinical therapies, it would be ideal to have cardiomyocytes which can restore the function of lost myocardium, and currently, stem cell-derived cardiomyocytes are only able to generate a small fraction of the contractile strength of

adult cardiomyocytes [10]. Second, current engineered cardiac tissues are unable to recapitulate native cardiac structure. The heart is a highly organized organ, and the structure of the developing and adult heart is critical to cardiomyocyte development and cardiac function. However, current engineered cardiac tissues are restricted to unidirectional [11-13] or randomly organized 3D tissues [14, 15]. Finally, many cardiac tissue engineering strategies incorporate a 3D scaffold. Although 3D scaffolds are often scalable to tissue-relevant sizes, the use of a scaffold inherently reduces cell-cell contacts, which is critical for a cell-dense tissue such as myocardium. Further, scaffolds also often cause an uneven distribution of cardiomyocytes within the engineered tissue, leading to heterogeneity between tissue constructs. As there currently remains no restorative treatment option for heart disease, we believe systematic and purposeful improvements in strategies to engineer heart tissue can advance the field and subsequent therapies.

1.2.2 Cardiac biology and structure-function relationship of the heart

The heart is a well-ordered organ, demonstrating specific multiscale organization from the nano- to macroscale. Beginning with the cardiac extracellular matrix (ECM), structural proteins within the cardiac (ECM) support, mechanically couple, and orient cardiac cells [16]. Fibrillar ECM proteins, such as collagen, are well-aligned with cardiomyocytes, providing topographical and alignment cues at the nanoscale. Cardiomyocytes subsequently connect to the extracellular matrix through focal adhesions, which are connected to their cytoskeletal proteins, intrinsically binding cardiomyocyte morphology with that of its extracellular microenvironment [16]. This morphology is highly specific: adult cardiomyocytes have a rectangular shape, aligned cytoskeletal proteins, and well-ordered sarcomere arrays [17]. This cellular structure is necessary for the transmittance of stress as well as the generation of anisotropic contractile forces throughout the cell. In order to transmit these forces as well as other signals, such as an action

potential, to one another, cardiomyocytes are connected through junctions called intercalated discs. These junctions are located at the lateral end of each cell and run transversely between cardiomyocytes [18]. The location and structure of intercalated discs is critical for cell-cell communication throughout the entire tissue.

In the myocardium, cardiomyocytes are organized in an anisotropic, laminar fashion [19, 20]. These myofiber sheets are anisotropic, transmit both electrical and mechanical forces, and are layered together to create the thick tissue of the myocardial wall. In 3D, the orientation of these sheets in the ventricle changes gradually from a right-handed helix in the subendocardium to a left-handed helix in the subepicardium [21-23]. This change in myofiber sheet orientation leads to a transmural helical structure in 3D [23]. Studies have found that this complex heart structure is critical to many aspects of adult heart function. Electrically, the depolarizing action potential is anisotropic, with the current guided by the fiber orientation in the heart [24-26]. Mechanically, the fiber orientation is an important determinant of the myocardial stress and strain [27, 28], additionally affecting the perfusion and oxygen consumption of the heart [29]. Finally, the helical fiber orientation allows for the unique twisting contractile motion of the heart [30-32]. This wringing motion is critical for appropriate blood clearance and cardiac output [33, 34]. Fiber orientation is also altered in disease states such as ischemic heart disease and ventricular hypertrophy, and can also contribute to arrhythmias after cardiac injury [35-37]. Thus, normal heart function is intrinsically tied to the physiological heart structure, and the disruption of cardiac structure at both a single cell and tissue level due to disease can exacerbate a deterioration in cardiac function.

1.2.3 The current state of the art in tissue engineering of the myocardium

Due to the lack of treatment options for heart disease and the advent of a reliable, renewable source of cardiomyocytes from pluripotent stem cells, cardiac tissue engineering is a popular and diverse field of study. Specifically, the ability to engineer an entire human heart is often seen as an ultimate goal of cardiac tissue engineering. Whether or not this is achievable in the near future remains to be seen, however even the engineering of small portions of the heart, such as heart valves, pacemakers, or a piece of myocardium, can yield drastic benefits, both therapeutically and in advancing discoveries or developments of other promising interventions.

Broadly, cardiac tissue engineering can be separated into two main approaches: scaffold-free or scaffold-based. Scaffold-free approaches, as the name suggest, do not rely on a supporting structure or scaffold to engineer 3D tissues. Instead, scaffold-free tissues are cell-dense aggregates or layers of cardiac tissues. Scaffold-free human cardiac tissue patches have been created by simply using an orbital shaker and a suspension of cardiomyocytes [38], and human cardiac micro-tissue particles have been engineered by using PDMS molds to allow for the aggregation of 3D cardiac spheroids [39]. Another approach, termed cell sheet engineering, utilizes a thermoresponsive release layer on a culture surface to release sheets of cells, which can then be stacked into 3D tissues. This technique has been successfully applied to engineer multilayered, human cardiac tissues [40]. Scaffold-free approaches such as these have the advantage of engineering cell-dense tissues, allowing for cell-cell contacts, transmission of electrical signals and transmission of force. Additionally, these scaffold-free tissues can also be vascularized simply with the incorporation of endothelial cells and a stromal support cell [41, 42], offering promising approaches to address the oxygen diffusion limitations (~80μm) of thicker, avascular tissues [43]. However, due to the relatively uncontrolled nature of the formation of these tissues, scaffold-free approaches do not allow for the manipulation of tissue structure beyond overall tissue size. Indeed, histological examination of scaffold-free cardiac tissues often reveal

no cellular or tissue alignment [42]. Additionally, although cell-cell connections in a dense tissue allow for the transmission of an action potential, cells in the native heart are also elongated and demonstrate organized gap junctions which allow for the anisotropic spread of the action potential across the cardiac tissue [18]. The lack of physiologically-relevant cellular organization of scaffold-free patches may thus also play a role in preventing electrical coupling with host tissue [39].

Thus, in order to engineer reproducible and more controllable cardiac tissues, often a supporting scaffold is used. The simplest methods incorporating a scaffold typically use a polymerized extracellular matrix component to encapsulate cardiac cells, such as collagen [13, 44], fibrin [45], or even broadly decellularized, digested, cardiac ECM [46]. Utilizing natural, structural protein components of the cardiac ECM provides structural and mechanical support to encapsulated cardiomyocytes, as well as biochemical cues allowing for cell attachment and migration, which allow the encapsulated cells to then actively remodel and compact the supporting scaffold [44]. Additionally, the mechanical properties of such natural ECM scaffolds allow for the incorporation of uniaxial strain [47] and even dynamic, cyclic stretch [13]. Such scaffolds can also incorporate vascularization to a degree [13], and due to the biocompatible nature of these proteins, can be implanted into the heart without long-term foreign body responses [48, 49]. However, although promising, these scaffold-based approaches suffer from a number of limitations, namely in the controllability of overall tissue architecture. Specifically, all approaches using such scaffolds with any structural organization have all been uniaxial, utilizing mechanical forces and active cell remodeling to orient cardiomyocytes through extended culture [13, 44, 47].

These tissues can therefore only exert force and transmit an action potential in a single direction. However, *in vivo*, the myocardial wall changes alignment from interior to exterior, which leads to a unique, 3D activation of both depolarization and contraction: endocardium to epicardium, with an anisotropic wave form subsequently spreading across the ventricle [50, 51].

Uniaxially-aligned tissues are thus incapable of investigation of tissue function in 3D, such as the effects of infarct location on tissue contraction and conduction or helical tissue geometry on cardiac output. This, in turn, limits both the application and relevance of such engineered tissues.

Finally, investigations have also analyzed the use of topographical or patterned culture surfaces to structure and orient cardiac monolayers. Utilizing microfabrication techniques such as microcontact printing, lanes of well-aligned cardiac tissues have been generated with robust intercalated discs [52]. This technique has also been applied to flexible thin films to analyze the effects of cardiac tissue alignment on force generation [53], and by manipulating thin film shape, could even be used to engineer “walking” and “swimming” tissues [54]. Additionally, larger-scale patches have utilized microtopography to create flexible cardiac tissues for therapeutic transplant purposes [55]. Our previous investigations have utilized sub-cellular, nanoscale cues to align and orient cardiac monolayers [56]. There are numerous advantages over using nanotopography over microtopography: (1) the cues are subcellular and do not restrict or confine cell morphology, (2) the cues allow for rapid and scalable generation of cardiac monolayers without preventing cell-cell contacts, and (3) the use of biomimetic structures has also shown to modulate cardiomyocyte function dependent on the specific dimension used, indicating a more profound effect on cardiomyocytes than simple tissue alignment [56]. However, although these fabrication techniques offer more precise control over engineered tissue structure than indirect mechanical cues, such as uniaxial strain, these approaches also suffer a number of limitations. Namely, the scaling of these tissues into 3D, thick tissues, remains a technical challenge. Many studies have demonstrated differences in cellular morphology, gene expression and differentiation when cultured as 3D tissues [28], limiting the utility of monolayer-focused approaches. More importantly, a sufficient tissue volume is necessary to generate physiologically relevant forces and pressure. For example, more recent approaches utilizing ~500 million human stem cell-derived

cardiomyocytes and whole decellularized human hearts were only able to generate ~2.4 mmHg [57]. For applications which would require generation of larger forces, such as engineered tissue for therapeutic transplantation to increase contractile function (>10 mmHg to restore pulse pressure [58]), a single, 2D cardiac monolayer, even while structured, would presumably be insufficient.

Altogether, the field of cardiac tissue engineering offers numerous promising approaches towards the lofty goal of engineering whole, human hearts. However, limitations remain in every approach which has, thus far, prevented the engineering of even pieces of cardiac tissues which can mimic the physiological structure and function of the native heart.

1.3 Summary

Heart disease remains the leading cause of death both in the United States and worldwide, with a heart transplant as the only cure for end stage heart failure. Advancements in stem cell biology as well as engineering technologies offer new hope to the millions afflicted with heart disease worldwide of the possibility of engineering a functioning human heart. However, the lack of current methods to engineer physiologically-structured tissues ultimately inhibits the utility of engineered cardiac tissues for transplantation and functional purposes. Further, the lack of such tissues also prevents *in vitro* investigations, specifically for the study of stem cell-derived cardiomyocytes and tissue level structure-function relationships.

In this dissertation, we sought to address some of the limitations facing stem cell-derived cardiac tissue engineering by first developing a platform to reliably generate scaffold-free, 3D tissues with controllable structures in Chapter 2. This developed platform allows for the investigation of structure-function relationships of a number of tissues, and was used to show the

effects if tissue structure on the morphology and formation of skeletal muscle tissue in Chapter 3. More importantly, our platform has allowed us to engineer 3D, cardiac tissues with complex tissue architectures in Chapter 4. We found that by organizing individual cardiac sheets, we can significantly improve cardiac tissue function over unstructured tissues. Further, simply changing sheet orientation to a helical structure can further affect contractile characteristics of the engineered tissues. We believe that our developed platform will thus allow for the reproducible engineering of structured, 3D cardiac tissues, which can be further utilized in investigations of new therapies or *in vitro* diagnostic and modeling systems.

CHAPTER 2. A Thermoresponsive Nanofabricated Substratum for the Engineering of Three-Dimensional Tissues with Layer-by-Layer Architectural Control

2.1 Abstract

Current tissue engineering methods lack the ability to properly recreate scaffold-free, cell dense tissues with physiological structures. Recent studies have shown that the use of nanoscale cues allows for precise control over large area 2D tissue structures without restricting cell growth or cell density. In this study, we developed a simple and versatile platform combining a thermoresponsive nanofabricated substratum (TNFS) incorporating nanotopographical cues and the gel casting method for the fabrication of scaffold-free 3D tissues. Our TNFS allows for the structural control of aligned cell monolayers, which can be spontaneously detached via a change in culture temperature. Utilizing our gel casting method, viable, aligned cell sheets can be transferred without loss of anisotropy or stacked with control over individual layer orientations. Transferred cell sheets and individual cell layers within multilayered tissues robustly retain structural anisotropy, allowing for the fabrication of scaffold-free, 3D tissues with hierarchal control of overall tissue structure.

2.2 Introduction

Tissue engineering seeks to fabricate physiological tissues by utilizing a combination of cells, biomaterials, and engineering methods. However, one of the challenges inherent in tissue engineering is replicating the complex, three dimensional (3D) structures of most tissues which

are critical to their function [59-61]. The importance of replicating physiological tissue structure can be seen in the structure-function relationships of many tissues, such as in the orthogonal layering of sheets of connective tissues in the annulus fibrosus of intervertebral discs, which allow for their ability to withstand forces applied in multiple directions [62, 63]. Other examples of tissue-level structure-function relationships include the complex 3D structure of both the sinoatrial and atrioventricular nodes and connected Purkinje fiber network, which are responsible for the appropriate depolarization sequence of the heart [64], and the pennation or angling of muscle fibers in most muscle tissues to the line of action, which allows for a greater degree of control through mechanically diverse functions [65, 66]. Tissue structure is also often altered in disease states, such as the disarray of cardiac muscle in hypertrophic cardiomyopathy [67] and the thinning of bone trabeculae in osteoporosis [68], which can contribute to a deterioration of tissue function.

Despite significant efforts to study physiologically-relevant tissue structures and functions, however, only recently have technological advancements allowed for the engineering of more complex tissue structures. Microfabrication techniques have been used to engineer tissues with defined microscale structures, such as strips, squares, and wells, and have been successful in studies to understand single cell or tissue-like structure-function relationships [52, 69]**.** Other methods such as directionally-defined mechanical strain [70-72], magnetic fields [73, 74] and electrical stimulation [75, 76] have also allowed for the simple alignment or orientation of tissues**.** Additionally, 3D scaffolds, such as self-assembling peptides [77], are commonly employed to organize cells on biomaterials that can more accurately replicate tissues [78]. Finally, methods utilizing thermoresponsive polymers, such as poly(N-isopropylacrylamide) (PNIPAM), termed cell sheet engineering, have been able to fabricate 3D, cell-dense tissues without the use of a supporting scaffolds [79-82]. All these methods have started to bridge the gap between the simple

plating and culture of cells on flat culture surfaces and the complex tissue structures which are actually found in the human body. However, although promising, most of these techniques are ultimately still constrained to simplified aligned tissue structures [71, 75, 80], or sacrifice the cell-dense nature of physiological tissues [83, 84].

Subcellular nanoscale cues are a promising alternative for engineering cell and tissue structures which do not restrict the growth of cells. For instance, the addition of nanoscale cues, such as protein-based nanoparticles [85], nanorods [86], and nanotubes [87] have been explored to align both individual cells as well as 2D tissues. Additionally, nanotopographically-defined matrix guidance cues have been explored as an alternative method to structurally organize monolayers of tissues [88]. Topographical cues at the nanoscale are subcellular and can replicate the well-defined architectures of the local cellular microenvironment, such as mimicking structures of the extracellular matrix [79]. The use of scalable soft nanofabrication techniques thus can allow for the multiscale analysis of complex cell-matrix interactions and their role in tissue engineering. Further, the use of nanotopography has shown more precise control of self-assembled monolayer tissues over conventional alignment techniques and has also shown differential effects on morphological characteristics of cells [88]. We previously explored the effects of nanoscale surface topography on single cell and tissue level morphology and function with precise control over cell and tissue structure, such as guided migration in response to topographical gradient[89, 90] or self-assembly of anisotropic cardiac monolayers [56]. The use of these techniques allows for the study and characterization of specific monolayer tissue structures at a larger scale while utilizing a platform which can mimic the local cellular microenvironment.

In this study, we report the development of a thermoresponsive, nanofabricated substratum (TNFS) which can be used to structurally organize cell monolayers. By reducing culture temperature, the monolayers detach spontaneously as intact cell sheets. Using an

additionally developed tissue manipulation method termed “gel casting’, the cell sheets can be transferred to a flat surface and will maintain structural organization long term. Further, the sheets can be stacked using the gel casting method to engineer three dimensional, scaffold-free tissues. These multilayered tissues robustly maintain both individual layer structure as well as the specific angle at which the layers are stacked, providing layer-by-layer control over the fabricated tissue structure. Thus, the developed TNFS and gel casting method can be used as a platform to reproducibly engineer more complex tissues structures which can then be used in tissue engineering applications, drug screening and disease modeling.

2.3 Materials and Methods

2.3.1 Fabrication of a poly(urethane acrylate)-poly(glycidyl methacrylate) (PUA-PGMA) nanopatterned substratum

A UV-curable poly(urethane acrylate) (PUA, Minutatek, Korea) mold was fabricated using capillary force lithography as published previously [89-91] and was used as the nanopatterned template for the PUA-PGMA substratum (Fig. 2a). To allow for epoxy functionalization of the fabricated nanopatterned substratum, 1% GMA weight/volume monomer (Sigma-Aldrich) was added to the liquid PUA precursor (Norland Optical Adhesive) sonicated for 1 h and then hand mixed for 10 min. Solution was then degassed under a vacuum for 1 h to remove air bubbles. A glass coverslip (Ø18mm, Fisher) was cleaned using isopropyl alcohol and brush coated with an adhesion promoter to allow for attachment of the polymer to the glass surface and air dried. 20µl of PUA-PGMA prepolymer was added to the coverslip and covered with the PUA template. The PUA-PGMA prepolymer was spontaneously drawn into the nanofeatures of the PUA template via

capillary force. The template-prepolymer-glass was cured via 365nm UV light to initiate photopolymerization for 5 min. After polymerization, the PUA template was peeled off from the PUA-PGMA substratum via forceps and the substratum was UV cured overnight to finalize polymerization.

2.3.2 PNIPAM-grafting to the PUA-PGMA substratum

Amine groups react spontaneously with epoxy groups in an addition reaction to form a hydroxyl group and a secondary amine (Fig. 2a). Amine-terminated poly(N-isopropylacrylamide) (M_n: 2500, Sigma-Aldrich) was dissolved in deionized (DI) water at room temperature at a concentration of 1g/30ml. The PNIPAM solution was reacted with the PUA-PGMA substratum in a shaker at room temperature for 24 h at 55 rpm to allow for thermoresponsive functionalization. The TNFS was then washed 3 times with DI water and sterilized with 294nm UV light overnight prior to use.

2.3.3 Characterization of the TNFS

Scanning electron microscopy (SEM, FEI Sirion) was used to confirm nanotopographical fidelity. X-ray photoelectron spectroscopy (XPS, Surface Science Instruments S-probe spectrometer) was utilized to determine surface composition of the TNFS.

2.3.4 Cell culture and seeding on the TNFS

C2C12 mouse myoblasts were cultured in Dulbecco's Minimal Essential Media (DMEM, Gibco) supplemented with 20% Fetal Bovine Serum (FBS, Sigma), 1% penicillin-streptomycin (Sigma) and 1% amphotericin-B (Sigma) in an incubator at 37ºC, 5% CO_2. Cells were split at 80% confluency to prevent spontaneous differentiation. To seed cells onto the TNFS, cells were split

and seeded at a density of 40k cells/cm^2 to form a confluent monolayer within 24 h of culture and cultured normally with a daily media change. Cells were imaged with a bright field microscope (Nikon TS100) during culture. To visualize individual layers, cells were labeled with either 2μM CellTracker CMFDA Green (Invitrogen) or 2μM CellTracker Red CMTPX (Invitrogen) for 30 min before seeding onto the TNFS, and then washed gently 2 times with warmed media after attachment.

2.3.5 Gel casting transfer and stacking of nanopatterned cell sheets

To prevent loss of anisotropy after sheet detachment, a gel casting method was developed to preserve cell morphology. A 7.5% (wt/v) gelatin (Sigma) in media solution was made, which forms a solid at room temperature but melts at 37ºC. To detach the cell sheet, the TNFS was removed from the incubator and placed in a tissue culture hood at 22ºC, the media was aspirated and room temperature (22ºC) DPBS (Gibco) was added to the TNFS and incubated for 25 min to initiate cell sheet detachment. After room temperature incubation, the DPBS was aspirated and melted gelatin solution (37ºC) was then added to the TNFS, and the TNFS and gelatin were then incubated at 4ºC for 5 min to allow the gelatin to solidify rapidly. The solidified gelatin (gel cast) was then removed from the TNFS surface with forceps with the cell sheet adhered to the bottom surface and transferred to a new surface. The cell sheet was allowed to adhere to new surfaces in a 28ºC, 5% CO_2 incubator for 1 h and then the gel cast was melted by transferring the sheet to the 37ºC, 5% CO_2 incubator for 1 h. After the gel cast was melted, the transferred cell sheet was washed gently 3 times with warm media and cultured as normal. To create multilayered tissues, during the 4ºC incubation of the top sheet, the next layered sheet would first be removed from the 37ºC incubator, placed in the tissue culture hood, and the media removed. The gel cast from the first cell sheet (with the first sheet still adhered) would then be carefully placed on top of the

second cell sheet (still attached to the TNFS) with forceps, and the gel cast, cell sheets, and the TNFS would then be transferred to the 28ºC incubator and allowed to attach for 30 min (Fig. 7a). After the 30 min incubation, the gel cast, cell sheets, and the TNFS would then be incubated at 4ºC for 5 min to firm the gel cast for handling, at which point a subsequent cell sheet could be prepared for stacking or the multilayered tissue could be transferred to a new surface (Fig. 7a).

2.3.6 Use of orientation key to control stacked layer angle

To create tissues with specific layer orientation, an orientation key was fabricated out of transparent polystyrene. After gel casting, the gel cast and the TNFS could be visualized under a microscope at a 20x objective, and the nanopatterns were aligned to the 0 degree position of the orientation key. The gel cast was then cut parallel to the 0 degree position as a reference. During stacking, the detaching layer was then placed upon the orientation key and oriented to the desired angle relative to the casted layer and confirmed under the microscope. The gelatin cut line of the casted layer was then oriented to the key and the casted layer was then stacked and allowed to attach as normal (Fig. 7b).

2.3.7 Assessment of transferred cell sheet viability

A Live/Dead fluorescent staining kit (Invitrogen) utilizing calcein AM as a live cell reporting dye and ethidium homodimer-1 as a dead cell reporting dye was used according to manufacturer's instructions. Briefly, the kit reagents were added to sterile 1x DPBS to create a 1mM calcein AM and 4mM ethidium homodimer-1 solution. Cells were washed gently with warm 1x DPBS and then 200uL of calcein AM/ethidium homodimer-1 solution was added to the cells and incubated protected from light for 30 min at 37ºC, 5% CO_2. After incubation, cells were gently rinsed with 1x DPBS and then imaged with a confocal microscope (Nikon A1R).

2.3.8 Immunofluorescent staining and imaging

Cells were washed with phosphate buffered saline (PBS, Sigma) and fixed in 4% paraformaldehyde (Sigma) for 15 min at room temperature (22ºC). Fixed cells were then washed with PBS, and permeabilized and blocked with a solution of 5% bovine serum albumin (Sigma) and 0.25% Triton X-100 (Sigma) in PBS for 1 h at room temperature, then washed with PBS. For F-actin staining, cells were then incubated in AlexaFluor488-conjugated phalloidin (Invitrogen) at a dilution of 1:200 in 1% BSA in PBS for 1 h at 37ºC. All samples were then stained with a Hoechst stain (Sigma) at a dilution of 1:1000, washed with PBS once, and then treated with Vectashield (Vector Labs) and mounted on coverslips and imaged using a confocal microscope.

2.3.9 Quantitative analysis of cell alignment

To assess alignment, phase contrast or immunofluorescent images of phalloidin or CellTracker stained cells were taken at 3 representative fields at 10x magnification and analyzed using a modified, previously published MATLAB script utilizing pixel gradient analysis. Briefly, the images were passed through a Gaussian low pass filter and Sobel horizontal edge-emphasized filter (predefined MATLAB Image Analysis toolbox functions) to generate a 2D convolution. The Sobel filter was then transposed to extract the vertical edge, and the horizontal and vertical edges were combined to calculate the gradient magnitude of each pixel in the image. The image was then thresholded to determine the borders of the areas of interest, and the orientation of the gradient was calculated via respect to the x-axis (0 degree). A representative image of the filtering, vector generation and histogram creation process is demonstrated in Figure 1. The orientation gradient data obtained from the pixel gradient analysis MATLAB script was then used to generate representative plots of overall cell alignment using a second custom MATLAB script. Each image

was segmented into a grid of user-designated size. The gradient orientation angle for each pixel in a given grid square was then shifted in order to take a circular average with respect to the angle present with the highest incidence within that grid square's orientation angle data. This circular average is representative of the mean orientation of each pixel gradient within a given grid square.

2.4 Results

2.4.1 Fabrication of a polyurethane-epoxy copolymer nanofabricated substratum for thermoresponsive polymer functionalization (TNFS)

To develop a thermoresponsive, nanofabricated substratum, we sought to functionalize substrata engineered with our well-established capillary force lithography (CFL)-based nanofabrication techniques [89-91] with a thermoresponsive release layer while preserving pattern fidelity. To do this, we utilized epoxy-amine chemistry (Fig. 2a) to covalently bind amine-terminated poly(N-isopropylacrylamide) (PNIPAM) to surface epoxy groups present in our composite polymer substratum fabricated with CFL (Fig. 2b). Our composite polymers consisting of glycidyl methacrylate (GMA) and polyurethane acrylate (PUA) as a copolymer allowed for GMA incorporation up to 75% wt/v in the PUA prepolymer mixture and still allow for photopolymerization of the mixture and nanofabrication of topographical cues. Scanning electron microscopy (SEM) analysis confirmed nanopattern fidelity of a TNFS consisting of 1% GMA (Fig. 2c), and the UV-assisted CFL technique could scale the TNFS to large-area sizes (up to 25cm^2), which were useful for tissue-level fabrication and analysis. X-ray photoelectron spectroscopy analysis showed an increase in nitrogen surface compositions of the TNFS reacted with amine-terminated PNIPAM, confirming PNIPAM functionalization of the TNFS (Fig. 2d and Table 1).

2.4.2 Biocompatibility of the TNFS and effects of PNIPAM grafting density on monolayer formation

In order to determine the biocompatibility and thermoresponsive characteristics of the TNFS, C2C12 mouse myoblasts were used as the cell model. As varying PNIPAM grafting densities have been previously shown to affect cell adhesion and sheet formation [92], we fabricated the TNFS using varying GMA percentages (1%-75%) to create various density of available epoxy groups, and then reacted with PNIPAM for 24 h. C2C12 cells were seeded at a high density ($4x10^5$ cells/cm^2) and allowed to attach for 24 h at 37ºC on the TNFS with varying GMA percentages. Cells displayed increased attachment and monolayer formation with decreasing GMA percentage, indicating that high-density grafted PNIPAM inhibits cell adhesion (Fig. 2e and Fig. 3). Specifically, the TNFS consisting of 1% GMA (1% GMA TNFS) as well as a 1% GMA unpatterned, thermoresponsive substratum (controls) formed confluent monolayers within 24 h after seeding. Cells on the 1% GMA TNFS also aligned to the direction of the nanopatterns, indicating sensitivity to nanoscale topography (Fig. 2e). Cells attached to the 1% GMA TNFS within 2 h of seeding, and continued to spread to form a confluent monolayer within 24 h. The self-organization of cells and monolayers to nanoscale cues happened quickly – within 2 h of seeding cells on the TNFS, which allows for rapidly, aligned monolayer formation. Additionally, the cell monolayers are very well aligned to the nanotopographical cues even under varying culture conditions such as cell seeding density or culture time, removing variability in the degree of alignment of the forming monolayer. Other studies have shown that topographical guidance cues to align cells even in the presence of conflicting cues such as mechanical strain [93] or electrical stimulation [93, 94], suggesting these topographical cues provide a high degree of control over structural organization.

2.4.3 Thermoresponsive detachment of anisotropic cell sheets from the TNFS

To assess thermoresponsive, spontaneous detachment of cell sheets, the 1% GMA TNFS seeded with cells was removed from the culture incubator (37ºC) and incubated in DPBS for 30 min at room temperature (22ºC). Within 20 min, edges of the cell sheet began to detach from the TNFS and controls and retract inwards and soon after, the cell sheet on the 1% GMA TNFS as well as controls detached spontaneously (Fig. 4). During detachment from the 1% GMA TNFS, cells contracted along the longitudinal axis and lost anisotropic morphology, with the entire cell sheet shrinking and losing alignment (Fig. 5). The detached cell sheet could be transferred to a new surface via forceps or pipets and allowed to reattach. However the sheet continued to contract and became extremely cell-dense, aggregated tissues with no discernible anisotropy or organization. Based on the ability to form confluent monolayers rapidly, as well as detach a cell sheet spontaneously, the 1% GMA TNFS were used for all subsequent experiments and will be referred to simply as the TNFS.

2.4.4 Use of the gel casting method to transfer nanopatterned cell sheets without loss of structure

To transfer and manipulate anisotropic cell sheets without loss of structural organization, a previously published cell sheet transfer method was investigated [79]. Using this plunger-like manipulator method, a fully intact cell sheet was only able to be transferred from the unpatterned thermoresponsive controls. The cell sheet from the TNFS only partially detached, allowing for transfer of a partial cell sheet or cell sheet fragments. Further, the transferred cell sheet from the TNFS demonstrated some loss of anisotropy immediately after transfer and subsequently lost all anisotropy after 5 days of culture on the flat surface of a standard tissue culture dish (Fig. 6a).

We hypothesized that the lack of adhesion strength to the gelatin-coated manipulator from the TNFS may result in partial or difficult cell sheet detachment as well as the lack of morphological maintenance. As a result, a new method was developed to transfer nanopatterned cell sheets, termed the gel casting method (Fig. 7a), in which we aimed to encase the cell sheet in the gelatin in order to increase cell sheet-gelatin adhesion strength and preserve morphology. Briefly, melted gelatin is added to the TNFS which is incubated at room temperature and then cooled to solidify and encase the detaching cell sheet prior to full sheet detachment. These sheets can then be stacked onto another TNFS to form multilayer tissues or transferred to a new surface. Using a developed orientation key (Fig. 7b), the relative layer angle between the top and subsequent layers can also be controlled during the stacking process. The use of gelatin also allows for the easy manipulation of delicate cell sheets using forceps (Fig. 7c). Using the gel casting method, cell sheets from both the TNFS and controls were able to be recovered intact and transferred to glass coverslips. After transfer, cell sheets remained firmly attached to the glass and could be cultured as normal. The transferred nanopatterned cell sheet retained anisotropic cytoskeletal structure immediately (24 h) after transfer as well as up to 7 days post-transfer (Fig. 8a). Gel casted transferred cell sheets also maintained near 100% viability 24 h after transfer (Fig. 9), and cell growth continued outward from the edges of the cell sheets, albeit in a random growth pattern for the transferred nanopatterned cell sheet. Immunofluorescent staining of cellular cytoskeletal proteins also indicated that cells within the transferred nanopatterned cell sheet demonstrated a well aligned cellular cytoskeleton in addition to cell morphology (Fig. 8b). Automated image analysis was used to quantify alignment of transferred cell sheets from both TNFS and controls 24 h and 7 days after transfer to a flat glass coverslip. The transferred nanopatterned cell sheet demonstrated significant structural alignment immediately after transfer, which was maintained

overall tissue alignment long term (7 days) comparable to the transferred, unpatterned cell sheet (Fig. 8c).

2.4.5 Engineered orthogonal bilayer tissues

To determine whether the gel casting method could be used to successfully fabricate 3D tissues, nanopatterned cell sheets were stained with fluorescent live cell red and green membrane dyes to discern individual layers when stacked. The gel casting method was then used sequentially to transfer a green-dyed nanopatterned cell sheet onto a red-dyed nanopatterned cell sheet and then the bilayer tissue onto a glass coverslip. After 3 days of culture after stacking and transfer, the transferred bilayer tissue was fixed and imaged. The gel casting method was able to successfully fabricate the bilayer tissue which maintained individual layer morphologies even after transfer (Fig. 10a,c) with distinct red and green layers, indicating no layer mixing or migration of cells between layers (Fig. 10b). The average overall thickness of the bilayer tissue was 33.2µm, with both layers having the same thickness.

2.4.6 Fabrication of helical, trilayer myoblast tissues which retain structure

Next, using the gel casting method and orientation key, a 3D tissue with specific layer orientations, and specific inter-layer angles, was fabricated. To confirm this, stained red and green nanopatterned cell sheets were detached and stacked sequentially with specific inter-layer angles (Fig. 11a) to form a trilayer tissue and transferred to a flat glass coverslip and cultured for 3 days. The fabricated tissue demonstrated 3D, multi-colored structures when analyzed using confocal microscopy (Fig. 11b). Individual layers were easily discernible (Fig. 11d) and did not mix. Further, the red/green signal from individual cell sheets was analyzed using a modified image analysis technique to quantitatively evaluate alignment of individual layers within the tissue. The

individual layers maintained alignment as well as the specific layer angle at which they were stacked, indicating no reorganization both within the sheets and between layers (Fig. 11c). The overall thickness of the layered tissue was 48.9μm, with an average layer thickness of 16.3μm, similar to the results from the bilayer stacking experiments. The tissue maintained this distinct structural organization 3 days after transfer, and no retraction or detachment of either individual sheets or the whole tissue was noted during this time.

2.5 Discussion

While other groups have fabricated aligned tissues using cell sheet engineering [80] and have demonstrated multilayered tissues with specifically arranged layers [81], to our knowledge, this is the first demonstration of 3-layered tissues with clear anisotropy, defined individual layers, and fabricated utilizing a method to control the specific inter-layer angles. Interestingly, we observed the maintenance of both layer anisotropy and stacked layer angle of tissues utilizing myoblasts. It has recently been reported using human myoblasts that aligned cell sheets reorganize themselves to match the alignment of the top sheet, generating a completely aligned 3D muscle tissue [80]. Further, this rearrangement of all bottom sheets happens within 24 h of stacking, and cells within individual sheets migrate between sheets, indicating intermixing between layers of fabricated tissue. In a clear contrast to these results, our method allows the maintenance of individual layer orientations as well as prevention of intermixing of individual sheets for 3 days.

Myoblasts are well known as migratory cells due to their migration to sites of injury for muscle repair, and recent studies have also shown that myoblasts can migrate vertically through multilayered tissue constructs [95, 96]. This cell fluidity has been hypothesized to contribute to the loss of individual layer orientations in multilayered myoblast tissues constructs. However, we

did not observe this phenomenon in our experiments utilizing a mouse myoblast line and our nanotopography-based platform. Our recent study showed an upregulation of myogenic markers of myoblasts when cultured on the nanopatterned substratum, and an increase in dystrophin expression when nanopatterned monolayer muscle patches were implanted in an *in vivo* mouse muscular dystrophy model, relative to unpatterned controls [97]. Other studies have reported differential response of myoblasts to nanotopography versus micropatterning [98]. It is possible that the utilization of nanotopographical cues to structurally organize monolayers may evoke a different biological response within the chosen cell model when compared to methods such as micropatterning. With such results, we believe this platform can allow for the facile, reproducible fabrication of well-defined 3D tissue structures which may not be achievable via other means.

In this study, we have developed a simple, yet versatile platform for the fabrication of scaffold-free 3D tissues using our newly developed TNFS and gel casting method. This platform enables the reproducible and robust fabrication of scaffold-free 3D tissues with control of overall tissue architecture via nanoscale control of cell and tissue structure. Although other groups have demonstrated the fabrication of 3D tissues using scaffolds with controllable 3D architectures [78, 99] or micropatterned molds or scaffolds functionalized with thermoresponsive polymers [80, 81, 100], in contrast, the use of nanotopographical cues allows for the structural organization of cells and cell monolayers at a sub-cellular level, thus not preventing or restricting cell growth and reducing variabilities such as degree of alignment due to pattern size or cell seeding density. Additionally, the fabrication method of our TNFS is highly reproducible, cost-effective, and scalable, allowing for a variety of applications in cell biology and tissue engineering. The developed substratum incorporated our CFL-based nanofabrication method, which allows us to fabricate a variety of nanotopographical cues in a large-area format with an epoxy-based

chemistry which allowed the surface immobilization of a thermoresponsive polymer. The TNFS had variable cell attachment based on GMA percentage incorporation and thus PNIPAM grafting density, with the 1% GMA TNFS allowing for both rapid monolayer formation as well as spontaneous, thermoresponsive detachment of intact cell sheets. Next, the gel casting method was used to transfer aligned sheets to a flat surface, and the transferred cell sheets maintain long term structural organization without presentation of additional nanotopographical cues. Finally, the gel casting method also allowed for the stacking of aligned sheets at specific angles between subsequent layers. The multilayered tissues retained specific layer organization, layer integrity, and overall tissue architecture upon transfer to a flat surface for 3 days, demonstrating the feasibility of our platform in the creation of complex 3D tissues with highly controllable architecture. Interestingly, when stacked into multilayered tissues, individual sheets also retain their specific alignment and cells from individual sheets do not mix or migrate. This allows for the fabrication of 3D tissues with defined layer structures which can also have precisely controlled architectures, or changing of the tissue organization in three dimensions, allowing for the engineering of complex and physiological tissues. Our developed platform could be readily extended to the engineering of other complex, defined 3D tissues of interest and used in quantitative studies of structure-function relationship.

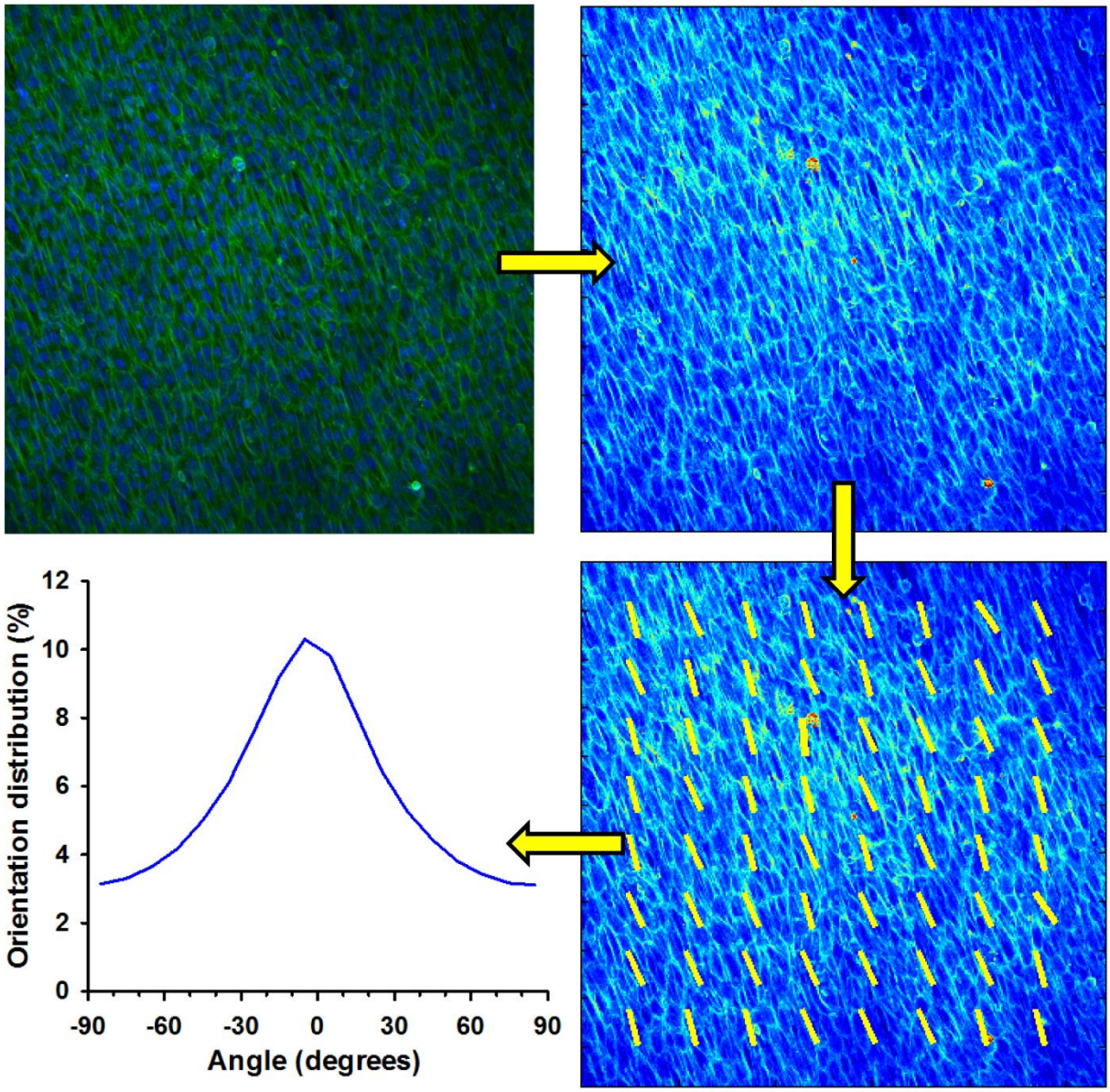

Figure 1. Quantitative analysis of alignment using pixel gradient algorithm. Confocal image of phalloidin stained, transferred anisotropic cell sheet. Image is then converted to grey scale and gaussian filtered. Pixel gradient vectors are calculated based on filtered image (representative gradient vectors overlaid on image). Vectors are then binned to 10 degree ranges with major vector angle set to zero and a histogram plot is displayed.

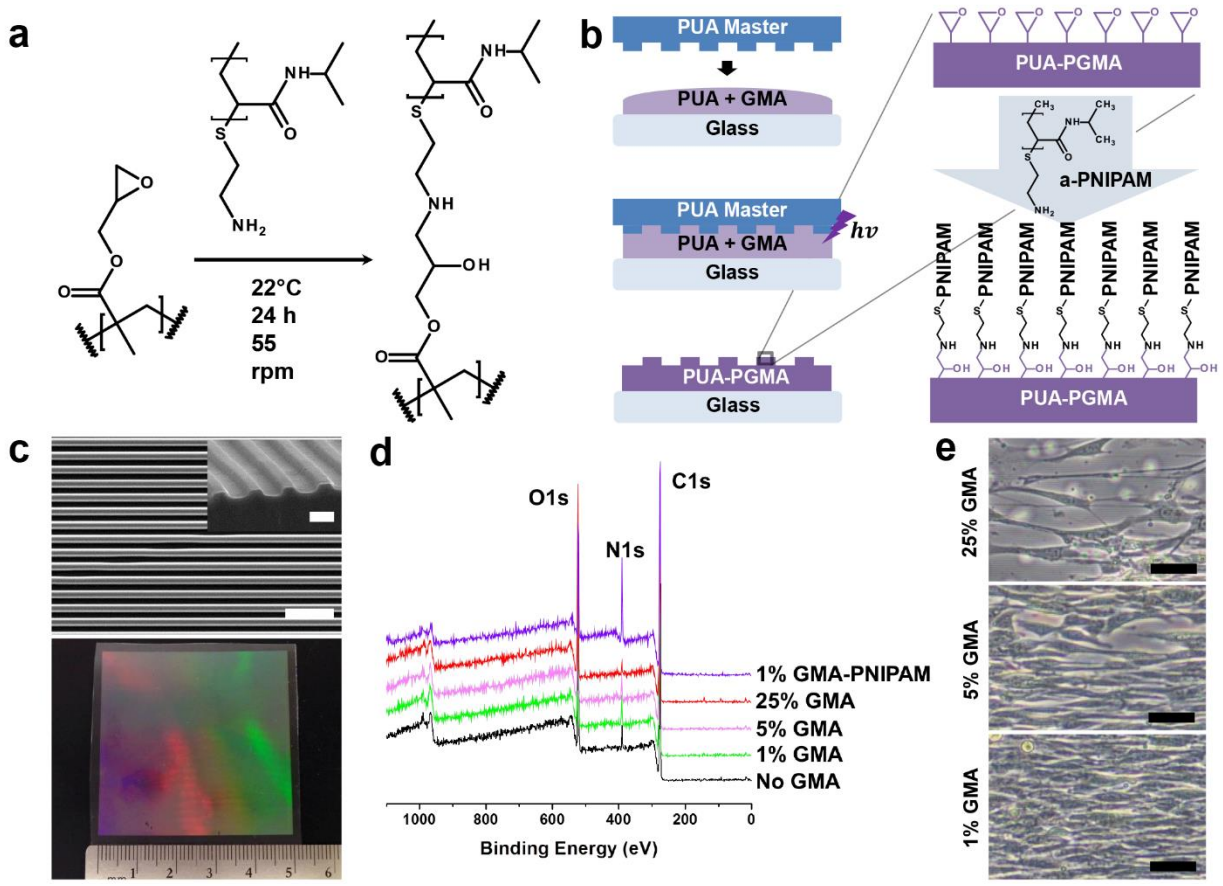

Figure 2 Fabrication and characterization of the thermoresponsive nanofabricated substratum. (a) Epoxy amine addition reaction equation and experimental conditions. (b) Schematic of capillary force lithography to create the nanofabricated substratum and subsequent functionalization of the substratum with amine-terminated PNIPAM (a-PNIPAM). (c) SEM image of PNIPAM-functionalized polymeric nanofabricated substratum (top) and photo of a large-area, scalable TNFS (bottom). Scale bar, 5 μm; 1 μm (inset). (d) XPS analysis of the TNFS surface chemical composition with varying GMA prepolymer concentration before PNIPAM reaction and after 1% GMA TNFS PNIPAM reaction. (e) DIC image of C2C12 cells cultured on 25, 5, and 1% GMA TNFS after PNIPAM reaction for 24 h at 37 °C. Cells demonstrated varying degrees of confluent monolayer formation. Scale bar, 50 μm.

Table 1. Atomic concentration percentages of various substrate surfaces.

Sample	Percent		
	C1s	O1s	N1s
0% GMA	72.1 ± 1.0	23.6 ± 0.9	4.3 ± 0.2
1% GMA	72.4 ± 0.6	23.0 ± 0.5	4.5 ± 0.2
5% GMA	71.9 ± 1.0	23.8 ± 0.9	4.2 ± 0.2
25% GMA	71.2 ± 0.4	25.3 ± 0.6	2.4 ± 0.1
1% GMA-PNIPAM	75.0 ± 0.6	12.4 ±0.3	12.3 ± 0.3

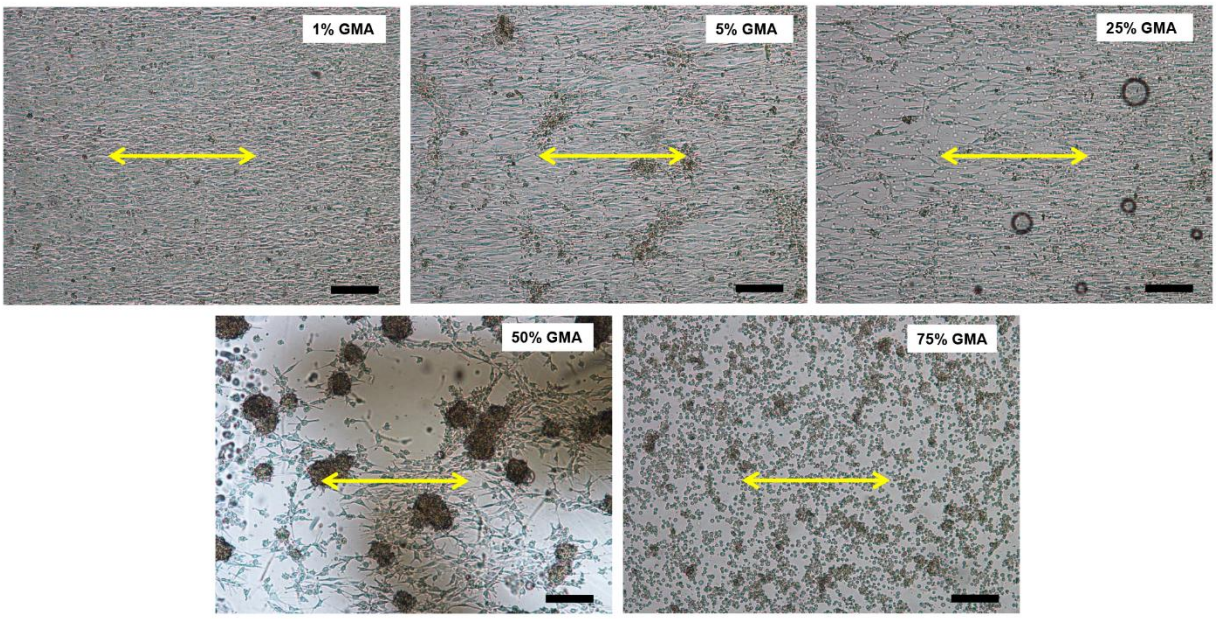

Figure 3. Varying GMA incorporation prior to PNIPAM functionalization affects cell attachment. Phase contrast image showing varying substrate GMA composition and subsequent cell attachment and monolayer formation after 24 h culture at 37°C. Scale bars, 200µm.

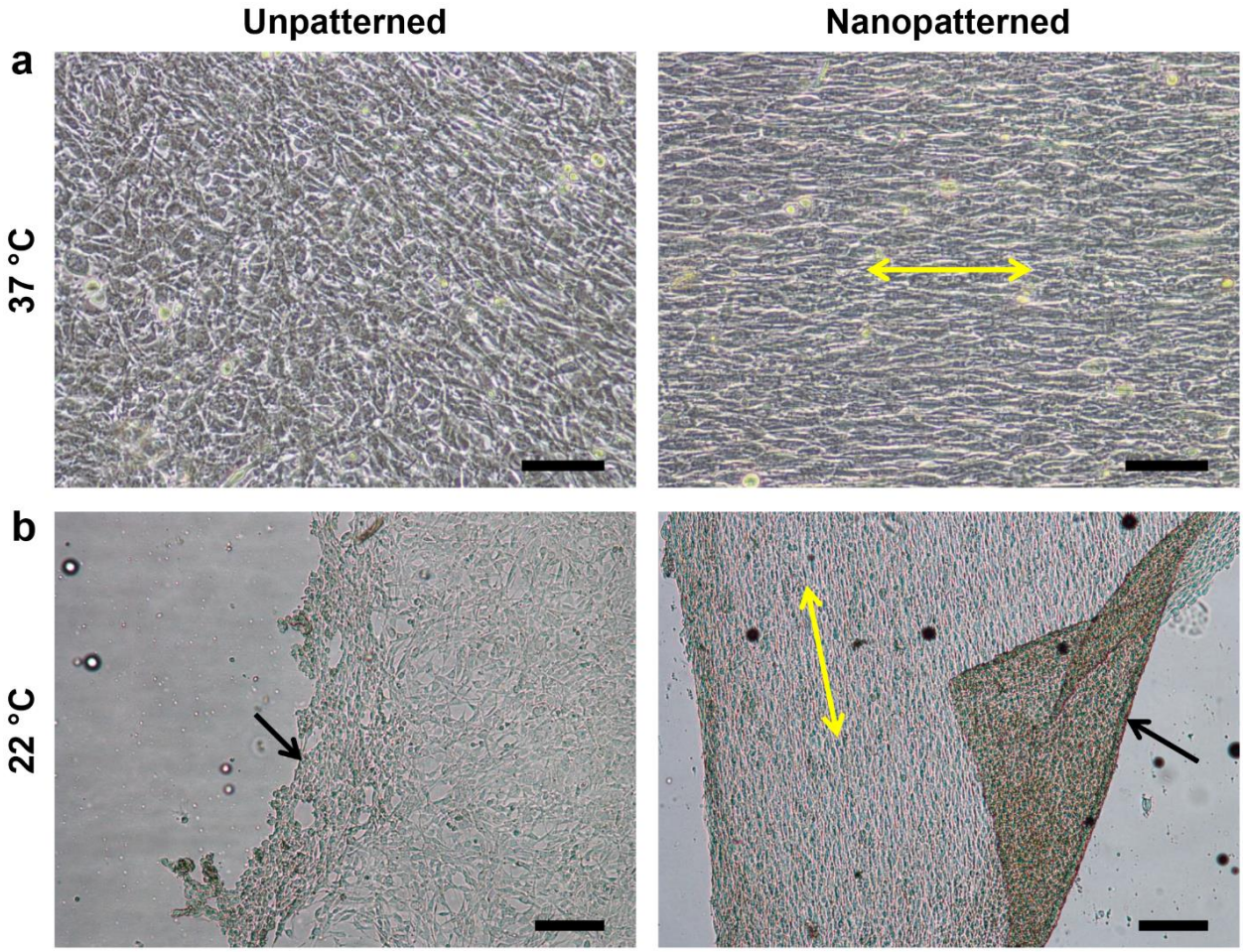

Figure 4. TNFS aligns cell monolayers and spontaneously detaches cell sheets in response to temperature change. (a) Bright field image of C2C12 myoblasts cultured on the TNFS and control at 37 °C 24 h after seeding. The TNFS aligns the cell monolayer. Scale bar, 100 μm. (b) Phase contrast image of C2C12 monolayers after incubation at 22 °C for 30 min undergoing spontaneous detachment on both the TNFS and control. Black arrows indicate detaching edge of cell sheet. Yellow arrows indicate TNFS nanopattern direction. Scale bar, 200 μm.

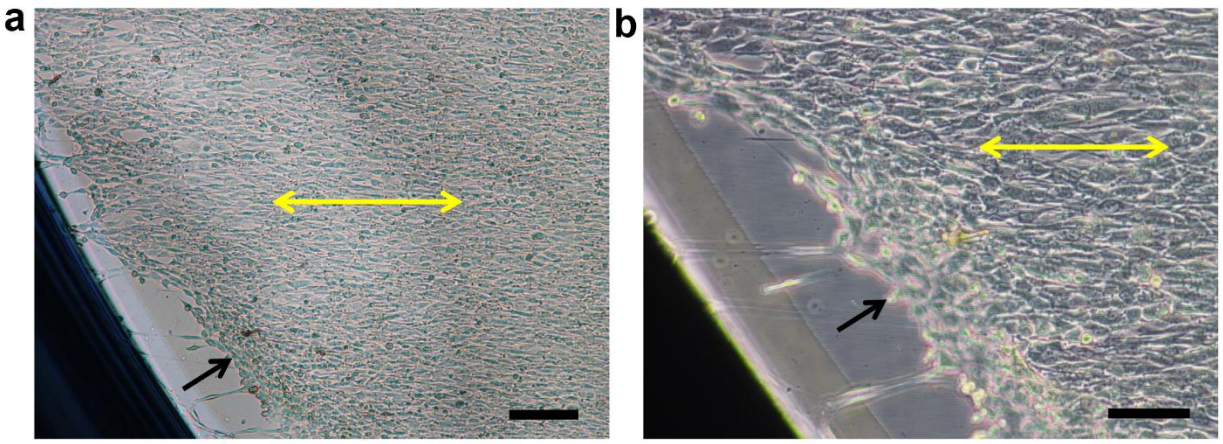

Figure 5. Cells lose anisotropic morphology during detachment. (a) Phase contrast image showing detachment of nanopatterned cell sheet and subsequent loss of anisotropic cell morphology. Scale bar, 200µm. (b) Magnified DIC image of detaching edge of a nanopatterned cell sheet. Scale bar, 100µm.

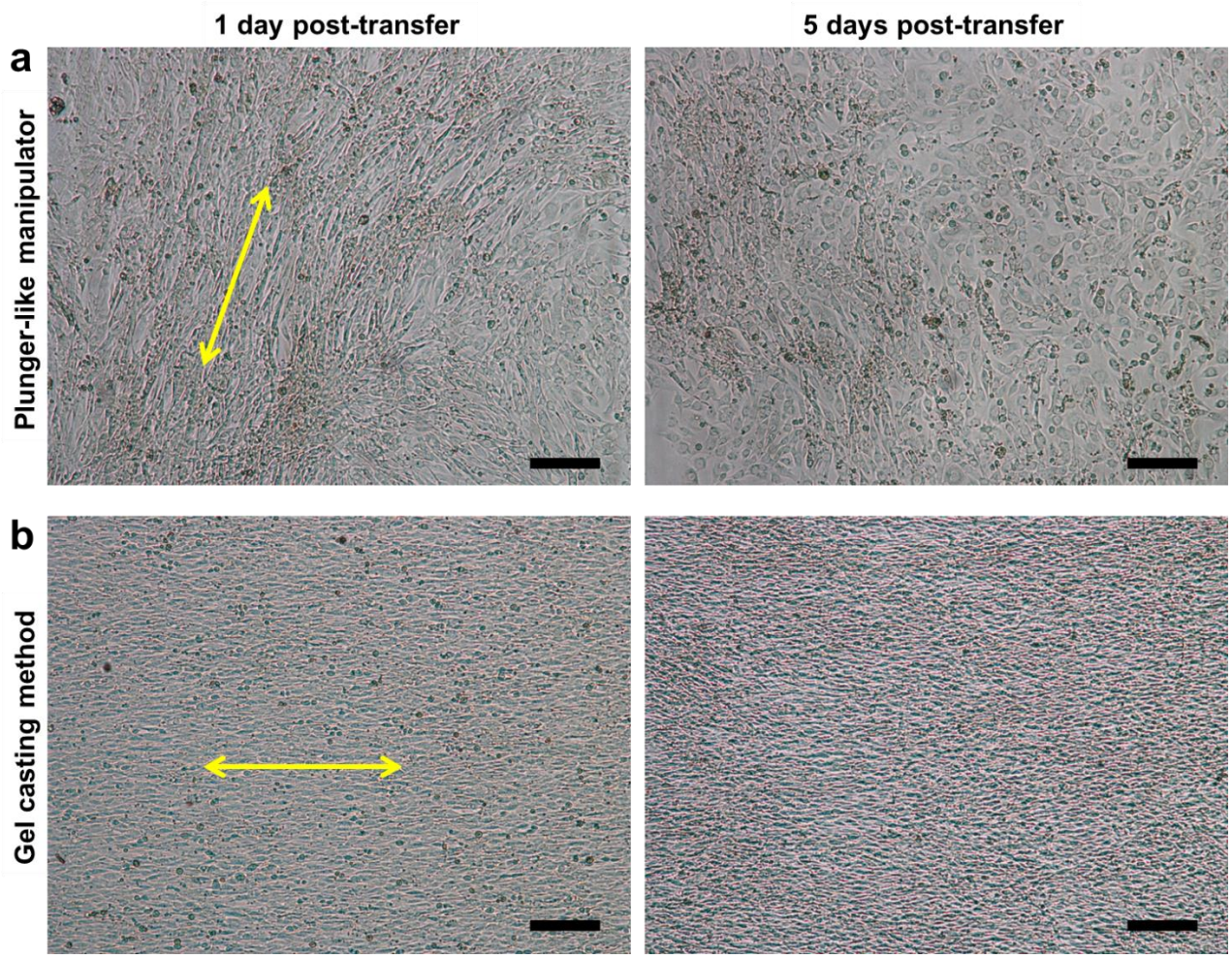

Figure 6. Comparison of two methods to transfer nanopatterned cell sheets. (**a**) Phase contrast image of nanopatterned cell sheets transferred using the plunger-like manipulator method 1 day and 5 days after transfer onto a flat surface. Scale bar, 200μm. (**b**) Phase contrast image of nanopatterned cell sheets transferred using the gel casting method 1 day and 5 days after transfer onto a flat surface. Yellow arrows represent cell sheet alignment. Scale bars, 200μm.

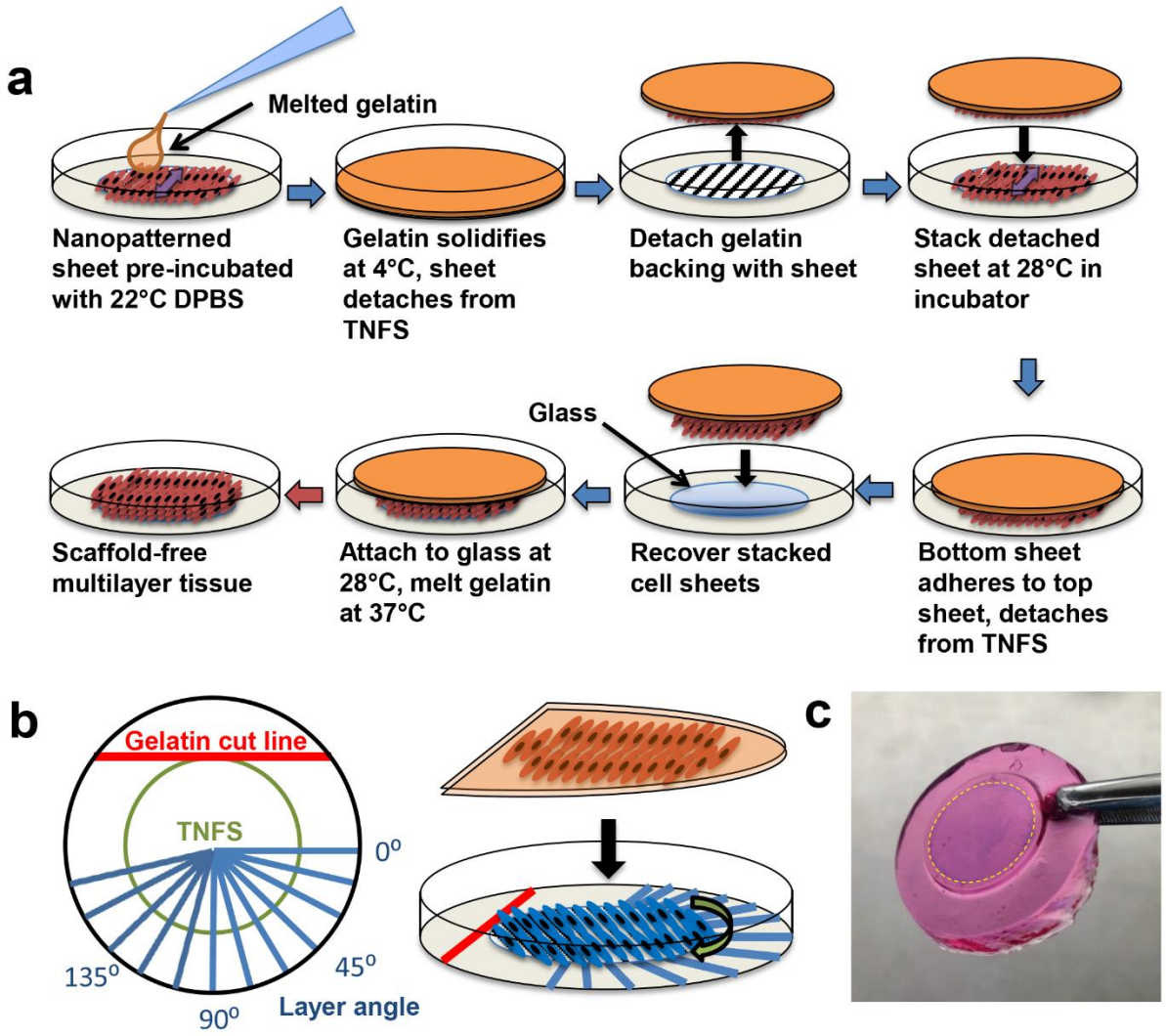

Figure 7. Gel casting method to preserve cell sheet anisotropy and control relative layer angle during stacking. (a) Schematic showing the gel casting method process to stack and transfer nanopatterned cell sheets. (b) Schematic of the orientation key (left) used to control relative layer angle during nanopatterned sheet stacking (right). (c) Image of gel cast sheet after gelatin solidification. Sheet was fixed and stained with trypan blue while casted to enhance visibility.

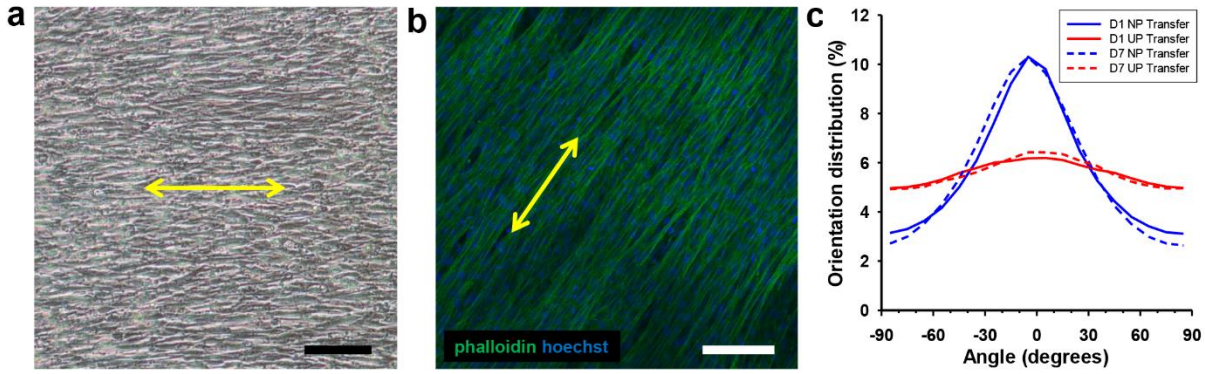

Figure 8. Transferred nanopatterned cell sheets are viable and maintain alignment. (a) DIC image of a transferred nanopatterned cell sheet 7 days after transfer onto glass. Scale bar, 100 μm. (b) Confocal image of phalloidin (green) and Hoechst (blue) staining showing maintenance of aligned cytoskeletal structure of nanopatterned cell sheets. Scale bar, 100 μm. (c) Quantitative analysis of cytoskeletal alignment of transferred nanopatterned (NP) cell sheets and unpatterned (UP) controls 1 day and 7 days after transfer. Yellow arrows indicate direction of transferred cell sheet alignment.

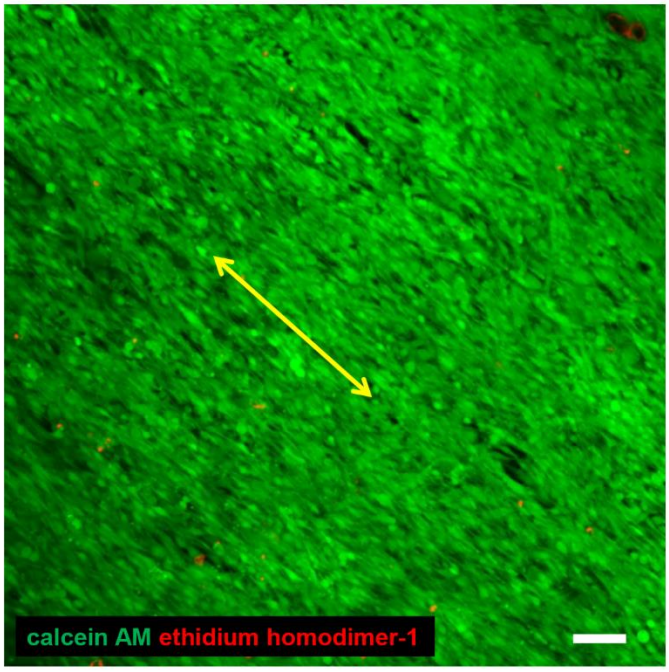

Figure 9. Viability of gel casted, transferred nanopatterned cell sheets. Confocal image of a live (green)/dead (red) assay performed on a transferred cell sheet indicating near 100% viability. Scale bar, 100µm.

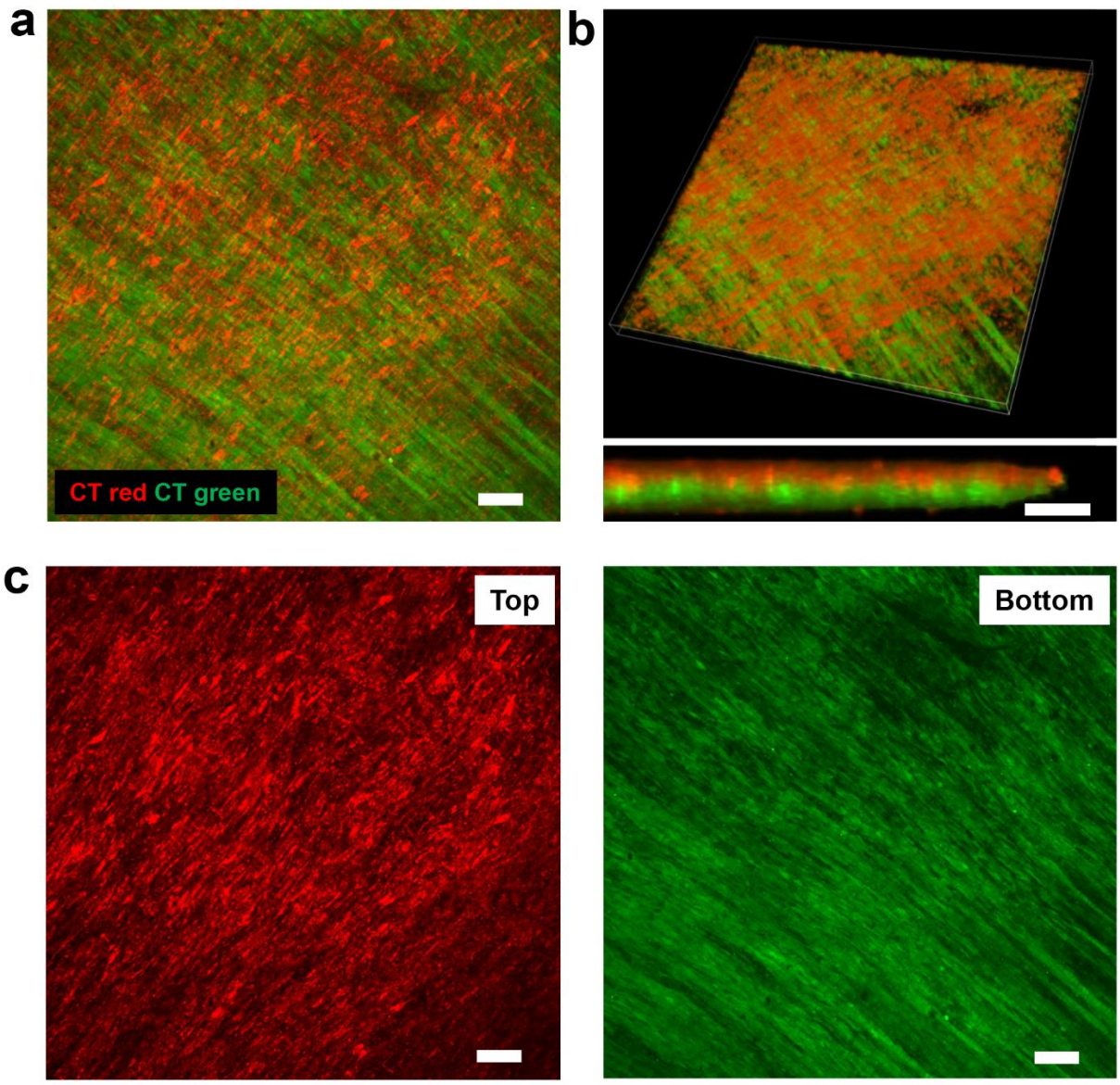

Figure 10. Individual nanopatterned cell sheets can be stacked together using the gel casting method. (a) Max projection confocal image of a z-stack showing two membrane-stained nanopatterned cell sheets stacked together to form a bilayer tissue. Top layer stained with red membrane dye, bottom layer stained with green membrane dye. Bilayer tissue was transferred to a glass coverslip and cultured 3 days before fixation and imaging. Scale bar, 100 μm. (b) Three-dimensional tissue rendering utilizing confocal z-stack images of membrane-stained cell sheets stacked into bilayer tissue, with individual layer colors discernible when magnified (bottom). Scale bar, 40 μm. (c) Confocal image of top and bottom sheets. Scale bar, 100 μm.

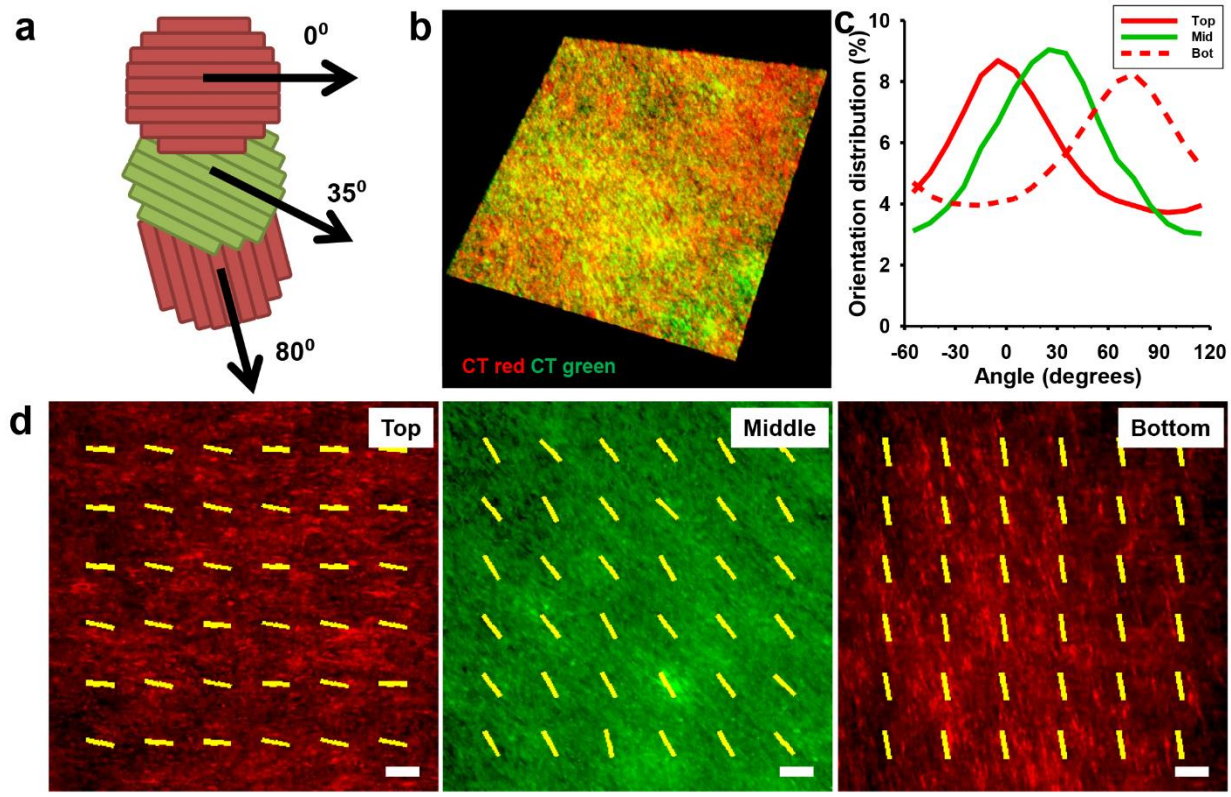

Figure 11. Stacked nanopatterned cell sheets maintain individual layer alignment and demonstrate precise control over 3D structure. (a) Schematic of the trilayer myoblast tissue with individual layer orientations. (b) Three-dimensional tissue rendering utilizing confocal z-stack images of membrane-stained cell sheets stacked into trilayer tissue. Top and bottom layers were stained with red membrane dye; middle layer was stained with green membrane dye. Trilayer tissue was transferred to a glass coverslip and cultured 3 days before fixation and imaging. (c) Quantitative analysis of cell sheet alignment of individual layers demonstrates retained alignment 3 days after stacking as well as maintained interlayer angles. (d) Confocal images of the individual layers with representative alignment vectors generated via the image analysis program overlaid. Scale bar, 100 μm.

CHAPTER 3. Nanoengineered Myoblast Constructs to Assess Tissue Structure on Myoblast Fusion and Myotube Morphology

3.1 Abstract

Skeletal muscle is comprised of aligned myofibers encased in an extracellular matrix sheath or lamina. Within this lamina resides satellite cells, which migrate to the site of injury to dedifferentiate into myoblasts and fuse with myofibers to regenerate muscle tissue. Biochemical cues have most often been implicated to direct cell migration and fusion, however other microenvironmental stimuli, such as ECM or tissue structure, are largely unstudied. We hypothesize that the structure of skeletal muscle tissue in both 2D and 3D can affect the organization and morphology of differentiating myoblasts and formed myotubes. Further, we believe that cellular and extracellular matrix cues, in the absence of biochemical factors, can be a strong director of myoblast function in a 3D tissue environment. In this study, we utilized a thermoresponsive nanofabricated substratum (TNFS) to engineer anisotropic sheets of myoblasts which can be transferred and stacked into multilayered tissues. We found that myoblasts rapidly sense topography and deposit structured ECM proteins. Further, the initial tissue structure was a strong determinant of eventual myotube formation and organization. When organized into bilayers, competing alignment cues led to formation of disorganized myotubes, whereas alignment allowed for larger, organized myotubes. Finally, when transferred to a 3D hydrogel cylinder as a muscle surrogate, myoblasts fused and formed myotubes along the original tissue structure, even when oriented circumferentially to the cylinder, providing insights into additional strategies to repair damaged muscles.

3.2 Introduction

The cellular microenvironment comprises of local physical and chemical stimuli surrounding the cells which often dictate or regulate cell function. These stimuli include the extracellular matrix, which often has an inherent structural organization which is also critical to the appropriate function of cells and tissues [101]. The structure of tissues is dictated by a complex interplay between cells and ECM: the extracellular matrix imparts topographical cues which can direct cell orientation and migration, and many cells also actively secrete and remodel their ECM [102-104]. One well known example of a cellular microenvironment with defined structure is that of the satellite cell niche. Satellite cells are skeletal muscle stem cells which aid in muscle regeneration after injury and are located at the periphery of individual adult skeletal muscle myofibers, in between the basal lamina (endomysium) and the plasma membrane of the myofiber (sarcolemma) [105, 106]. Under normal conditions, these satellite cells are quiescent, however, after injury, satellite cells have remarkable regenerative capable and can both self-renew as well as fuse with existing myocytes to repair damaged muscles [105]. In development, myoblasts also fuse end to end to form myotubes, which then mature and become myocytes [107]. When engineering tissue, it is thus important to analyze the structure of both cells and ECM when engineering tissues in order to impart correct physiological function.

Cell sheet engineering utilizes thermoresponsive polymers on culture surfaces to detach monolayers of cells intact as a sheet [108]. Contrasting enzymatic digestion, cell sheet engineering preserves cell-deposited ECM and cell sheets detach with their ECM intact [109]. The use of such thermoresponsive culture platforms thus allows for the engineering of cell-dense tissues which also contain cell-secreted ECM. This additionally allows for the analysis of more physiological microenvironments, which natively consist of both cells and extracellular matrix.

However, typical cell sheet engineering utilizes a substrate which cannot organize cells or tissues, subsequently generating randomly organized and structured 3D tissues [110]. This, in turn, prohibits investigation of cell microenvironments which have specific structures, such as the endomysium [106, 111], on satellite cell fate and function. To this end, we previously have developed a platform utilizing nanotopographical cues to align cell monolayers as well as a thermoresponsive release layer termed thermoresponsive nanofabricated substratum or TNFS [112]. Nanopatterned cell sheets can be transferred from the TNFS and maintain alignment long term, even when stacked into multilayered tissues. This contrasts other methods using cell sheet engineering which cannot maintain independent sheet alignment after stacking [80].

We hypothesize that the TNFS also allows for organization and transfer of cell-deposited ECM, which provides alignment cues and prevents cell sheet reorganization after detachment and transfer. Further, we believe that, due to the necessity of myoblast alignment to form myotubes [113], multilayered, aligned myoblast tissues will be able to form aligned myotubes from myoblasts in both sheets while orthogonally oriented myoblast tissues will only be able to form myotubes within the individual sheets, with the respective sheet alignment dictating myotube alignment. Using C2C12 mouse myoblasts, we found that cells quickly sensed nanotopographical cues and structurally organized deposited ECM. After 24 hours in culture, cell cytoskeleton and cell-deposited ECM was structurally organized and well aligned to the nanotopographical cues and could be transferred to flat surfaces with maintained cell and ECM alignment of up to 1 week after transfer. To analyze the effects of cell and ECM structure on myoblast function, bilayer orthogonally stacked tissue maintained both cell and ECM structure for up to 7 days post-stacking, even in the absence of nanotopographical cues from the TNFS, while maintained in a growth state. However, while undergoing differentiation, only myoblasts in the top layer were able to fuse to form myotubes, whereas the bottom layer remained as myoblasts. Contrasting that, aligned

bilayers formed myotubes from both layers of myoblasts. The myotubes formed from the aligned bilayers also demonstrated larger morphology and maturity. Finally, to assess the formation of myotubes in a transplanted, nanopatterned cell sheet onto a 3D structure as a possible therapeutic cell patch, we transferred single nanopatterned myoblast sheets circumferentially onto a crosslinked gelatin cylinder as a surrogate of muscle tissue. We observed that the cell sheets maintained alignment after transfer and differentiated into myotubes in accordance to the original cell and ECM alignment rather than to the longitudinal direction of the cylinder as would be more typical of regenerating or developing muscle. These results highlight the importance of tissue and ECM structure on the function of myoblast differentiation and fusion to provide insights into satellite and stem cell biology towards development of novel and more effective engineered tissues and therapeutics.

3.3 Materials and Methods

3.3.1 Fabrication of a poly(urethane acrylate)-poly(glycidyl methacrylate) (PUA-PGMA) thermoresponsive nanofabricated substratum (TNFS)

PUA-GMA TNFS were fabricated as previously described [112]. Briefly, a UV-curable PUA mold was fabricated and used as the nanopatterned template for the PUA-PGMA substratum. Glass coverslips were primed with an adhesion promotor and allowed to dry. A previously mixed and degassed 1% PUA-GMA (w/v) prepolymer was aliquoted onto a PUA template consisting of 800 nm ridge and groove width and 500 nm deep parallel grooves and ridges; a dried coverslip was then placed primed-side down onto the prepolymer. The template-prepolymer-glass was cured under 365 nm UV light to initiate photopolymerization for 5 min. After polymerization, the

PUA template was peeled off from the PUA-PGMA substratum using forceps and the substratum was UV-cured overnight to finalize polymerization. To functionalize the surface of the nanofabricated substrate with a thermoresponsive polymer, amine-terminated poly(N-isopropylacrylamide) (PNIPAM) solution (1g/mL) was reacted with the PUA-PGMA substratum in a shaker at room temperature for 24 h at 55 rpm to allow for thermoresponsive functionalization. The TNFS was then washed with DI water to remove excess PNIPAM and sterilized with 294 nm UV light for 1 hour prior to use.

3.3.2 Cell culture and seeding on the TNFS

C2C12 mouse myoblasts were cultured in Dulbecco's minimal essential media (DMEM, Gibco) supplemented with 10% fetal bovine serum (FBS, Sigma) and 1% penicillin-streptomycin (Sigma) in an incubator at 37℃, 5% CO2. Cells were split at 80% confluency to prevent spontaneous differentiation and used within 7 passages of a thaw. To seed cells onto the TNFS, cells were split and seeded at a density of $1x10^6$ cells/cm^2 to form a confluent monolayer within 48 hours of culture for subsequent transfer. Cells were imaged with a bright-field microscope (Nikon TS100) during culture. Cell sheets were allowed to reach 100% confluency (2 to 3 days in culture after seeding) before transfer onto treated glass or stacked on top of another cell sheet using our gel casting method. Once transferred, the single or bilayer tissues were cultured either in growth media (10% FBS) to maintain quiescence or differentiation media (2% horse serum, HS) to induce myotube fusion for up to 7 days after transfer. Tissues were subsequently fixed at 24 hours and 7 days after transfer.

3.3.3 Gel casting transfer and stacking of nanopatterned cell sheets

To transfer individual cell sheets or to engineer bilayer tissues, the gel casting method was used as previously described. Briefly, the cells on the TNFS are rinsed and incubated with room temperature DPBS for 25 minutes to promote sheet detachment, at which point the DPBS is removed and melted (37C) 7.5% wt/v gelatin is added to the culture dish and incubated at 4C for 10 minutes to allow for the gelatin to solidify. The solidified gelatin can then be transferred with the adhered cell sheet to a new surface or transferred to another cell sheet cultured on a TNFS for multilayered stacked tissues. An orientation key is used to allow for orthogonal or aligned tissue stacking. The single and bilayer sheets are then transferred to a glass coverslip for subsequent culture. Using the gel casting method, complex tissue and ECM microenvironments can be engineered for studies on myoblast function (Fig. 12).

3.3.4 Engineering nanopatterned myoblast sheet-wrapped gelatin cylinders

To engineer tissue surrogates for subsequent analysis of myotube formation of transferred nanopatterned cell sheets in a 3D environment, first the TNFS was adapted to a surface treated, flexible, polyethylene terephthalate film (SKC films) instead of a treated glass coverslip. The cells were seeded on the flexible TNFS (fTNFS) as described previously. For transfer onto a gelatin cylinder, the fTNFS and attached cell sheet was first incubated with room temperature DPBS for 30 minutes to initiate sheet detachment, then rolled into a tube structure and placed into a plastic cylindrical mold (Ø: 3mm). 7.5% wt/v gelatin in DMEM with 4% v/v transglutaminase (used to crosslink and thermally stabilize the gelatin) was melted and then added to the mold, and the mold, fTNFS and gelatin was incubated at 4C for 10 minutes and then room temperature for 30 minutes, at which point the plastic mold and fTNFS were removed, with the nanopatterned cell sheets attached to the outside of the gelatin cylinder. A schematic of the engineering process is

shown in Figure 12. Cells and cylinder were then cultured as normal for up to 7 days in either growth media or differentiation media, then fixed, stained, and sectioned for imaging.

3.3.5 Immunofluorescent and CellTracker staining and imaging

Cells were washed with phosphate buffered saline (PBS, Sigma) and fixed in 4% paraformaldehyde (Sigma) for 15 min at room temperature (22℃). Fixed cells were then washed with DPBS, permeabilized and blocked with a solution of 5% bovine serum albumin (Sigma) and 0.25% Triton X-100 (Sigma) in PBS for 1 h at room temperature, then washed with PBS. For fibronectin (produced in rabbit, Abcam) and myosin heavy chain staining (produced in mouse, Abcam), cells were incubated with the respective primary antibody at a dilution of 1:1000 (fibronectin) or 1:500 (MHC) in 1% BSA in PBS over night at 4C. After primary incubation, cells and sheets were subsequently washed with DPBS and incubated with the respective fluorescently labeled secondary antibodies for 1 hour at 37C. For F-actin staining, cells were incubated with AlexaFluor488-conjugated phalloidin (Invitrogen) during the secondary staining step. For CellTracker cell sheet labeling, cells were incubated with either CellTracker Red CMTPX dye (ThermoFisher) or CellTracker Green CMFDA dye (ThermoFisher) at 2μM concentration in serum free media prior to TNFS seeding.

3.3.6 Quantitative analysis of cytoskeletal alignment

To assess cytoskeletal alignment, immunofluorescent images were analyzed using an automated, modified pixel gradient-based MATLAB script as previously published. Briefly, images of phalloidin-stained cells were taken at three representative fields at 10x magnification and analyzed by being passed through a set of filters to calculate the gradient magnitude of each

image pixel and generate an orientation vector. This orientation gradient data is then used to generate a histogram plot of overall cell alignment.

3.3.7 Quantification of myotube alignment and morphology

Confocal microscope images were taken at 10x magnification at 3 randomly chosen locations per sample stained for MHC (n=3 per condition). The MHC channel was isolated from each image and subsequently analyzed using ImageJ. To quantify myotube morphology, a free-hand trace of myotubes with a positive MHC signal was drawn per each identifiable myotube. An ellipse was fit to the freehand trace to determine overall orientation angle and length, and the area of the trace was divided by the length of the major ellipse axis to determine average myotube width. At least 10 myotubes were traced per sample, yielding at least 30 myotube measurements per condition. Myotube lengths and widths were averaged and statistical significance was characterized using a 2-way ANOVA, with significance determined as a p-value < 0.05. Myotube orientations were binned into 10 degree increments, with each myotube having 1 orientation and counted. The orientations were then plotted as a histogram, with the major axis of alignment set to 0 degrees, and the y-axis as a percent of myotube population per bin.

3.4 Results

3.4.1 Seeded myoblasts sense nanotopography quickly and deposit aligned ECM shortly after attachment

We have previously shown that myoblasts grown on the TNFS align within 24 hours to form an anisotropic cell sheet, but the time course of morphological alignment as well as

deposition and structure of extracellular matrix has not been investigated. After initial seeding of cells on the TNFS, microscope images were taken and samples were fixed at 15 minutes, 1 hour, 4 hours and 24 hours to assess the speed at which myoblasts sensed the underlying substrate topography. We found that cells were able to attach to the TNFS within 15 minutes but remained spherical in shape, similar to a cell in suspension. However, the cells remained firmly attached even after washing prior to fixation and cell processes were apparent even in bright field microscopy. Within 1 hour, cells began to elongate along the direction of the topography, with a confluent, anisotropic sheet formed within 4 hours. By 24 hours, cells were tightly packed in a confluent monolayer and cell borders were not readily apparent.

Subsequent immunostaining and confocal microscopy imaging revealed that cell cytoskeletal filaments were primarily on the periphery of cells (15 min) and were predominately concentrated at the leading edges of the cells aligned to the topography (1 hour) (Fig. 13a). Clearly filamentous cytoskeletal structure was evident within 4 hours of seeding, well aligned to the nanotopographical cues, and continued to develop throughout culture. As we were interested as to the presence and structure of the ECM during anisotropic sheet formation of cells seeded on the TNFS, we also analyzed fibronectin through immunostaining and confocal imaging. Within 15 minutes, the presence of fibronectin was apparent within the body of the attached cells, but was not present on the remainder of the TNFS surface. As cell morphology started to elongate, ECM was still predominately within the cell body. After 4 hours of culture, ECM was deposited around the periphery of the cells and began to assume an aligned structure. Within 24 hours, the ECM deposited had a well-defined anisotropic, web-like structure characteristic of fibronectin and indicative of a cell-deposited basal lamina (Fig. 13a). Control sheets also had cell-deposited ECM, however these were predominately isotropic, web-like structures. These results demonstrate that cells rapidly attach to the TNFS, sense topographical cues and elongate, and then deposit ECM,

which subsequently is also aligned to the cells and nanotopographical cues. Quantification of the alignment of both cytoskeleton and fibronectin demonstrated a time-dependent increase in alignment (Fig. 13b).

3.4.2 Cell-deposited ECM is transferred along with the cell sheet, maintains structure long term, and direct myotube fusion alignment

To analyze the effects of the gel casting method and the TNFS on cell-deposited ECM, we transferred nanopatterned myoblasts sheets and analyzed cytoskeletal and ECM structure 24 hours after transfer and 7 days after transfer to a flat surface via immunofluorescent staining and imaging. We observed that both cytoskeletal structure as well as cell-deposited ECM structure are maintained when a nanopatterned cell sheet is transferred from the TNFS using the gel casting method (Fig. 14a). Further, when maintained in a growth state long-term, both cells and ECM structure maintained overall anisotropy, with cytoskeletal alignment actually increasing during a growth state, presumably as cells continue to divide and compact the transferred sheet further (Fig. 14b). Additionally, under differentiation conditions, nanopatterned myoblast sheets differentiated along the original tissue alignment (Fig. 14b). To determine the effects of cell and ECM structure on myotube fusion, we also differentiated nanopatterned cell sheets while on the TNFS (presence of nanotopography) as well as a transferred to a flat surface (no nanotopography). Myoblasts in both cell sheets fused along the direction of alignment to form myotubes aligned to either the nanotopography or overall sheet alignment, however myotubes still on the TNFS were better aligned than transferred cell sheets, presumably due to the presence of physical nanotopographical cues restricting transverse migration (Fig. 15). However, sheets of differentiated myotubes were unable to be transferred from the TNFS, indicating that myotube studies would have to be conducted on transferred nanopatterned cell sheets which are

subsequently differentiated. As myoblasts remodel their cytoskeleton and microenvironment both in growth and differentiation conditions, we quantified F-actin and fibronectin alignment of transferred nanopatterned sheets over time and by condition (Fig. 16a,b). Interestingly, for transferred and differentiated nanopatterned cell sheets, ECM alignment increased (Fig. 16d), as large areas of fibronectin were removed and the remaining areas remodeled to allow for myotube formation, however for growth conditions, cytoskeletal alignment increased (Fig. 16c) as the cells began to demonstrate more elongated morphologies (yet still stained negative for MY-32). This indicates that the transferred ECM structure alone is sufficient to dictate myotube formation in a specified direction without needing continued culture on a nanofabricated substrate, and further, that myoblasts actively remodel either their cytoskeleton or ECM depending on culture conditions.

3.4.3 Nanopatterned cell sheets can be stacked into multilayer tissues while retaining overall tissue and ECM structure

We previously demonstrated that nanopatterned cell sheets can be stacked into multilayered tissues while maintaining overall sheet alignment and stacked tissue architecture. Based on the results of single nanopatterned sheet transfers, we hypothesized that transferred, anisotropic ECM provides a sufficient alignment cue to allow for maintenance of cell morphology when cultured long term in a growth environment. To test this, we stacked nanopatterned cell sheets using our gel casting method in an orthogonal configuration and cultured the bilayer tissues in growth media for up to 7 days after transfer. Bilayer stacked tissues had a noticeable cross-hatching structure apparent in bright field microscopy images (Fig 17a,b) immediately after transfer, which was subsequently maintained throughout culture in growth media. Interestingly, myoblasts continued to grow out of the edge of the bilayer tissues aligned to the direction of the bottom sheet (Fig. 17b). Confocal microscopy images revealed that both layers maintained both

cytoskeletal as well as ECM anisotropy immediately after stacking (Fig. 18a) long term (Fig. 18b). These results demonstrate the utility of our developed TNFS for engineering tissue environments with complex tissue and ECM structures for the subsequent analysis of tissue structure-function relationships.

3.4.4 Tissue and ECM structure affects myotube formation and morphology

To assess the effects of tissue and ECM structure on myoblast function, nanopatterned myoblast sheets were stacked either orthogonally or parallel and subsequently differentiated, with the hypothesis that the individual sheet anisotropy would direct myotube fusion to form bilayered, myotube tissues with either orthogonal or parallel oriented myotubes in 2 separate layers. Interestingly, in both conditions, differentiation caused myoblast remodeling of the overall tissue structure, such that the ECM was remodeled significantly and cells migrated between sheets in order to form myotubes in a single layer. For bilayer, orthogonal myoblast sheets, bilayer tissues “flattened” into a monolayer with the differentiated myotubes aligned primarily in two directions, the original orthogonal alignments, with no dominant alignment direction (Fig. 19a). Additionally, the ECM of the bilayer, orthogonal tissue, lost anisotropy in either cell sheet direction. Conversely, parallel bilayer sheets “flattened” to form aligned myotubes in the original direction of the stacked sheets (Fig. 19b). Myotubes formed in parallel bilayer tissues also demonstrated significantly larger average morphologies as measured by average length and width than myotubes formed in orthogonal bilayer tissues, as well as more unified orientation in the original sheet direction (Fig. 19c). Myotubes in parallel conditions also formed denser myotube tissues, possibly because the cells were already aligned and in parallel, allowing for more efficient myotube fusion and organization. These results demonstrate that tissue and ECM structure can affect the formation and alignment of myotubes. Further, myoblasts within cell sheets actively remodel their

microenvironment during differentiation and can migrate between cell sheets in order to form myotubes. Finally, aligning myoblasts in a singular direction for differentiation facilitates the formation of larger myotubes.

3.4.5 Nanopatterned myoblast sheets can be transferred to 3D structures and differentiate into structured skeletal muscle tissues

To determine whether transferred nanopatterned myoblast sheets would retain original sheet and tissue alignment and could differentiate into aligned muscle tissue after transplantation onto a 3D surface, nanopatterned cell sheets were transferred onto a cross-linked gelatin cylinder and cultured for up to 7 days with the sheet alignment oriented circumferentially. Cells transferred using the fTNFS and gelatin cylinder retained their alignment immediately after transfer as confirmed via bright field microscopy. The gelatin cylinders noticeably compacted in the differentiation conditions compared to growth. Immunofluorescent staining of the cylinders in both conditions indicated that cytoskeletal alignment was maintained during culture. Further, in the differentiation condition, the nanopatterned cell sheet was able to form circumferentially oriented myotubes (Fig. 20b), indicating that the initial nanopatterned cell sheet alignment was the greatest determinant of myotube direction during fusion, even in a 3D cylinder environment (Fig. 20c). Quantification of cytoskeletal and ECM alignment matched that of transferred nanopatterned cell sheets to flat surfaces (Fig. 20d). Finally, using z-stack imaging and analysis, it was determined that the basal lamina deposited by the cells during culture remained on the outside of the cylinder (Fig. 20a), mimicking the endomysium or basal lamina sheath found in native muscle tissue. These results demonstrate the feasibility of transplanting aligned, myoblast patches onto tissues to generate myotubes and subsequent muscle tissue with a specific structure.

3.5 Discussion

We previously have demonstrated the feasibility of engineering multilayered tissues stacked in specific configurations which maintained alignment after stacking and subsequent culture. Other groups have used cell sheet engineering and microfabrication to engineer aligned cell sheets that have also been stacked into multilayered configurations, however these tissues subsequently reorganized into uniaxially aligned, multilayered tissues using similar cell types [80]. As maintained tissue structure is often advantageous for creating multilayered tissues with complex architectures, and allows for more robust structure-function analysis, we sought to understand the phenomenon of maintained tissue architecture using our TNFS system. We found that cells rapidly sensed the underlying nanotopographical cues, subsequently changed morphology, and then subsequently deposited ECM along the periphery of the cell, creating an anisotropic, confluent cell sheets within 24 hours of culture. The nanopatterned sheets could then be transferred and stacked as individual sheets or multilayered tissues with intact ECM structure which does not reorganize during growth conditions. We hypothesize that the use of nanotopographical cues allows for the rapid deposition of ECM to form a structurally organized basal lamina, which is then transferred as part of the nanopatterned cell sheet. This basal lamina thus prevents reorganization and migration of myoblasts during a growth state. However, under differentiation conditions, myoblasts actively migrate and remodel their microenvironment in order to fuse to form nascent myotubes, expressing matrix metalloproteinases both during *in vitro* studies of myoblast fusion as well as *in vivo* studies of muscle regeneration [114, 115]. In lines with these studies, we observed the remodeling of tissue ECM during the fusion process for both 2D and 3D tissues.

During in vivo regeneration of damaged muscle tissues, satellite cells migrate to the site of injury and differentiate to form multiple small myotubes within the basal lamina sheath of the original myofiber [116]. Many studies have focused on the chemotactic response of satellite cells and myoblasts to form myotubes, but few studies have examined the specific role of microenvironment structure on myoblast biology. As satellite cells have been well documented to mobilize from up or downstream of the site of injury [117], and as the muscle basal lamina survives various types of tissue injury and is believed to play a critical role on regeneration [118], our studies indicate the structure of the basal lamina can be an important determinant of myotube alignment during differentiation in the absence of chemotactic signals. Further, other studies have shown the importance of F-actin remodeling and structure for myoblast fusion [116]. The alignment of 2 layers of myoblasts could thus make it easier for myoblasts to form larger and more numerous myotubes due to the structural organization of the cells and cytoskeleton versus the orthogonally-layered constructs. Finally, during muscle injury and regeneration, myotubes form within the basal lamina in the original orientation to fuse and regenerate the injured myofiber. It has been hypothesized that the lamina structure may allow for orientation of myoblast fusion, however a number of different cues are present, such as longitudinal stress and strains and mechanical forces. Although only in a muscle tissue surrogate, the transfer of nanopatterned cell sheets with the cells directly contacting the transfer surface (as opposed to transferred with the lamina contacting the surface) allows for the engineering of a pseudo-lamina, which maintains orientation and directs myotube fusion in 3D. These studies could thus inform future strategies for engineered skeletal muscle tissues for repair. Specifically, the use of structurally organized, 3D myoblast tissues could be used as a promising patch or tube, which could be transplanted on the site of injured tissues and maintain structure.

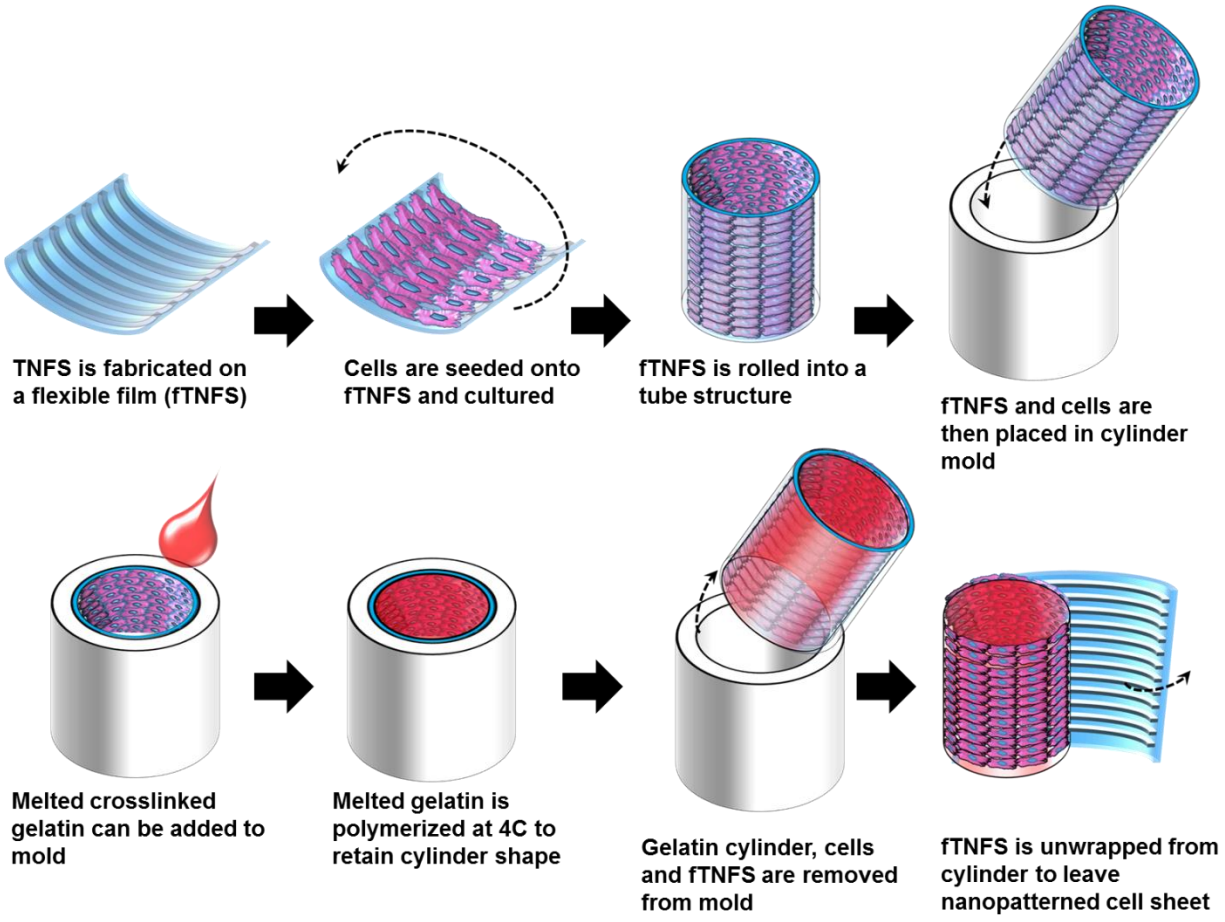

Figure 12. The use of a flexible TNFS to engineer nanopatterned cell sheet-wrapped hydrogel cylinders for 3D tissue engineering. Schematic showing the use of a flexible TNFS which can be rolled to form 3D shapes and subsequently casted to engineer 3D tissues while utilizing cell sheet engineering.

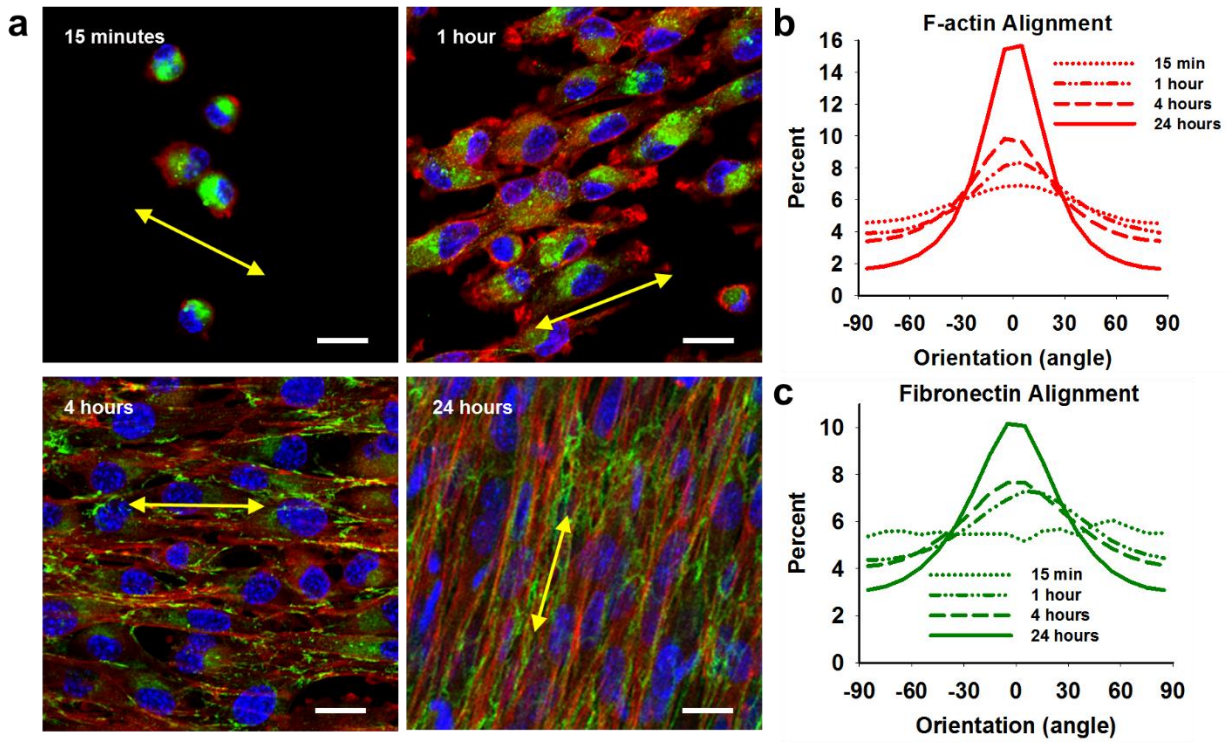

Figure 13.Time course analysis of myoblast attachment and subsequent morphological and cell-deposited extracellular matrix alignment. (a) Confocal microscope image of phalloidin (red), fibronectin (green), and Hoecsht (blue) staining showing TNFS-seeded C2C12 myoblasts at various times after seeding, demonstrating the rapid detection and subsequent alignment due to nanotopographical cues. Scale bar, 20μm. Quantitative analysis of cytoskeletal alignment (b) and cell-deposited extracellular matrix alignment (c) over time of seeded cells. Yellow double-sided arrows indicate substrate nanopattern direction.

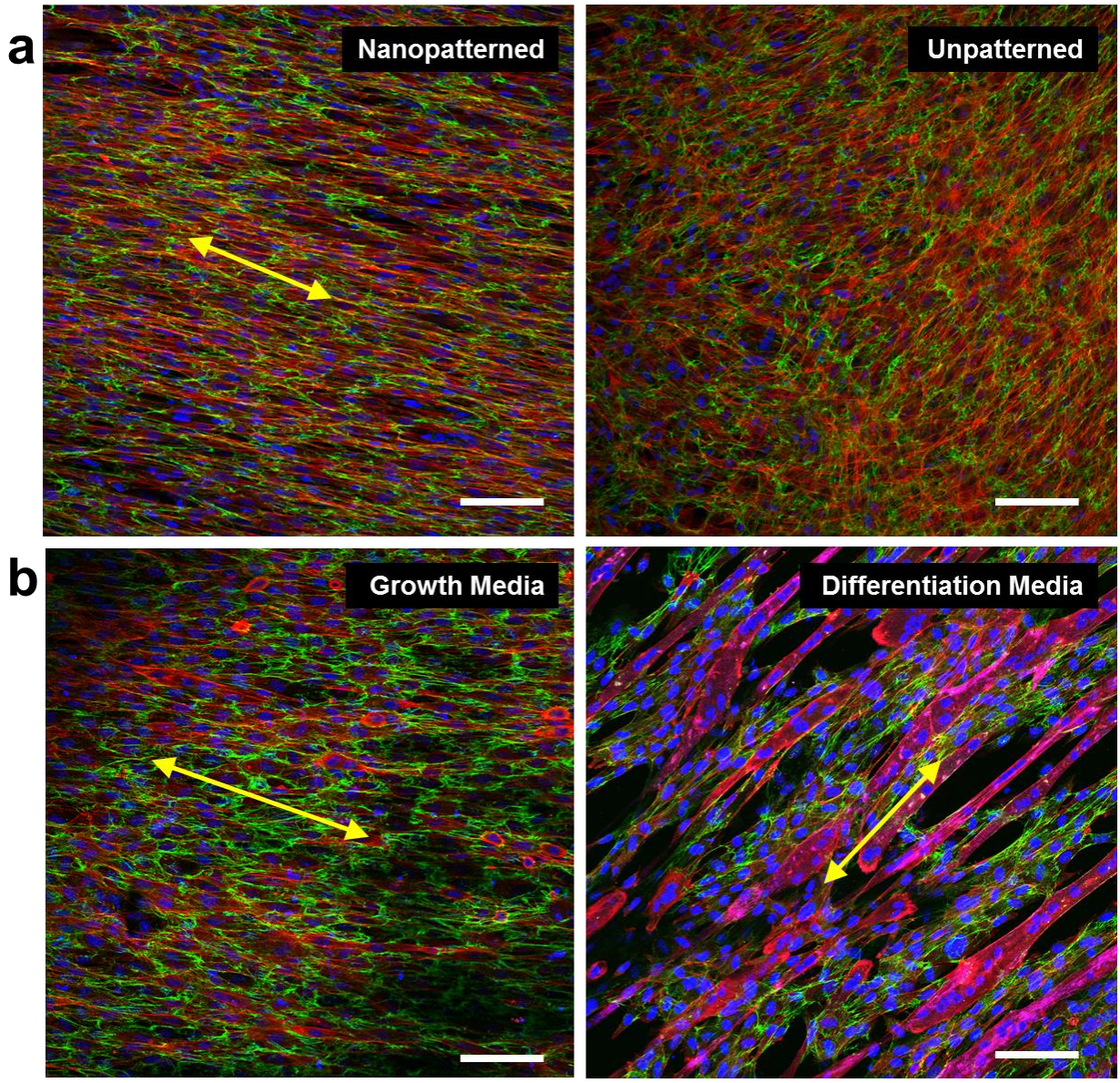

Figure 14. Nanopatterned myoblast sheets are transferred with retained cytoskeletal and extracellular matrix structure, can maintain structure long-term, and can differentiate along initial alignment. (a) Confocal microscope image of phalloidin (red), fibronectin (green), and Hoecsht (blue) staining showing a gel-casted, transferred nanopatterned myoblast sheet and unpatterned control 24 hours after transfer onto a flat glass surface. Scale bar, 100µm. (b) Confocal microscope image of phalloidin (red), fibronectin (green), MY-32 (magenta) and Hoecsht (blue) staining showing transferred nanopatterned myoblast sheets after 7 days of culture in growth and differentiation conditions maintaining original alignment even during myotube fusion. Scale bar, 100µm. Yellow double-sided arrows indicate initial substrate nanopattern direction.

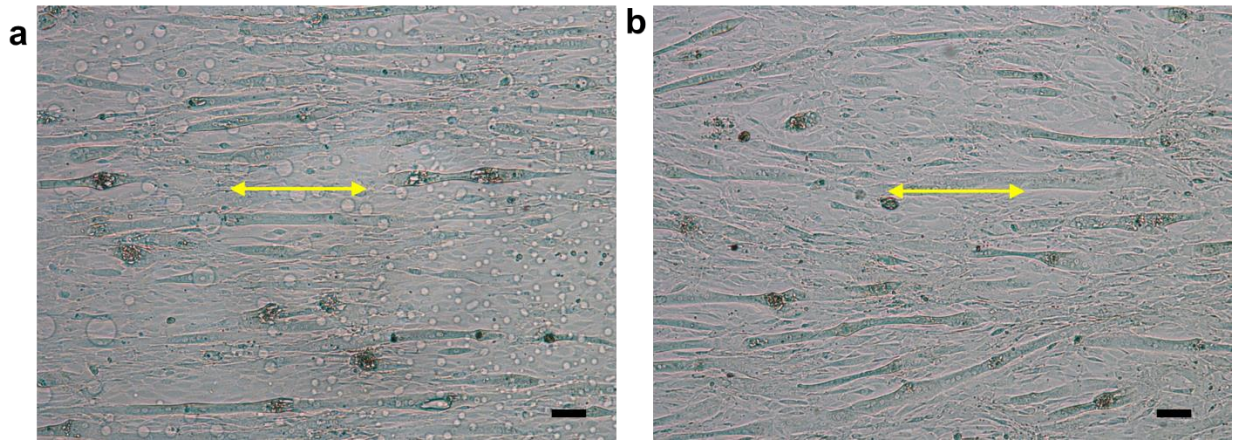

Figure 15. Persistent topographical cues are not necessary to induce aligned, myotube tissue formation of myoblasts. Bright field microscope images of myoblast monolayers differentiated for 7 days while on TNFS (a) or transferred to a flat glass surface (b) demonstrating the formation of aligned myotubes. Scale bar, 100µm. Yellow double-sided arrows indicate initial substrate nanopattern direction.

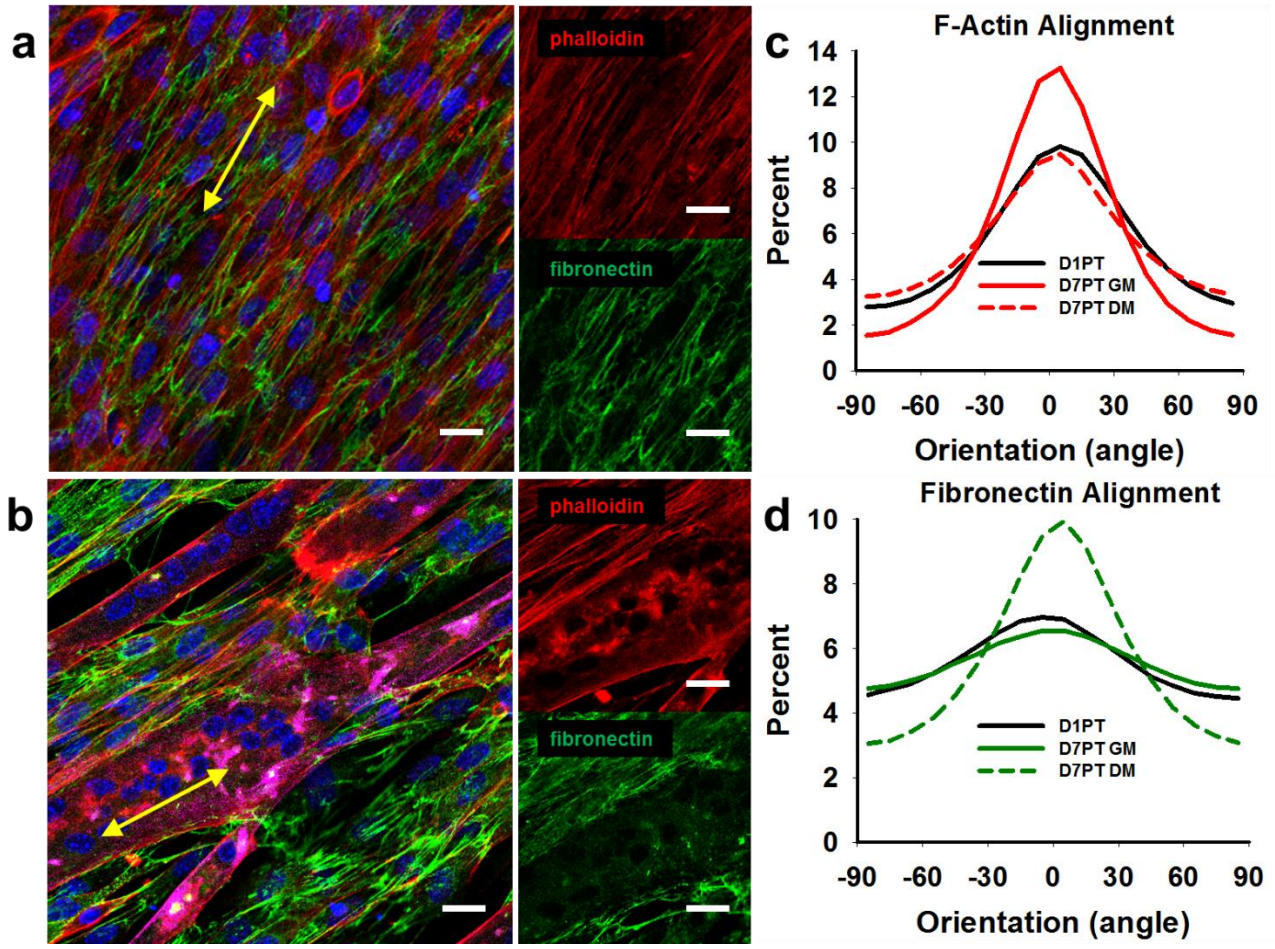

Figure 16. Transferred nanopatterned myoblast sheets remodel cytoskeletal and extracellular matrix structure depending on culture condition. Confocal microscope image of phalloidin (red), fibronectin (green), MY-32 (magenta) and Hoecsht (blue) staining structural organization of transferred myoblasts under growth conditions (a) and differentiation conditions (b). Sheets cultured under growth conditions did not stain positive for myotubes. Scale bar, 20μm. Quantitative analysis of cytoskeletal alignment c) and cell-deposited extracellular matrix alignment (d) under different culture conditions of transferred, nanopatterned myoblast sheets. Yellow double-sided arrows indicate initial substrate nanopattern direction.

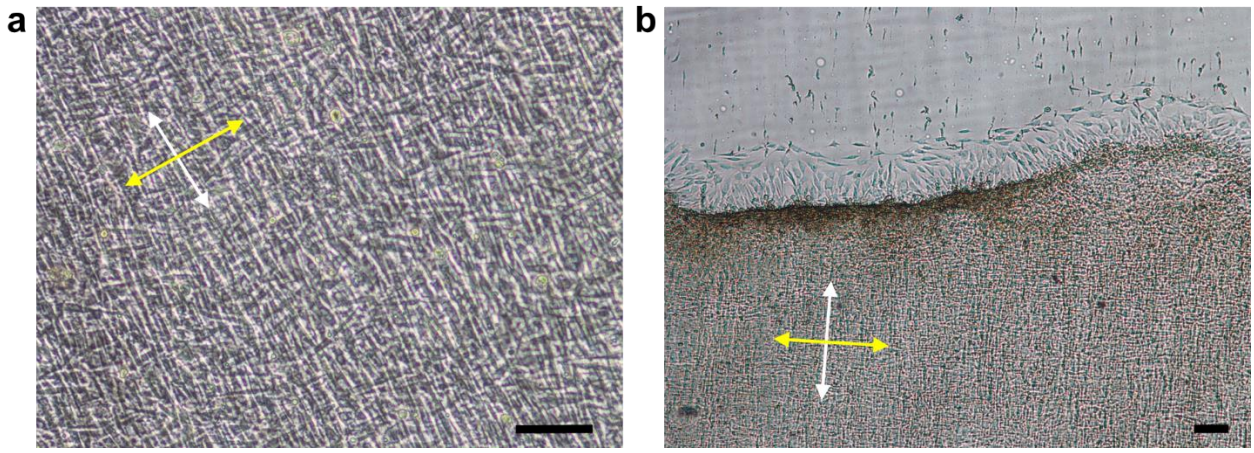

Figure 17. Stacked myoblast bilayers maintain structural alignment and can affect subsequent morphology of proliferating cells. (a) Bright field microscope images of an orthogonally stacked myoblast bilayer maintained in growth media for 24 hours after transfer showing cross-hatching pattern. Scale bar, 100µm. (b) Bright field microscope image of the edge of an orthogonally stacked myoblast bilayer showing continued cell proliferation in the orientation of the bottom sheet 24 hours after transfer in growth media. Scale bar, 100µm. Yellow double-sided arrows indicate initial substrate nanopattern direction of top sheet, white double-sided arrows indicate initial substrate nanopattern direction of bottom sheet.

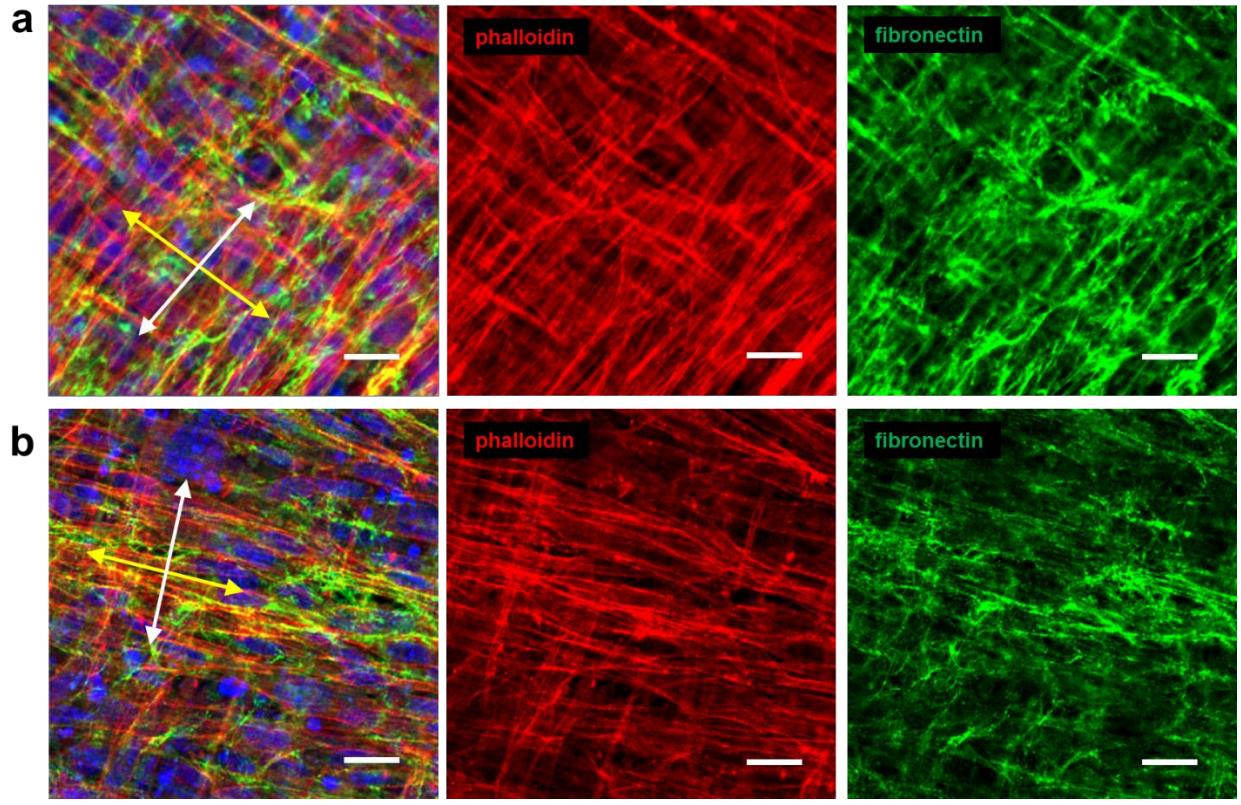

Figure 18. Stacked myoblast bilayers maintain cytoskeletal and extracellular matrix structure long term under growth conditions. Confocal microscope image of phalloidin (red), fibronectin (green), MY-32 (magenta) and Hoecsht (blue) staining structural organization of transferred myoblasts under growth conditions 24 hours (a) and 7 days (b) after transfer. Neither condition stained positive for myotubes. Scale bar, 20μm. Yellow double-sided arrows indicate initial substrate nanopattern direction of top sheet, white double-sided arrows indicate initial substrate nanopattern direction of bottom sheet.

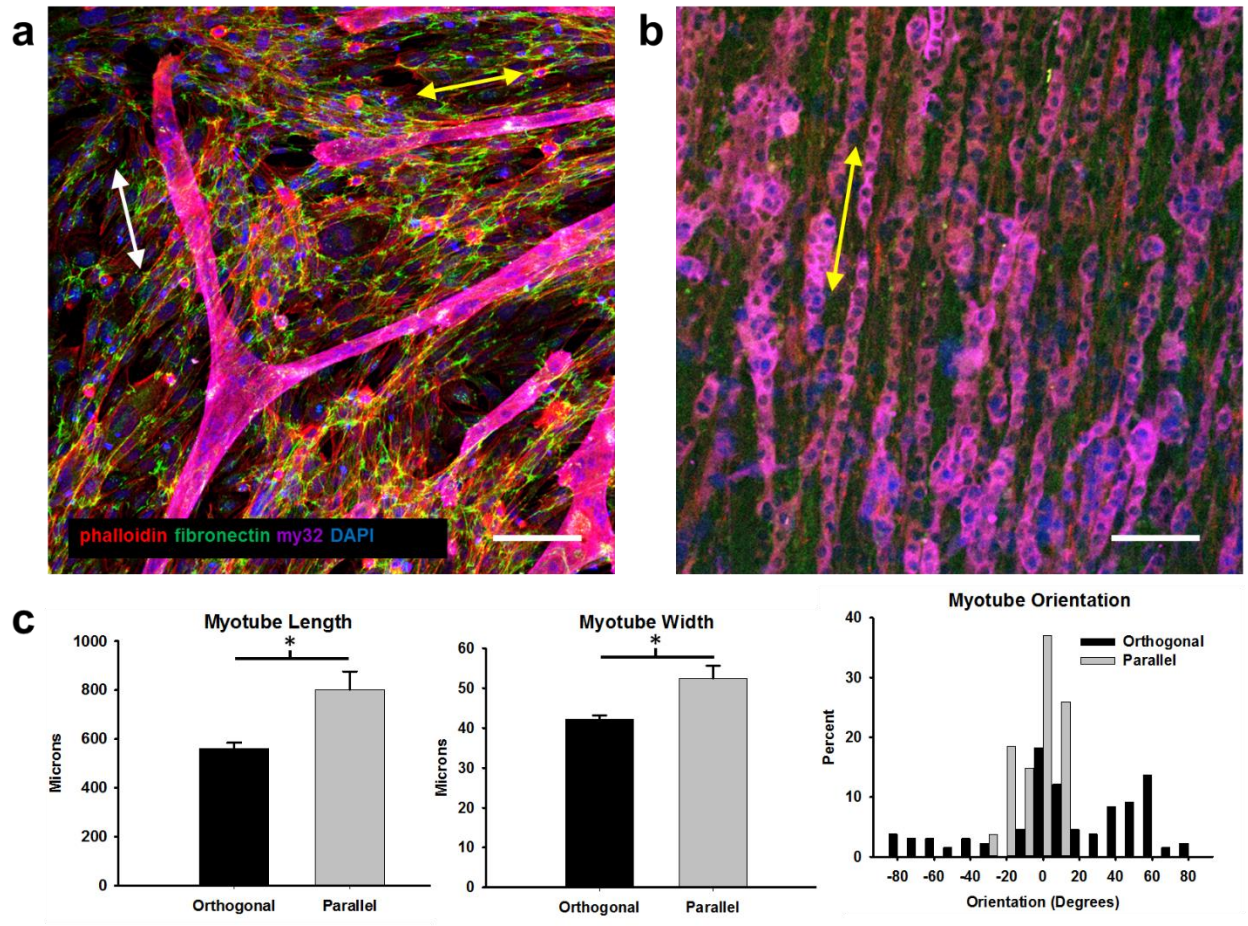

Figure 19. Structure of myoblast bilayers dictates subsequent myotube alignment and structure. Confocal microscope image of phalloidin (red), fibronectin (green), MY-32 (magenta) and Hoecsht (blue) staining structural organization of transferred orthogonal (a) and parallel (b) myoblast bilayers under differentiation conditions for 7 days. Both conditions formed myotubes after differentiation. Scale bar, 100µm. (c) Quantification of myotube morphology and orientation from orthogonal and parallel differentiated bilayers. Error bars are SEM. Asterisks indicate p value < 0.05. Yellow double-sided arrows indicate initial substrate nanopattern direction of top sheet, white double-sided arrows indicate initial substrate nanopattern direction of bottom sheet.

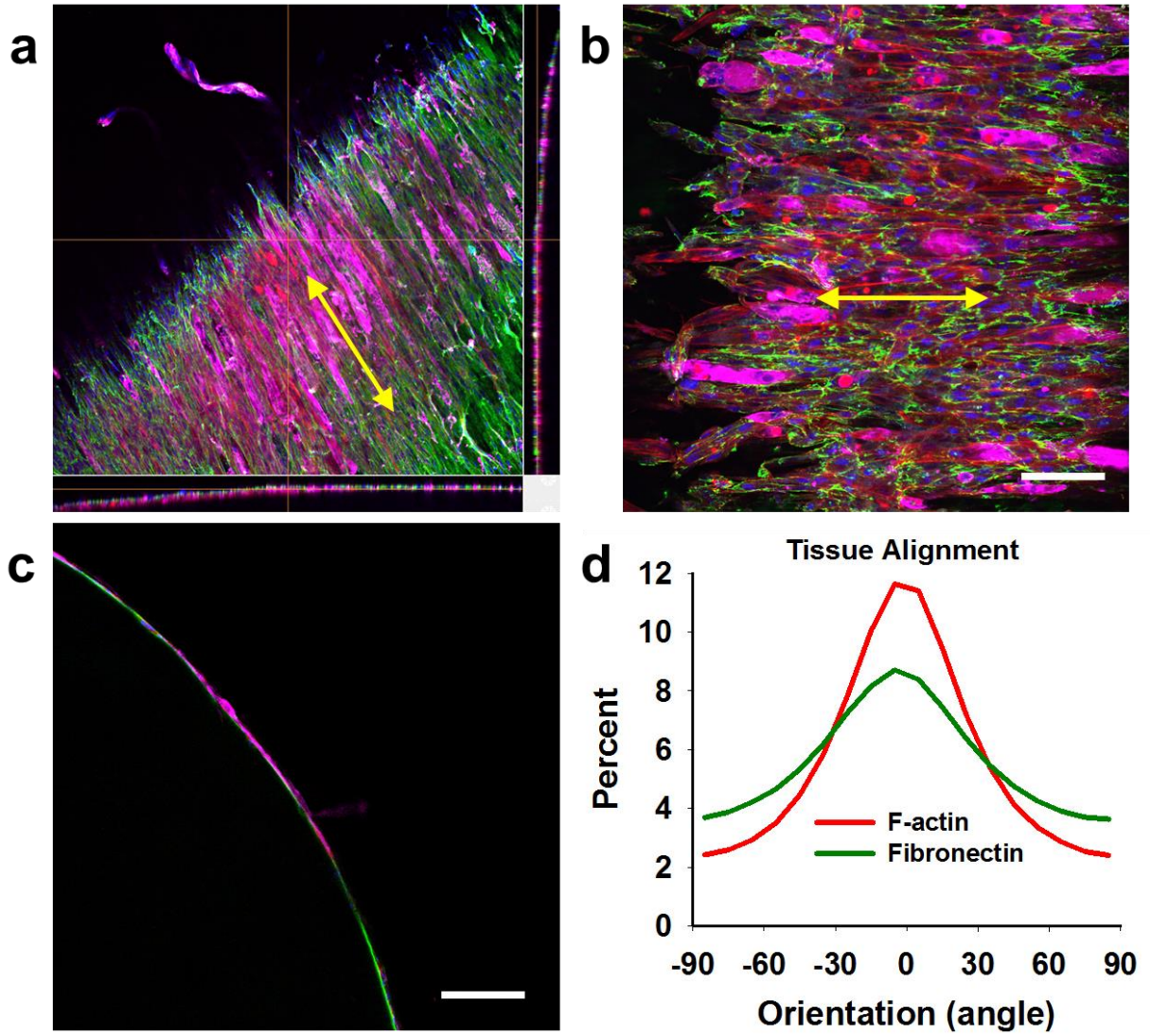

Figure 20. Nanopatterned myoblast sheets can be transferred onto 3D hydrogel structures and subsequently differentiated while maintaining original tissue structure. Z-stack slices view of confocal microscope images of phalloidin (red), fibronectin (green), MY-32 (magenta) and Hoecsht (blue) stained nanopatterned myoblast sheets casted around a gelatin cylinder. Transferred ECM (green) is on the outside edge, similar to the basal lamina sheath of myofibers. (b) Confocal image showing maintained cytoskeletal and myotube alignment. Scale bar, 100μm (c) Transverse section of cylinder-tissue construct showing curvature of cylinder and presence of myotubes. Scale bar, 200μm. (d) Quantitative analysis of cytoskeletal and cell-deposited extracellular matrix alignment of differentiated skeletal muscle tissue constructs. Yellow double-sided arrows indicate initial substrate nanopattern direction.

CHAPTER 4. Multiscale Engineering of Physiologically structured, Stem Cell-Derived, 3D Cardiac Tissues

4.1 Abstract

The heart has a complex, 3D structure comprised of sheets of aligned, elongated cardiomyocytes which form a transmural helical structure, crucial to appropriate function. However, current tissue engineering strategies are unable to precisely control 3D tissue architecture in cell-dense tissues *in vitro*. In this work, we engineered novel 3D cardiac tissue which can recapitulate the anisotropic, helical heart structure by utilizing nanofabrication-based cell sheet engineering and human induced pluripotent stem cell-derived cardiomyocytes (hiPS-CMs). We utilized a combination of our previously developed thermoresponsive, nanofabricated substratum (TNFS), endocardial-like endothelial cell coculture, and gel casting method to fabricate 3D, scaffold-free tissues with layer-by-layer structural control. We found that a high purity cardiomyocyte population combined with an ECM producing, cardiac-specific stromal cell coculture was able to yield aligned, synchronous cardiac monolayers which could be detached and transferred without loss of structure. Further, these nanopatterned cardiac sheets could be stacked into multilayered cardiac tissues in an aligned or helical fashion to mimic the physiological structure of the myocardium. Finally, the structure of the engineered, 3D multilayered cardiac tissues affected contractile function, with aligned cardiac constructs demonstrating improved contraction magnitude and velocity but with helical cardiac constructs generating a contractile torque, indicating a direct structure-function relationship of our engineered cardiac tissues.

4.2 Introduction

The human heart has a complex 3D structure consisting of layered anisotropic myofiber sheets [19, 20]. The myofiber sheets are comprised of elongated, parallel cardiomyocytes, which are well aligned to the underlying extracellular matrix (ECM) fibers [56]. In 3D, the orientation of these sheets in the ventricle changes gradually from a right-handed helix in the subendocardium to a left-handed helix in the subepicardium [21-23]. This change in myofiber sheet orientation leads to a transmural helical structure in 3D [23]. Studies have found that the complex, helical heart structure is critical to many aspects of adult heart function. Electrically, the depolarizing action potential is anisotropic, with the current guided by the fiber orientation in the heart [24-26]. Mechanically, the fiber orientation is an important determinant of the myocardial stress and strain [27, 28] and additionally affects the perfusion and oxygen consumption of the heart [29]. Finally, the helical fiber orientation allows for the unique twisting contractile motion of the heart [30-32]. This wringing motion is critical for appropriate blood clearance and cardiac output [33, 34]. Additionally, altered cardiac tissue structure is often an indication of disease and can also contribute to deteriorating cardiac function in diseases such as hypertrophic cardiomyopathy and dilated cardiomyopathy, amongst others [35-37].

Induced pluripotent stem cell (iPSC) technology allows for the reprogramming of adult cells into pluripotent stem cells, which can then be differentiated into cardiomyocytes and other cardiac-specific cells. These cells can subsequently be used to engineer cardiac tissues for therapeutic, diagnostic or screening purposes, showing great promise in advancing medical treatments for cardiovascular diseases. However, current attempts to engineer cardiac tissue often fall well short of recapitulating this complex cardiac architecture and are often restricted to unidirectional [11-13] or randomly organized 3D tissues [14, 15]. Newer attempts to utilize decellularized whole hearts as a scaffold for seeded cardiomyocytes in a top-down approach show promise but still ultimately lack well-defined cardiac tissue structure and cell density [57,

119]. This lack of physiologically structured, cell-dense cardiac tissues prevents optimal function due to the closely related structure-function relationship of the heart. This, in turn, limits the therapeutic and diagnostic efficacy of current engineered cardiac tissues. Alternatively, several groups have utilized a bottom-up approach to engineer cardiac tissues by manipulating surface cues, such as topography or patterned ECM proteins, to allow for the alignment of cardiomyocytes and cardiac monolayers [17, 52, 120]. The advantage of a bottom-up approach allows for finer control of cell morphology and the ability to form well-aligned, cell-dense monolayers which more closely mimic the native myofiber sheets. However, one major limitation using these surface cues to engineer structured tissues is the inability to generate thick, anisotropic cell dense tissues characteristic of the myocardium.

Inspired by the underlying extracellular matrix of the myocardium, we have developed nanofabricated substrates which allow for the robust and scalable alignment of single cardiomyocytes to anisotropic cardiac monolayers [56, 121]. We hypothesized that the successive stacking of these anisotropic cardiac sheets can yield aligned functional units of myocardium, similar to the 4 myocyte thick aligned myofiber sheets native to the heart, or even helically arranged multilayered cardiac tissues [27, 122-124]. Such an approach should yield 3D, cell-dense cardiac tissues which can be engineered for a variety of purposes, such as aligned tissues which demonstrate improved contractile function due to the alignment of force vectors or helical tissues that more physiologically represent the transmural structure of the myocardium. To this end, we have functionalized our nanofabricated substrates with a thermoresponsive polymer release layer, which would allow for the detachment of intact cell sheets by a reduction in culture temperature. However, cell sheets released by this method require cell-deposited extracellular matrix proteins to allow for the sheet to remain intact upon detachment. We additionally incorporated a stromal cell population of cardiac-specific endothelial cells to allow for the

deposition of ECM to detach intact, anisotropic cardiac cell sheets. Anisotropic cardiac cell sheets engineered using our TNFS are able to be transferred as viable individual monolayers or stacked together as 4-layered tissues. The stacked tissues can be engineered to be unidirectional or even helical in structure, which in turn affects contractile parameters such as contraction and relaxation velocity. These results demonstrate, for the first time, engineering of cell-dense cardiac tissues with precisely controllable structures, allowing for specific, reproducible and controllable investigations of the cardiac structure-function relationship.

4.3 Materials and Methods

4.3.1 Thermoresponsive nanofabricated substratum (TNFS) fabrication

The thermoresponsive nanofabricated substrate was fabricated as previously described [112]. Briefly, a polyurethane acrylate (PUA, Norland Optical Adhesive) and epoxy-containing glycidyl methacrylate (GMA, Sigma-Aldrich) solution was mixed together and utilized in capillary force lithography to fabricate nanotopographical substrata as previously published [19]. Once polymerized, the substrate was incubated with an amine-terminated PNIPAM solution (Mn: 2500, Sigma-Aldrich) in DI H2O and allowed to react for 24 h on a rocker at room temperature. The GMA percentage was varied (0.5%, 1%, 5%, 10%, 15%, 25% v/v) to change the PNIPAM grafting density.

4.3.2. Derivation and differentiation of human induced pluripotent stem cells (hiPSCs) into cardiomyocytes and endothelial cells

Human urine-derived iPS cells were obtained from the lab of Dr. Martin Childers at the University of Washington [125]. A modified monolayer-based directed differentiation method was used as previously published for cardiomyocytes [7]. Briefly, the day prior to induction, undifferentiated hiPSCs were treated with mTeSR 1 media (Stem Cell Technologies) supplemented with CHIR-99021 (Selleck). On the day of induction, undifferentiated hiPSCs were treated with RPMI-1640 media supplemented with B-27 without insulin and activin A (R&D Systems) and matrigel (BD Biosciences). 18 hours post-induction, the media was exchanged for media supplemented with BMP4 (R&D Systems) and CHIR-99021. Cells were then fed on day 3 with cytokine-free RPMI-1640 media supplemented with B-27 without insulin (ThermoFisher) and XAV-939 (Tocris Bioscience), on day 5 with cytokine-free RPMI-1640 media supplemented with B-27 without insulin, and then finally on day 7 and every other day thereafter using RPMI-1640 media supplemented with B-27 with insulin. Beating cells were first seen at ~7 days post-induction, cultured for 7 more days, and then were subsequently split and seeded at a lower density (100k cells/cm^2) into a new culture dish for cardiomyocyte purification using metabolic selection as previously published [126]. Cardiomyocytes used for subsequent experiments were 90% cTnT+ or higher and used between 28 to 35 days post-induction. For differentiation into endothelial cells, a similar monolayer-based directed differentiation method was used as previously published [127]. Briefly, after cytokine treatment, media was switched to StemPro media supplemented with ascorbic acid, BMP4, bFGF and VEGF for 3 days. Cells were split at day 5 post-induction and then fed with endothelial-specific media, EGM supplemented with CHIR-99021, bFGF and VEGF, to induce an endothelial phenotype. ECs were analyzed at 5 days post-induction to determine CD31+ purity via FACS and used at 14 days-post induction and were 85% CD31+ or higher and were maintained in endothelial-specific media.

4.3.3 Culture of cardiac and stromal cells on the TNFS for cardiac cell sheet engineering

Human bone marrow-derived stromal cells hs27a and hs5 were derived by and obtained from Dr. Beverly Torok-Storb at the Fred Hutchinson Cancer Research Center. They were thawed and maintained in DMEM (Lonza) supplemented with 10% fetal bovine serum (Lonza) and 1% penicillin/streptomycin (Sigma). Human dermal fibroblasts (hDFs) were acquired via a skin punch biopsy from the forearm of a healthy 52-year old male. Endocardial-like endothelial cells (ECs) were differentiated and maintained as described above. For cardiac cell sheet seeding, hiPSC-derived cardiomyocytes and stromal cells were split from their culture plates using 0.25% trypsin/EDTA (Lonza) and resuspended and mixed at stromal cell concentrations of 10%, 20% and 30% and seeded onto fibronectin-coated (5µg/cm2) TNFS at a seeding density of 175,000 cells/cm^2. Cells were cultured using a 1:1 mix of RPMI-1640 media with B-27 supplementation (Lonza) and EGM (Lonza) and cultured for 7 days after seeding. For fluorescent labeling of specific cell sheets, cells were suspended for 30 minutes in serum-free media supplemented with 2uM CellTracker Green or Red (ThermoFisher) prior to seeding.

4.3.4 Transfer and stacking of nanopatterned cardiac cell sheets using the gel-casting method

Cell sheets contract upon detachment from the TNFS surface and require a method to transfer sheets without loss of cell morphology. We utilized the gel-casting method as previously described [112] to transfer and stack nanopatterned cardiac cell sheets. Briefly, cell-seeded TNFS were incubated with room-temperature DPBS for 30 minutes to initiate cardiac cell sheet detachment. Prior to full sheet detachment, the DPBS was aspirated and melted 37ºC 7.5% w/v gelatin (Sigma-Aldrich) in media was added to the TNFS and then casted at 4ºC for 15 minutes to firm the gelatin and prevent full sheet detachment and subsequent compaction. The TNFS was

then incubated at 28ºC for 1 hour to allow for full cardiac cell sheet detachment. The gel-casted nanopatterned cardiac cell sheet could then be transferred to a new surface, such as a plasma-treated (100W, 5 minutes), matrigel-coated glass coverslip, or onto another cell-seeded TNFS and incubated for 2 hours at 28ºC to stack multilayered cardiac tissues. The stacking process was repeated up to 4 times to generate 4-layer thick nanopatterned cardiac sheets, which were then transferred to plasma-treated, matrigel-coated glass coverslips for subsequent culture. 4-layered cardiac tissues were either structured to have uniaxial alignment (aligned), 20º separation between individual cardiac sheets (helical), or were unpatterned controls. A schematic of the gel-casting method and stacking process is shown in Figure 21.

4.3.5 Immunostaining, imaging and image analysis of cardiac cell sheets

Cells were washed with PBS (Sigma) and fixed in 4% paraformaldehyde (Sigma) for 15 min at room temperature (22°C). Fixed cells were then washed with PBS and permeabilized and blocked with a solution of 5% bovine serum albumin (BSA, Sigma) and 0.25% Triton X-100 (Sigma) in PBS for 1 h at room temperature, then washed with PBS. Multilayered sheets were permeabilized and blocked for up to 4 hours. Cells and cell sheets were then incubated with primary antibodies to α-sarcomeric actinin (1:200, Abcam), fibronectin (1:1000, Abcam), or CD31 (1:20, Abcam) in 1% BSA in PBS overnight at 4C. For secondary antibody labeling, AlexaFluor488-conjugated phalloidin (1:200, Invitrogen) and the appropriate AlexFluor-conjugated secondary antibodies (Invitrogen) in a 1% BSA in PBS solution were added to the cells and cells sheets for 1 hour at 37 °C. All samples were then stained with a Hoechst stain (Sigma) at a dilution of 1:1000, washed with PBS once, then treated with Vectashield (Vector Laboratories), mounted on coverslips, and imaged using a confocal microscope. Imaging studies were supported by the Mike and Lynn Garvey Cell Imaging Lab at the Institute for Stem Cell and

Regenerative Medicine at the University of Washington. Images were collected on a Nikon A1 Confocal System attached to a Nikon Ti-E inverted microscope platform. To quantitatively assess cytoskeletal alignment, confocal microscopy images of phalloidin or CellTracker-stained cells were taken at three representative fields at 60× magnification and analyzed using a modified, MATLAB script utilizing pixel gradient analysis as previously published [112, 128].

4.3.6 Correlation-based Contraction Quantification (CCQ) analysis of cardiac cell sheet contractile function

In order to assess contractile function, videos of paced, contracting cell sheets were used. To acquire the videos, media was replaced with warmed Tyrode's solution and the cardiac sheets were field stimulated using the MyoPacer Field Stimulator (Ionoptix) at 1HZ, 10V, square waves with a 5ms duration. Videos of at least 4-5 contractions and 3-5 fields of view per sample were then analyzed. For the analysis, our CCQ method was used as previously published to quantify contractile function of cardiac cell sheets [129]. Briefly, a reference video frame is divided into a grid of windows of a set size. Each window is run through a correlation scheme with a second frame, providing the new location for that window in the second frame. This displacement is converted into a vector map, which provides contraction angles and, when spatially averaged, contraction magnitudes and velocities. The co-relation equation used provides a Gaussian correlation peak with a probabilistic nature that provides sub-pixel accuracy. The videos used to perform this analysis were taken with a (core camera info) at 60FPS.

4.3.7 Statistical analysis

Statistical significance between unpatterned control cardiac cell sheets and nanopatterned cardiac cell sheets was determined using Two-Way ANOVA with Tukey's pairwise

post-hoc analysis using SigmaPlot software unless otherwise stated. For the contraction angle analysis, a Chi square test run at 5% significance was utilized to quantify uniformity in alignment distributions. This test was calculated using MATLAB. For all statistical analyzes, a p-value less than 0.05 was considered significant. Error bars are standard error mean (SEM).

4.4 Results

4.4.1 Formation of anisotropic cardiac cell sheets on the TNFS requires consistent input cardiomyocytes and specific surface chemistry

To engineer 3D, anisotropic cardiac tissues, we first started by using bioinspired nanotopographical cues mimicking the aligned, native cardiac ECM fibers found in the myocardium (Fig. 21a). Although differentiation of hiPSCs into cardiomyocytes can yield highly pure cardiomyocyte populations, there are often variabilities between differentiation runs as well as a small percentage of non-cardiomyocytes which can increase variability of subsequent experiments. In order to ensure consistent formation of cardiac cell sheets, we incorporated metabolic selection to purify all cardiomyocyte differentiation runs. Using metabolic selection, non-cardiomyocytes detached within the first few days of purification, leaving highly pure populations of beating cardiomyocytes at the end of selection (Fig. 22), which were used for subsequent experiments. Next, to determine the appropriate surface chemistry parameters to allow for nanopatterned cardiac cell sheet engineering, we investigated altering the density of the grafted PNIPAM. The density of the grafted PNIPAM chains can affect the attachment and detachment of cell sheets, with too-densely grafted PNIPAM preventing formation of cell monolayers due to the hydrophobicity of the polymer. We seeded pure (99% cTnT+) cardiomyocytes on 0.5%, 1%,

5%, 10%, 15% and 25% GMA v/v TNFS, with the GMA concentration affecting PNIPAM grafting density. Cardiomyocytes were able to form aligned cardiac monolayers on 0.5%, 1% and 5% GMA TNFS, but did not form confluent monolayers on 10%, 15% or 25% GMA TNFS (Fig. 23). Cardiomyocytes seeded on 0.5% and 1% GMA TNFS demonstrated synchronous beating monolayers and especially well-aligned cytoskeletons and defined sarcomeric striations after 7 days of culture on the TNFS (Fig. 24, Fig. 25a). To test thermoresponsive detachment of cell sheets, TNFS were subsequently incubated with room-temperature DPBS to promote cell sheet detachment, however none of the tested conditions allowed for the detachment of intact cell sheets, with cells clumping together instead of detaching as intact sheets (Fig. 25b). Attempt to transfer cardiomyocyte clumps did not yield aligned cardiac sheets (Fig. 25c).

4.4.2 Endocardial-like endothelial cell incorporation promotoes detachment of nanopatterned cardiac cell sheets from the TNFS

Previous studies have shown that extracellular matrix must be deposited by the cells to allow for an intact cell sheet to detach from a thermoresponsive surface, and after a change in culture temperature below the PNIPAM lower critical solution temperature (32ºC), the deposited ECM and cell monolayer detaches spontaneously while maintaining cell-ECM and cell-cell connections [108]. To allow for deposition of ECM, four different cell cocultures comprised of stromal and vascular cells used in other cardiac tissue engineering studies were investigated towards the formation of detachable, nanopatterned cardiac cell sheets: primary human dermal fibroblasts (hDFs), stromal cell lines hs27a and hs5, and hiPSC-derived endocardial-like endothelial cells (ECs) in varying ratios. Confluent cardiac monolayers were unable to be formed utilizing stromal cell line hs5 (Fig. 26a), while hDFs, hs27as and ECs formed confluent, aligned cardiac monolayers (Fig. 26b-d). The remaining three stromal cell conditions were incubated with

room-temperature DPBS for 60 minutes to test for detachment capabilities. hDF cocultures were unable to be detached from the TNFS under any coculture ratio and additionally formed heterogeneous tissues with nodes of aligned cardiomyocytes beating asynchronously (Fig. 27a). This was likely due to an overproduction of ECM proteins during culture onto the TNFS which would not detach even after substrate swelling. Stromal cell line hs27a cocultures and EC cocultures detached spontaneously from the TNFS during DPBS incubation and were subsequently transferred using the gel-casting method, however hs27a cocultured cardiac cell sheets lost alignment after transfer (Fig. 27b); hs27a cells were also unable to detect nanotopography while cultured on the TNFS and subsequently overgrew remaining cardiomyocytes after transfer. Only EC cocultured cardiac cell sheets were able to be transferred with maintained alignment (Fig. 27c). From these experiments, 0.5% and 1% GMA TNFS seeded with 1:5 EC:CM ratio allowed for formation of confluent, synchronous, anisotropic cardiac monolayers which could detach spontaneously from the TNFS surface with a reduction in culture temperature (Fig. 28). Additionally, the detaching nanopatterned cardiac cell sheet maintained cell-cell connections during detachment, as evidenced by synchronous beating detached cardiac cell sheets. As the cardiac sheets were cultured for up to 14 days on the TNFS and would continue to beat throughout culture, premature detachment of cardiac sheets was occasionally noted on 1% GMA TNFS. As a result, subsequent transfer and stacking experiments utilized 0.5% GMA TNFS and controls.

4.4.3 Transferred nanopatterned cardiac cell sheets maintain alignment long term and can be stacked to form multilayered, aligned cardiac tissues with discrete cardiac layers

To determine feasibility of engineering aligned cardiac tissues for further structure-function studies, we first investigated transfer of single aligned cardiac sheets and then subsequently

multilayered, stacked aligned cardiac tissues. Using the gel-casting method, nanopatterned cardiac cell sheets were transferred to a matrigel-coated coverslip. Transferred sheets maintained alignment and beating immediately after transfer (Fig. 29a) as well as long term, 7 days post-transfer (Fig. 29b). Analysis of cytoskeletal alignment using automated image analysis demonstrated maintained structural alignment relative to unpatterned controls (Fig. 29c). Morphological analysis of cardiomyocytes within the transferred nanopatterned sheet demonstrate well-ordered sarcomeres, demonstrating a more mature structural phenotype (Fig. 29b). To engineer and visualize aligned multilayered cardiac tissues, nanopatterned cardiac cell sheets were first stained with CellTracker Red or Green dyes, then stacked uniaxially aligned to generate 4-layered thick cardiac tissues in alternating red-green fashion (Fig. 31a). Nanopatterned cardiac sheets that were only cultured for 7 days on the TNFS and subsequently stacked demonstrated a “loose” sheet morphology and formed gaps between cells as well as holes and tears within the sheet, but were still able to be stacked into 4-layer tissues. Confocal imaging of these tissues revealed subsequent reorganization within 24 hours after stacking between the sheets, indicating that individual layers were not maintained (Fig. 30). Nanopatterned cardiac sheets were then cultured for 14 days on the TNFS to determine if eventual deposition of ECM could allow for “thicker” cardiac sheets which could be stacked to form 4-layered tissues. Indeed, cardiac sheets cultured for 14 days demonstrated a different morphology, evidenced by the lack of distinct cell borders. When 14 day-cultured nanopatterned cardiac sheets were stacked, individual sheets would contract simultaneously but were connected loosely enough such that individual sheets were discernible during contractions, however, after 24 hours of culture, the sheets contracted and relaxed simultaneously, indicating some degree of tissue compaction or tighter cardiac sheet connections after culture. Analysis of CellTracker labeled tissues indicated that individual cardiac sheets did not intermix and instead maintained integrity

long term (7 days) after transfer to a new surface (Fig. 31b). Immunostained 4-layer aligned tissue images demonstrated maintained structural alignment similar to single nanopatterned sheet transfers throughout the entire multilayered tissue (Fig 31. c,d). Additionally, cardiomyocytes demonstrated well-ordered sarcomeres similar to the single nanopatterned sheets (Fig. 31e). Using z-stacked confocal microscope images of the tissues, individual nanopatterned sheets were measured as roughly 8-10μm thick, with a total tissue thickness of ~40μm. Staining for endothelial markers revealed that the incorporated ECs did not form vasculature in the laminae and instead remained as discrete individual cells within the tissue.

4.4.4 Engineered multilayered cardiac tissues retain individual layer alignment even when stacked in complex, 3D tissues, which subsequently affects tissue function

Based on the findings from the aligned, multilayered cardiac tissues, we sought to engineer more complex cardiac tissue structures using our developed platform and fabrication parameters. Nanopatterned cardiac sheets were thus cultured, detached and stacked in multilayered aligned, helical and unpatterned cardiac tissues. Aligned and helical cardiac tissues demonstrated cytoskeletal alignment in the individual nanopatterned sheets, as well as well-ordered sarcomere formation (Fig. 32c). Quantitative assessment of cytoskeletal alignment showed that overall multilayered tissue architecture was maintained as either aligned or helical long term in culture. Both conditions also demonstrated alignment of deposited and transferred ECM mimicking that of the individual layer alignment. Neither condition experienced reorganization or migration between cardiac sheets (Fig. 31b, Fig. 32a). To assess if alignment of cardiac tissues could affect function, and if multilayered tissues functioned differently than single cardiac sheets, we analyzed video recordings of the contracting tissues. Both aligned and helical multilayered tissues demonstrated significantly greater contraction velocities ($p < 0.05$)

than unpatterned controls (Fig. 33a), with aligned tissues also demonstrating greater contraction magnitude than helical tissues ($p < 0.05$, Fig. 33b). There were no significant differences between aligned and helical tissues for contraction velocity, or any of the conditions for relaxation velocity (Fig. 33c). Interestingly, helical multilayered cardiac tissue demonstrated a “swirl” or twisting contraction pattern, likely due to the differing orientations of the stacked, individual cardiac sheets (Fig. 32d). Contraction vectors of the aligned cardiac tissues were less disperse than helical tissues, which were less disperse than unpatterned controls (Fig. 33d).

4.5 Discussion

In the present study, we demonstrate a robust, “bottom-up” approach for engineering cell-dense cardiac tissues that allows for precise control of 3D tissue structure. By utilizing biomimetic nanotopographical cues, we are able to align entire cardiac monolayers. With the incorporation of a thermoresponsive release layer, as well as modifying tissue parameters such as the inclusion of a stromal cell population to allow for ECM deposition, the anisotropic cardiac sheets can be detached and transferred without loss of structure. Even more promisingly, the anisotropic sheets can be stacked to form multilayered cardiac tissues with a variety of tissue structures. The stacked nanopatterned cardiac sheets are able to beat in sync with one another while maintaining individual sheet anisotropy, allowing for the fabrication of both aligned and helical 3D cardiac tissues. Further, the different 3D cardiac tissue structures also demonstrated different contractile properties, highlighting the importance of overall cardiac tissue structure on tissue function even at the scale of individual cardiac sheets.

Although the heart contains an abundant amount of structurally organized extracellular matrix proteins, the myocardium is a cell-dense tissue. Cardiomyocytes must be in direct contact

with one another to transmit an action potential and transmit force during a contraction [130, 131]. As a result, the use of scaffolds to engineer cardiac tissue often limits the engineered tissue utility due to inflammatory response of implanted materials as well as difficulties with host tissue integration [13, 132]. The advent of scaffold-free cardiac tissue engineering has yielded promising results, specifically showing improvements in cardiac function after transplantation, but to our knowledge, all scaffold-free, engineered cardiac tissues thus far have lacked structural organization [42, 133]. Our engineered, structured, 3D cardiac tissues demonstrated improved contractile properties over unstructured controls. For aligned 3D cardiac tissues, the alignment of contractile direction, and subsequently, contractile force, would have an obvious additive effect. However, interestingly, even helically structured 3D cardiac tissues demonstrated improved contractile properties over controls, even though the top and bottom layer were oriented nearly perpendicularly. This could potentially be due to the fact that individual cardiac sheets in the helical tissue were still structured and therefore had an anisotropic, uniaxial direction of contraction, whereas control tissue contraction vectors were isotropic. This could lead to a greater overall contraction magnitude and velocity when summed throughout the 3D cardiac tissue, albeit blunted as the individual cardiac sheets were not aligned in a single direction. Thus, although a seemingly subtle experimental variable, our results demonstrate that tissue structure alone can play an important role in augmenting and improving tissue function. Our engineering approach could thus advance the already promising field of cardiac tissue engineering for therapeutic approaches.

Additionally, the ability to engineer more complex 3D cardiac tissue structures, like a helical architecture, also allows for more robust exploration of the role of cardiac structure into additional fields, such as developmental biology. For instance, although the adult cardiac structure is well-documented, the underlying processes regulating the development of this structure are still

under active research. Fibronectin and other ECM components assist in migration of cardiac precursors early in heart development [134], followed by elongation of individual cardiomyocytes which form lateral cell-matrix connections to aligned ECM fibers [135] and then self-organization of aligned fiber tracts into a helical structure late in fetal development and progressing through postnatal development [136]. These *in vivo* studies have suggested that both the ECM and the 3D cardiac microenvironment may contribute to the maturation of cardiomyocytes as well as the structural organization of the myocardium. Our platform could subsequently allow for the analysis of cardiac microenvironmental effects, including structure, on the development of embryonic stem cell-derived cardiomyocytes. Subsequently, as we have used our platform with a variety of other cell types, including cells derived from similar developmental lineages as cardiomyocytes, we could theoretically engineer complex, multilayered cardiac tissues, comprised of endocardium, myocardium, and epicardium, for the analysis of cardiomyocyte and supporting cell interactions during development. We believe that this initial proof of concept engineering of a variety of cardiac tissue structure thus could provide interesting insights into stem cell biology and development in addition to advancing tissue engineering for clinical purposes.

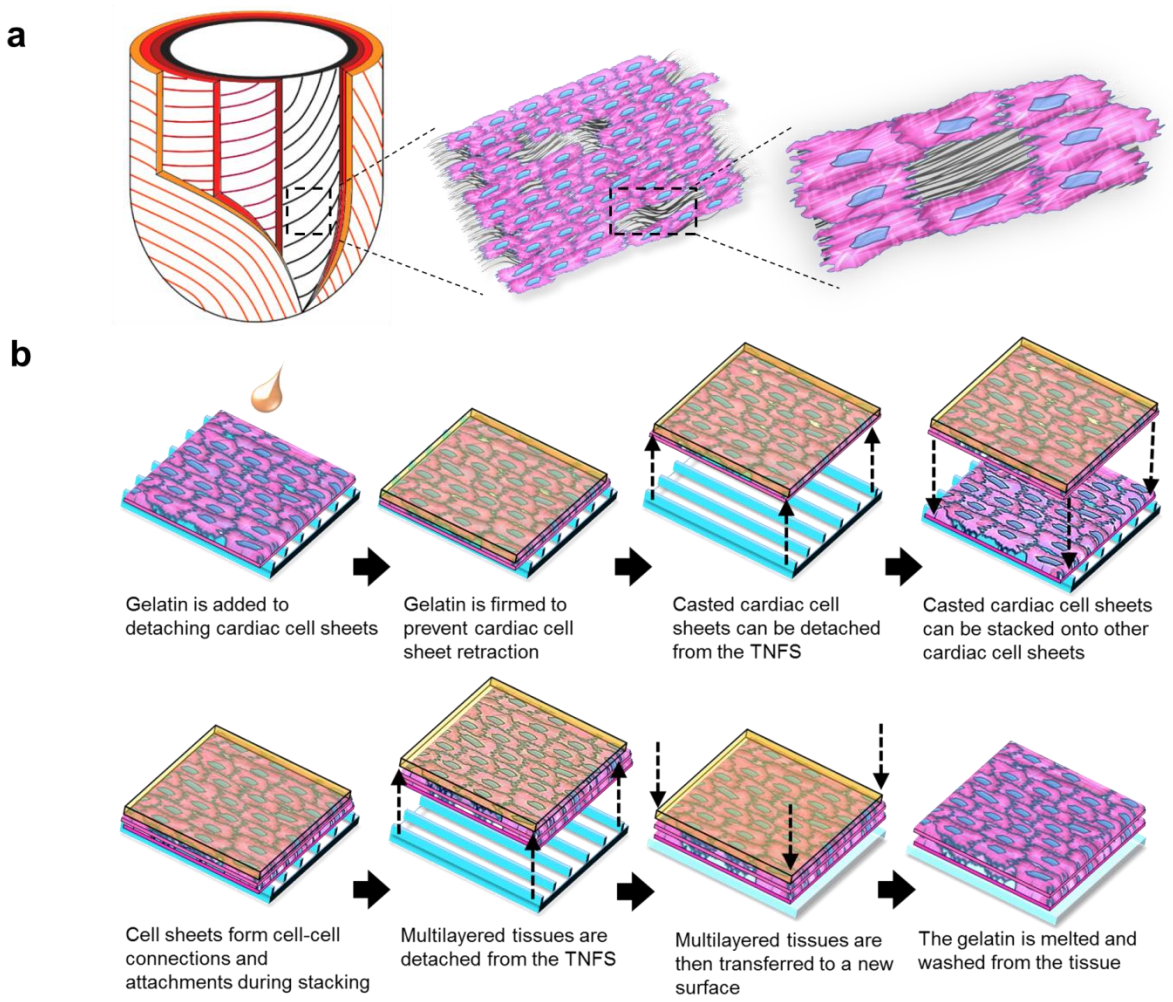

Figure 21. Bioinspired design and implementation of a flexible thermoresponsive, nanostructured substrate to engineer organized cardiac tissues. (a) Schematic illustration of helically structured myocardial sheets in the heart, which are organized in anisotropic cardiac layers comprised of aligned cardiomyocytes and extracellular matrix fibers 4-6 myocytes thick. (b) Schematic illustration of cardiac cell sheet engineering using the thermoresponsive nanostructured substrate (TNFS) to engineer multilayered cardiac tissues.

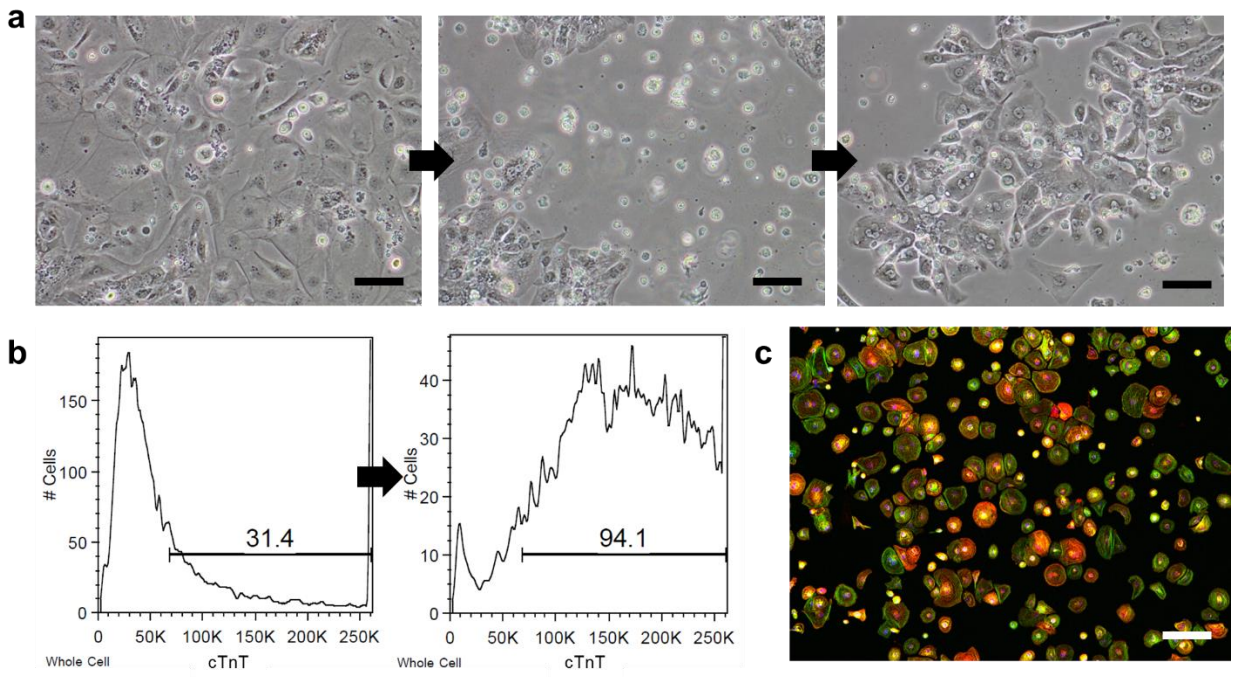

Figure 22. Metabolic purification of hiPS-derived cardiomyocytes yields high purity cell cultures. (a) Bright field microscope images showing the loss of non-cardiomyocyte cells due to metabolic purification in during cell culture over the course of 7 days. Scale bars, 100μm. (b) Flow cytometry analysis of FITC-cTnT stained cells before and after metabolic purification demonstrating a 3-fold increase in cTnT+ cells after selection. (c) A confocal microscope image of α-sarcomeric actinin (red), phalloidin (green), and Hoechst (blue) stained cells after metabolic purification. Scale bar, 200μm.

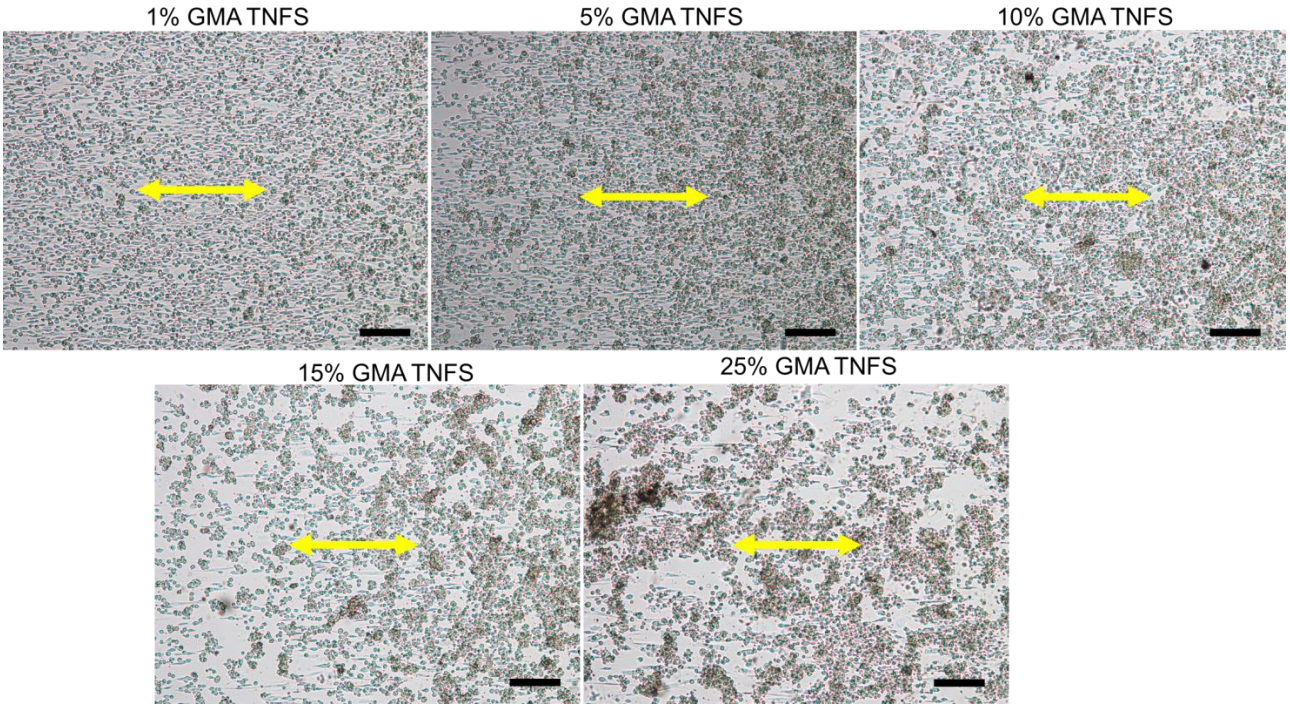

Figure 23. PNIPAM grafting density affects formation of anisotropic cardiac monolayers. Bright field microscope image demonstrating varying degrees of cardiac monolayer and subsequent sheet formation dependent on the concentration of GMA copolymer used in the TNFS. Scale bars, 200µm. Yellow double-sided arrows indicate substrate nanopattern direction.

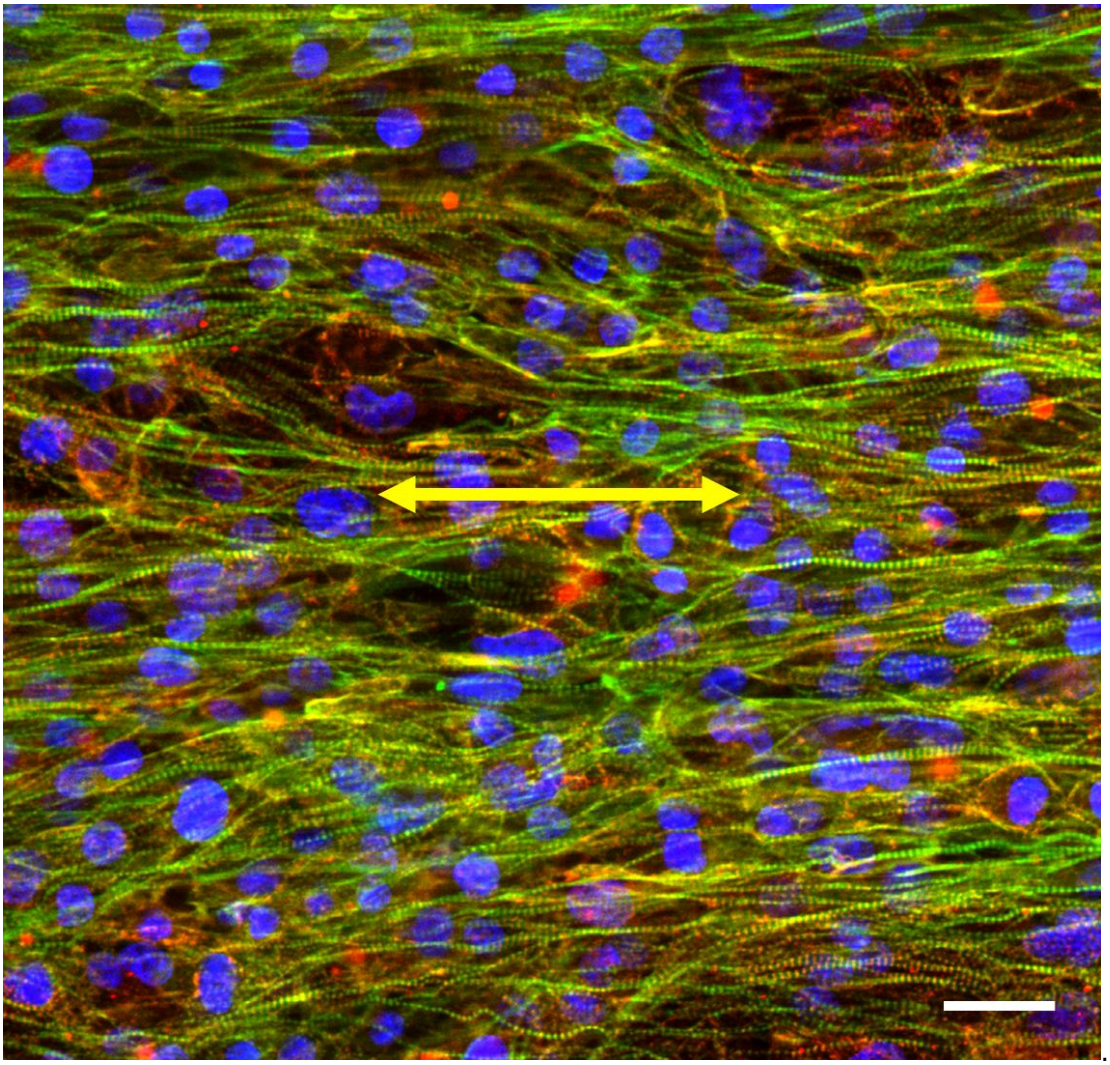

Figure 24. Pure cardiomyocytes form structurally-aligned monolayers on the TNFS. A confocal microscope image of α-sarcomeric actinin (red), phalloidin (green), and Hoechst (blue) stained cells demonstrating alignment of structural proteins and contractile apparatus in pure cardiac sheets seeded onto a TNFS. Scale bar, 50μm. Yellow double-sided arrow indicates substrate nanopattern direction.

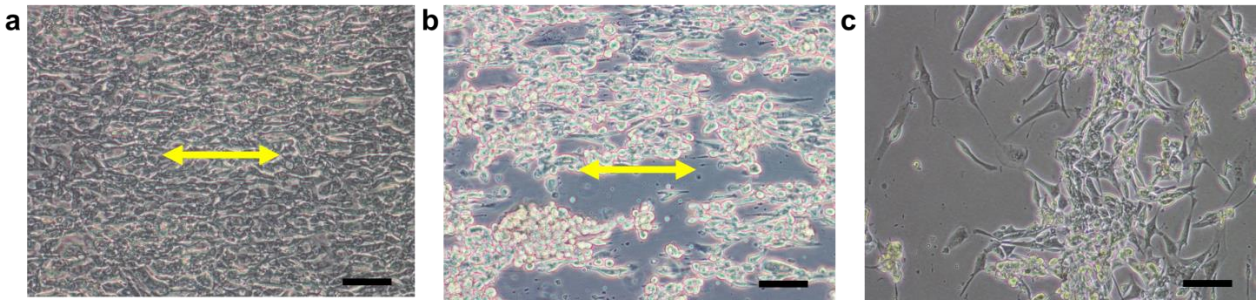

Figure 25. Pure cardiac sheets do not detach as intact, anisotropic cell sheets. (a) Bright field microscope image of 99% cTnT+ cardiomyocytes seeded on a 1% GMA TNFS show formation of elongated, aligned cardiomyocytes 24 hours after seeding. Scale bar, 100um. (b) Bright field microscope image of reduction of culture temperature from 37ºC to 22ºC causes cells to detach from the surface but not as an intact sheet. Scale bar, 100µm. (c) Bright field microscope image of gel-casted, transferred pure cardiac "sheets" demonstrating loss of initial alignment and only partial transfer. Scale bar, 100µm. Yellow double-sided arrows indicate substrate nanopattern direction.

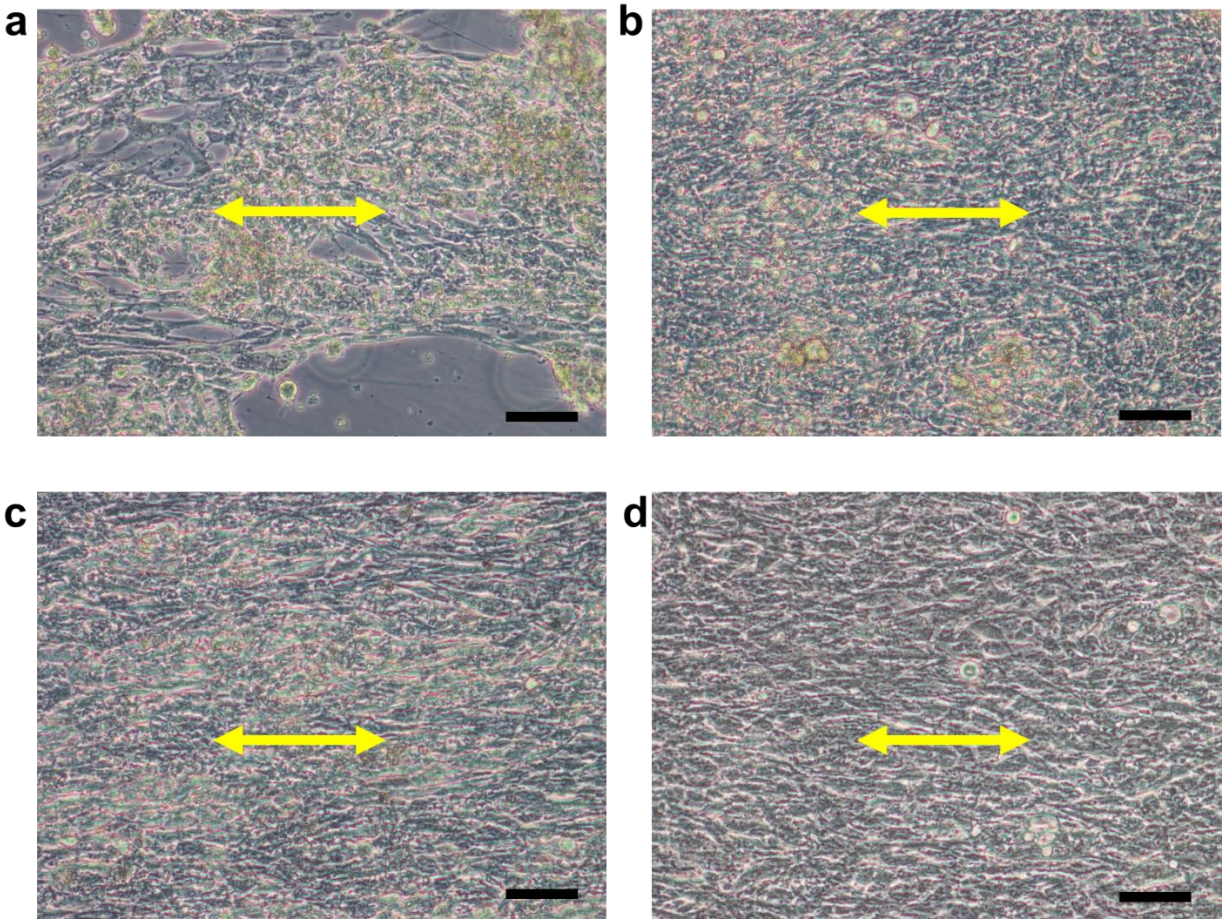

Figure 26. Stromal cell coculture with cardiomyocytes to engineer detachable, anisotropic cardiac sheets. Bright field microscope image showing incomplete cardiac sheet formation during coculture of the hs5 stromal cell line (a) and formation of aligned cardiac sheets of cocultures of the hs27a stromal cell line (b), primary human dermal fibroblasts (c), and hiPS-derived hemogenic anterior endocardial-like endothelial cells (d, ECs). All stromal cells mixed in a 1:5 ratio with cardiomyocytes. Scale bars, 100µm. Yellow double-sided arrows indicate substrate nanopattern direction.

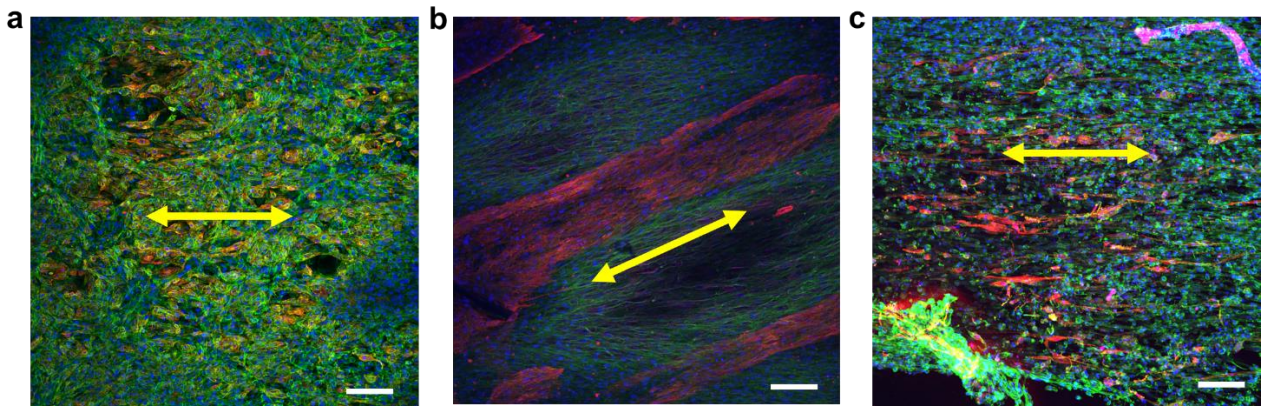

Figure 27. Endocardial-like endothelial cells (ECs) demonstrate best formation and transfer of aligned cardiac sheets. (a) Confocal microscope image of immunofluorescently stained, transferred hs27a cocultured cardiac sheets, demonstrating lost alignment after transfer to a glass surface. (b) Confocal microscope image of immunofluorescently stained, transferred hDF cocultured cardiac sheets, demonstrating sheet formation but asynchronous beating with uneven distribution of cardiomyocytes. (c) Confocal microscope image of immunofluorescently stained, transferred EC cocultured cardiac sheets, demonstrating but well-aligned, synchronous monolayers. α-sarcomeric actinin in red, phalloidin in green, Hoechst in blue. Scale bar, 200µm.

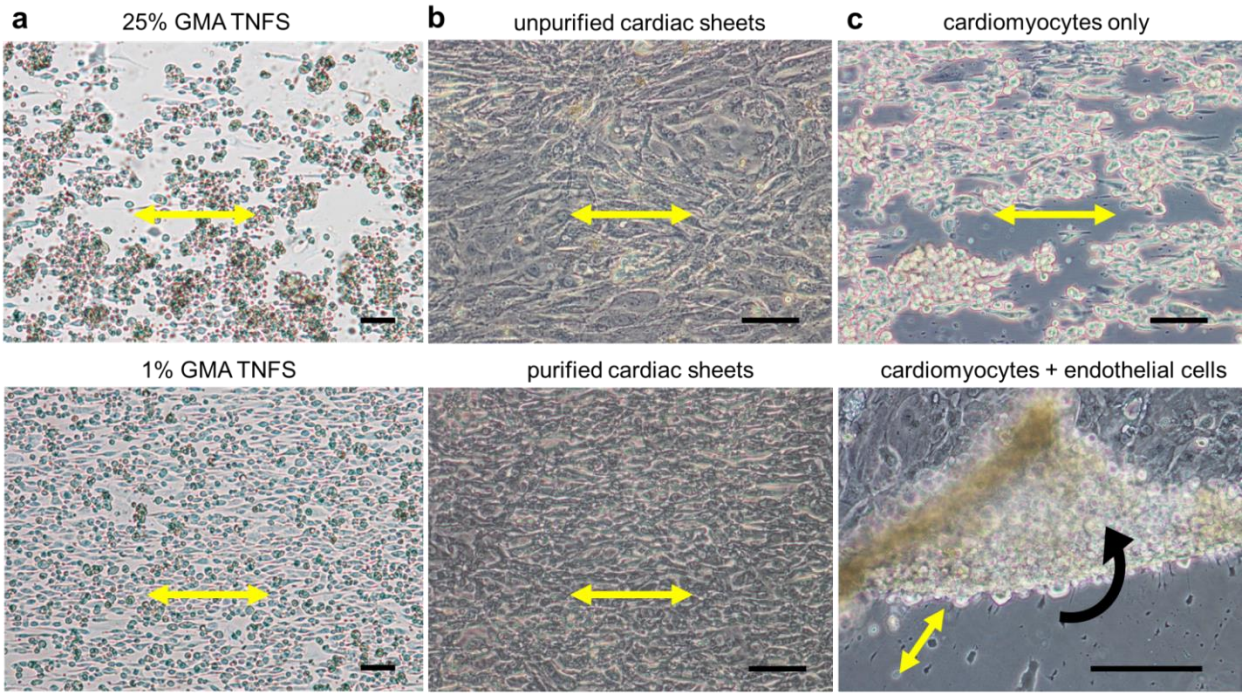

Figure 28. Tissue and substrate parameters to engineer anisotropic cardiac sheets. (a) Representative bright field microscope images of TNFS with varying GMA percentages, affecting PNIPAM grafting density and monolayer formation. Scale bars, 100µm. (b) Representative bright field microscope images of cardiac sheets with unpurified, hiPS-CMs (top) and metabolically purified hiPS-CMs (bot) on 1% GMA TNFS, demonstrating increased alignment and synchronous monolayer formation with incorporation of purified cardiomyocytes. Scale bars, 100µm. (c) Representative bright field microscope images of detaching nanopatterned (NP) cardiac sheets without incorporation of stromal cells (top) and with incorporation of 20% endocardial-like endothelial cells (bot) demonstrating intact, spontaneous cardiac sheet detachment only in the presence of an ECM producing stromal cell coculture. Scale bars, 100µm. Yellow double-sided arrows indicate substrate nanopattern direction.

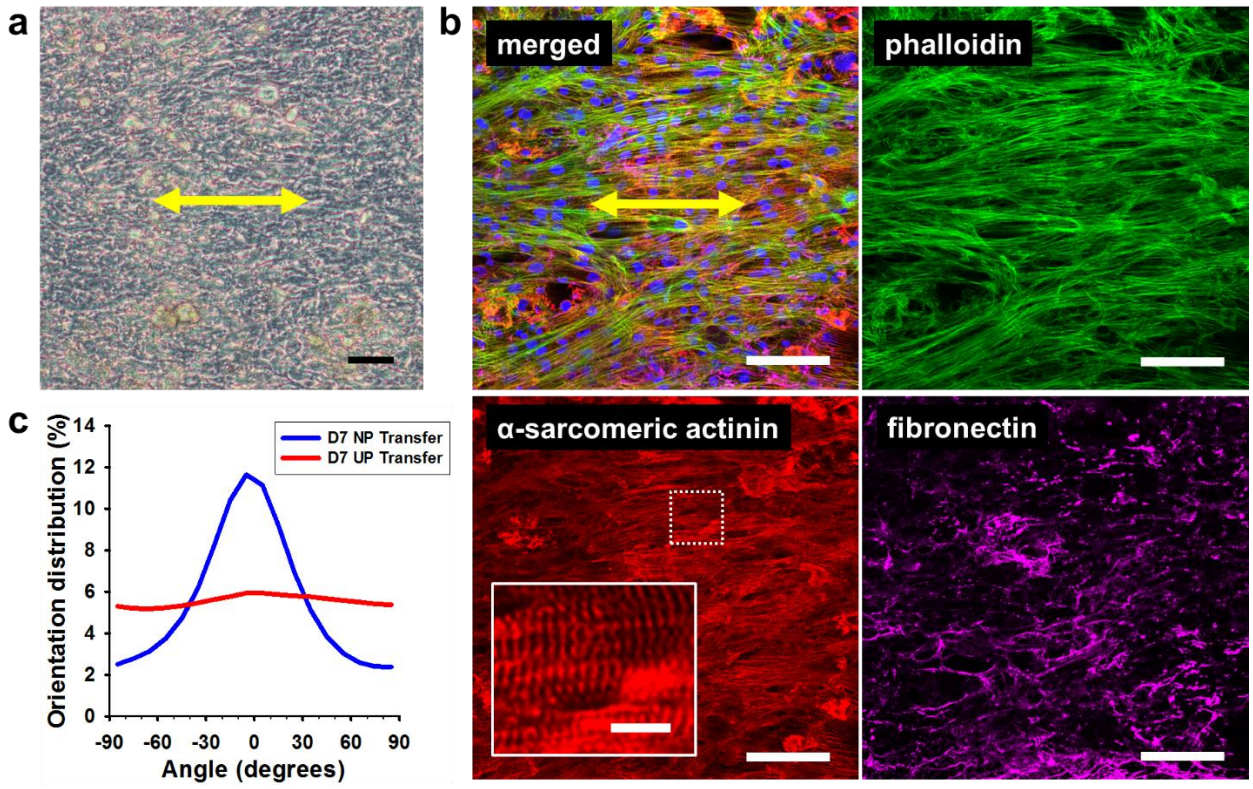

Figure 29. Nanopatterned endocardial-cardiomyocyte (cardiac) cocultured sheets can be transferred to other surfaces while maintaining alignment and deposited extracellular matrix proteins. (a) Bright field microscope image showing aligned structure of a transferred, nanopatterned cardiac sheet 24 hours after transfer onto a flat glass surface. Scale bar, 100µm. (b) Confocal microscope image of an immunofluorescently labeled cardiac cell sheet 7 days after transfer to a glass coverslip demonstrating maintained cytoskeletal alignment long-term, well-ordered sarcomeric arrays, and organized cell-deposited extracellular matrix proteins. Scale bar, 100µm, inset, 10µm. (c) Quantitative assessment of cytoskeletal alignment of both nanopatterned (NP) cardiac sheets and unpatterned (UP) controls illustrating the degree of alignment in NP cardiac sheets 7 days post-transfer to a glass coverslip. Yellow double-sided arrows indicate initial substrate nanopattern direction.

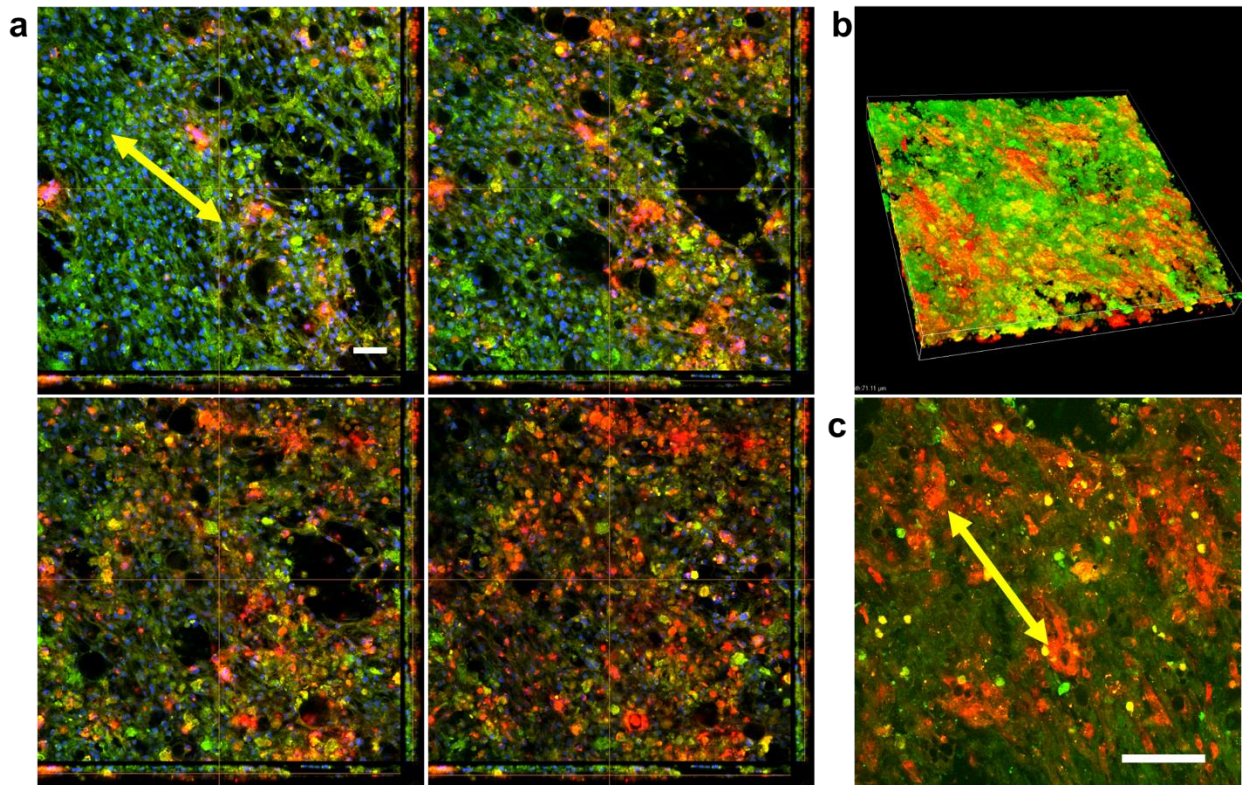

Figure 30. 7-day cultured anisotropic cardiac sheets can undergo sheet mixing and reorganization while maintaining alignment. (a) Confocal microscope z-stack image of red and green CellTracker-labeled, 4-layer aligned cardiac sheets, demonstrating layer mixing between sheets from bottom (upper left) to top (bottom right) 24 hours after transfer. Scale bar, 100μm. (b) Confocal microscope z-stack 3D-rendering of the CellTracker-labeled, 4-layer aligned cardiac tissue demonstrating intermixed red and green cardiac cells. (c) High resolution confocal microscope image demonstrating mixed red and green cells within a single layer. Scale bar, 100μm. Yellow double-sided arrows indicate initial substrate nanopattern direction.

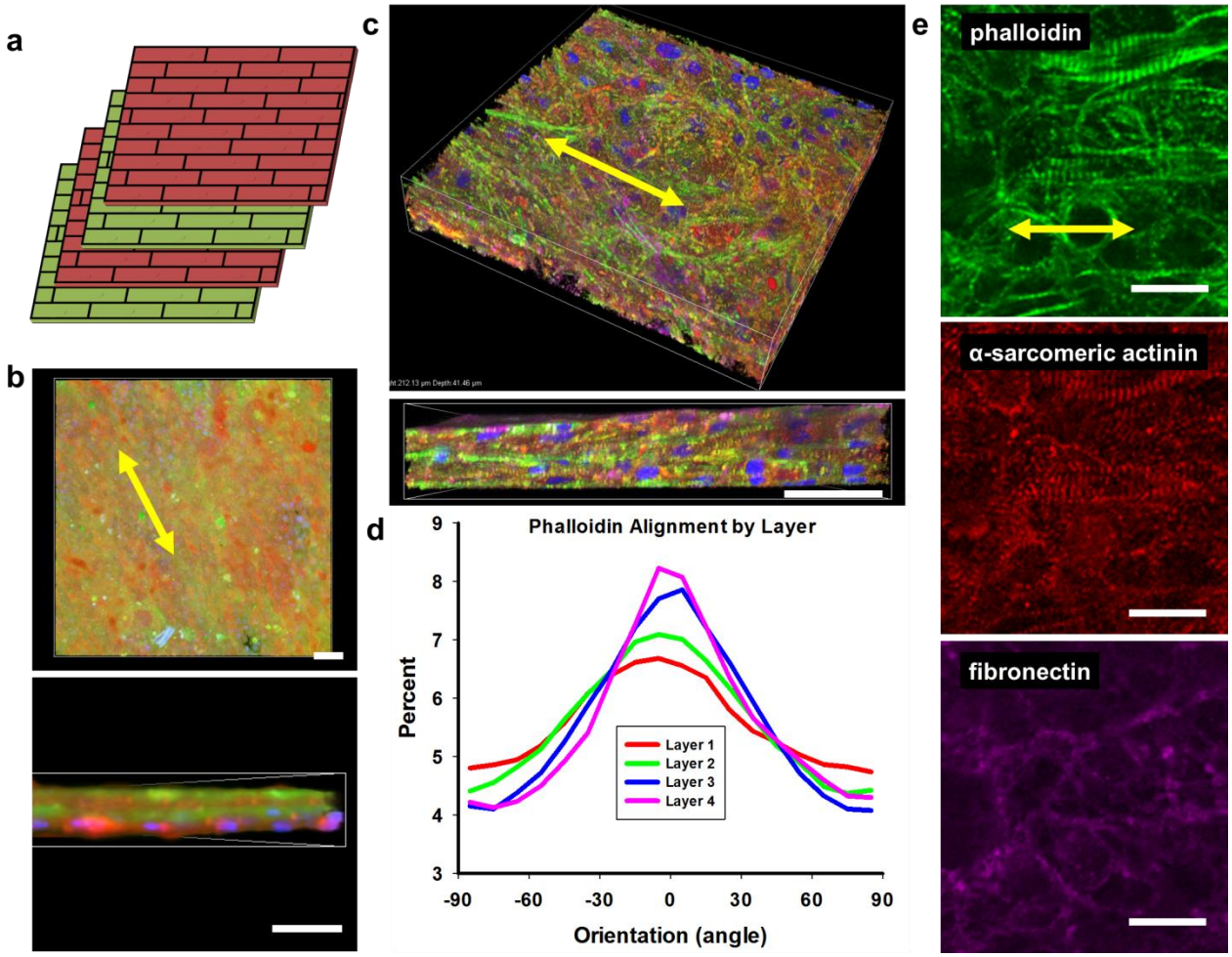

Figure 31. 14-day cultured, multilayered, aligned cardiac tissues maintain discrete layers and overall tissue alignment. (a) Schematic representation of the fluorescently labeled cell sheets stacked in a RGRG configuration with uniaxial alignment. (b) Confocal microscope image of CellTracker labeled cardiac cell sheet 1 day after stacking and transfer to a glass coverslip demonstrating maintained tissue alignment (top) while also maintaining discrete, individual layers (bottom). Scale bar top, 100μm, bottom, 40μm. (c) Confocal microscope z-stack 3D-rendering of the immunofluorescently stained cardiac sheet with α-sarcomeric actinin (red), phalloidin (green), fibronectin (magenta) and Hoechst (blue) demonstrating cytoskeletal alignment (top) and overall cell-dense, 3D tissue thickness (bottom). Scale bar, 40μm. (d) Quantitative assessment of cytoskeletal alignment throughout the 4-layer cardiac tissue, demonstrating maintained uniaxial alignment throughout the tissue and individual layers. Layer 1 is the top cell layer, Layer 4 is the bottom, surface-contacting cell layer. (e) Individual channels from a confocal microscope image of an immunofluorescently stained individual cardiac sheet within the multilayered tissue, demonstrating cytoskeletal alignment, well-ordered sarcomere structures, and presence of cell-deposited extracellular matrix. Scale bar, 50μm. Yellow double-sided arrows indicate initial substrate nanopattern direction.

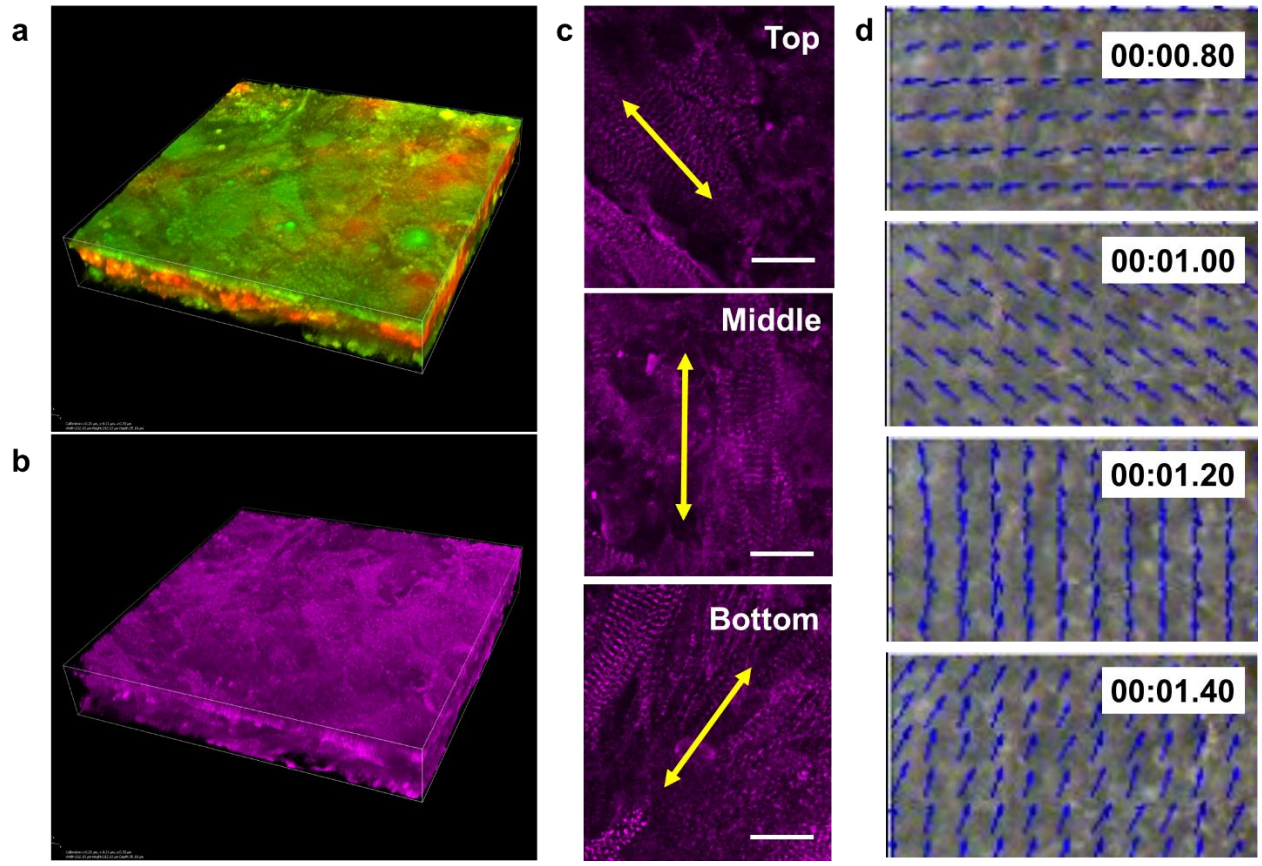

Figure 32. Helical cardiac tissues maintain discrete layers, helical alignment, and contract in a swirl pattern. (a) 3D rendering from z-stack confocal images of CellTracker Red and Green labeled, stacked cardiac tissues demonstrating maintained individual layers in helical tissues 24 hours after stacking. (b) Isolated channel from the same 3D rendering (a) of α-sarcomeric actinin labeled tissues, demonstrating high cardiac purity. (c) Isolated channels for α-sarcomeric actinin signal showing well-ordered sarcomere arrays aligned to different direction dependent on layer depth. Scale bar, 20μm (d) Freeze frames of videos of contraction with a quiver plot overlay based on CCQ analysis of contraction showing the swirl contraction pattern in helical tissues. Yellow double-sided arrows indicate initial substrate nanopattern direction.

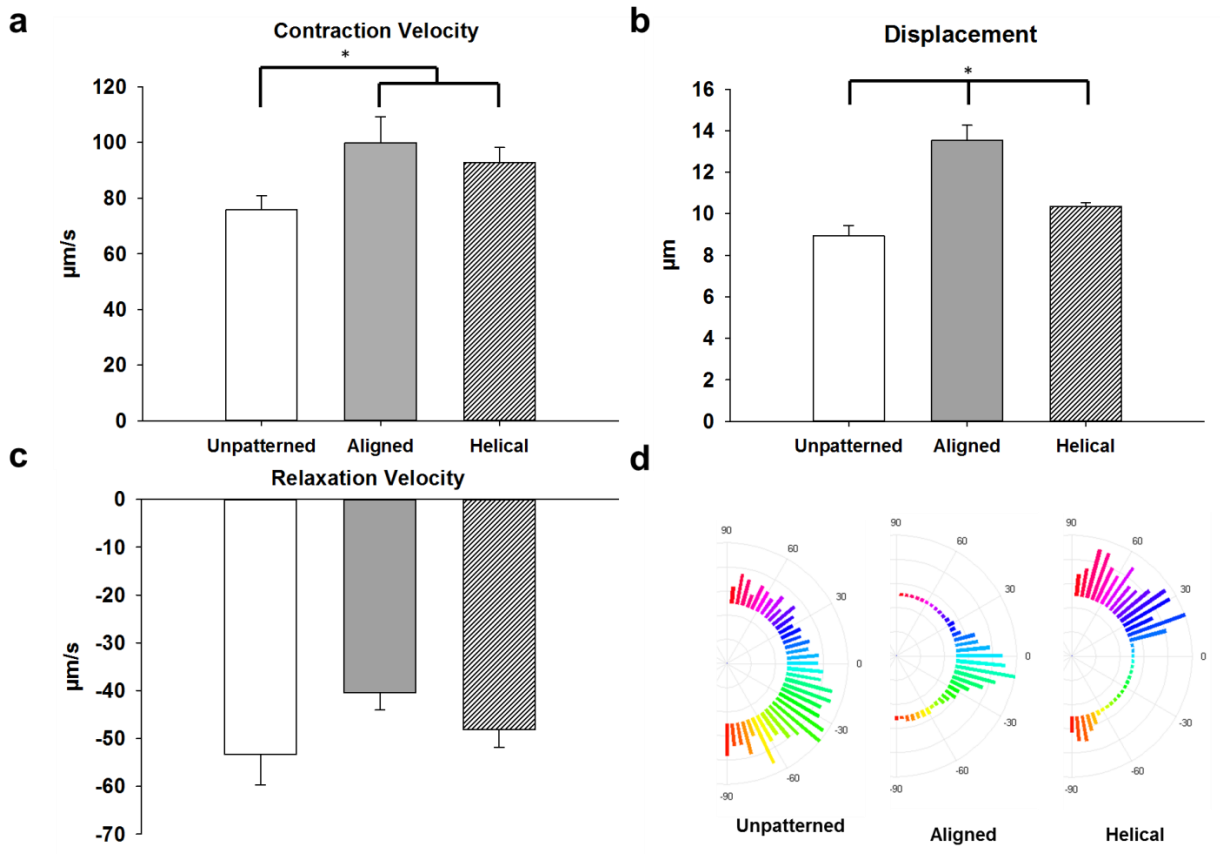

Figure 33. Structural organization of 3D cardiac tissue improves contractile function. CCQ-based quantification of contraction videos of nanopatterned (NP) cardiac sheets and unpatterned (UP) controls demonstrating increased contraction magnitude (**a**), velocity (**b**), and relaxation velocity (**c**). **d**, representative average contraction angle histograms of NP cardiac sheets and unpatterned controls.

CHAPTER 5. Conclusions and Implications for Future Studies

5.1 Summary

Towards the goal of engineering physiological skeletal and cardiac muscle tissues, we first considered some of the design parameters of a chosen approach. First, the approach would need to be able to align or structure cardiomyocytes so that the cellular cytoskeleton and contractile machinery within the cells would be able to generate and transmit force in a singular direction. Second, a scaffold-free approach would be necessary for subsequent engineering of cardiac tissues, as cardiomyocytes must be connected to one another via gap junctions and desmosomes in order to transmit electrical signals and mechanical forces. Finally, the approach would ultimately have to allow for control over the tissue structure in three-dimensions, as the native myocardial tissue has a complex, helical transmural structure which is critical to the clearance of blood. Thus far, no engineering platforms or methods have been developed to address these three design parameters for the engineering of more physiological cardiac tissues, and as a result, we proceeded to develop our own. Our platform would incorporate the use of biomimetic, nanotopographical cues due to its promising effects of rat cardiac tissue structure and function. We then hypothesized that by releasing structured monolayers of cells, cell sheets could be stacked to form multilayered tissues and allow us to control the structure and orientation of each individual cell sheet, ultimately allowing for control over 3D tissue architecture without relying on a supporting scaffold, fulfilling all three design parameters.

To achieve this, we first examined the fabrication of nanostructured polymer substrates utilizing a novel copolymer blend which would allow for the presentation of epoxy groups on the substrate surface. These epoxy groups could be functionalized with amine-terminated PNIPAM, a thermoresponsive polymer which would allow for the detachment of entire cell monolayers. We

found that our novel copolymer could be utilized to fabricate nanostructures with high fidelity, which could further be functionalized with PNIPAM – we termed the developed substrate as a thermoresponsive, nanofabricated substratum (TNFS). We then utilized C2C12 myoblasts and optimized TNFS parameters to allow for the formation and thermoresponsive, spontaneous detachment of anisotropic cell sheets. By developing a transfer method, termed the gel casting method, we could transfer viable, anisotropic cell sheets to new, unpatterned surfaces, with the transferred cell sheets retaining structure long term. Finally, we utilized our developed TNFS and gel casting method to engineer labeled, 3-layer myoblast tissues in a helical structure, which retained tissue architecture and sheet integrity after subsequent culture, demonstrating the feasibility of our developed platform for engineering structured, scaffold-free 3D tissues.

We then sought to investigate the biological underpinnings behind the maintenance of engineered tissue structure using the TNFS and gel casting method. Since tissues maintained individual layer alignments even after transfer to a new surface or other layers with competing alignment cues, we hypothesized that other alignment cues must be present with the transferred cell sheet to allow for tissue structure maintenance. Specifically, we believed that cells seeded on the TNFS would deposit and structure extracellular matrix proteins to form a basal lamina, which would subsequently be transferred with the cell sheet and provide structural cues for maintenance of cell and tissue structure. To test this, we analyzed the time course of C2C12 myoblast morphology changes and subsequent ECM structure after seeding onto our TNFS and found that cells rapidly sense the nanotopographical cues, elongate and change morphology, and then deposit ECM proteins. Both nanopatterned and unpatterned control cell sheets were transferred using our gel casting method without loss of tissue or ECM structure, and both retained initial structure while cultured under growth conditions. We also found that myoblasts undergoing differentiation would fuse and form myotubes along the direction of cell and ECM alignment.

Further, both cell cytoskeletal and ECM structure were reorganized during differentiation, indicating a dynamic and active microenvironmental remodeling process. To analyze the effects of 3D tissue structure on myoblast differentiation, myoblast bilayer tissues were engineered with orthogonal and parallel sheet structures. Interestingly, we found that bilayer orthogonal tissues maintained a specific crosshatched cellular and ECM morphology when cultured in growth conditions, but this structure was subsequently lost during differentiation. Further, we found that during differentiation, the initial alignments of the myoblasts was general lost after differentiation for orthogonal bilayers, whereas the parallel bilayers maintained overall alignment during myotube fusion. Additionally, parallel bilayers formed longer and thicker myotubes than the orthogonal bilayers. Finally, we transferred nanopatterned myoblast sheets onto a hydrogel cylinder to analyze whether myotubes would fuse in the direction of initial alignment in a curved, 3D microenvironment similar to that of a myofiber. We found that the nanopatterned cell sheets transfer onto 3D hydrogel surfaces, maintain a cell-deposited ECM, and differentiate into myotubes along the original axis of alignment. These findings demonstrate the importance of both tissue and ECM structure on engineered tissue function.

Finally, combining the findings from the previous two studies, we investigated the use of our TNFS to engineer 3D, stem cell-derived human cardiac tissues. Our initial findings indicated that immature, stem cell-derived cardiomyocytes are able to sense the nanotopographical cues and form anisotropic cardiac monolayers, however are unable to detach as an intact sheet. Based on the findings from our skeletal muscle studies, we hypothesized that the deposition of ECM proteins by the seeded cells was an important component of cell sheet engineering. We then analyzed varying cocultures of different, ECM-producing stromal cells and ultimately optimized our protocols to allow for the formation and transfer of nanopatterned, cardiac sheets by incorporating a coculture of endocardial-like endothelial cells. The transferred, nanopatterned

cardiac sheets maintained cytoskeletal and ECM alignment, demonstrated well-ordered sarcomere arrays, and maintained synchronous beating. Based on these results, we then proceeded to engineer multilayered, 3D cardiac tissues with varying tissue structures, specifically aligned cardiac tissues and helical cardiac tissues. We were able to successfully engineer 4-layered cardiac tissues of both structures. Both tissues were able to retain individual cardiac layer integrity after stacking, as well as individual layer alignment. Interestingly, both architectures also demonstrated improved contractile functions when compared to controls, with aligned cardiac tissues demonstrating the greatest overall contractile function, but with helical cardiac tissues demonstrating a "swirling" contractile motion. Based on these results, we successfully demonstrated, to our knowledge, the engineering of scaffold-free, 3D cardiac tissues with specific 3D architectures. Further, we also discovered that we are able to alter contractile function of the engineered tissues simply by manipulating the layer orientations.

5.2 Future Directions

Taken as whole, we believe that our developed platform and preliminary investigations into structured cardiac tissue engineering represents a modest but distinct advancement towards engineering whole human hearts as well as other structured tissues, specifically by incorporating and highlighting 3D cardiac tissue architecture. However, many investigations remain towards improving upon our developed platform for further cardiac structure-function analysis. One limitation of our current approach is the limited overall tissue thicknesses using the layer-by-layer stacking method. Each individual cell sheet thickness ranges between 8-10μm in thickness, with our thickest, 4-layered cardiac tissues only 40μm in thickness. As the native human myocardium ranges between 5-8mm in thickness [137], our engineered tissues are still hundreds of times

thinner than the myocardial tissue we seek to replicate. Although cardiac sheets can continued to be layered indefinitely, the continued addition of cardiac sheets to generate thicker tissues raises another potential hurdle, which is the diffusion limit of oxygen into thick, avascular tissues. Although we have incorporated endocardial-like endothelial cells within our cardiac sheets, we have been unable to observe the formation and presence of any vasculature. The native heart is highly vascularized, with capillaries closely apposed to cardiomyocytes and forming an anisotropic structure aligned to the laminar cardiac sheets [138]. Subsequent investigations towards engineering thicker cardiac sheets should thus be aware of the limitations of oxygen diffusion, and either incorporate an ad hoc vasculature or induce vascularization to allow for the engineering of thicker tissues. Should these limitations be addressed to engineer thick, structured cardiac tissue, such findings would represent a significant advancement towards the ultimate goal of engineering a human heart. It is our hope and belief that our modest contributions in this aspect may thus contribute to humanity's body of knowledge and eventually provide relief for millions of individuals afflicted with heart disease.

APPENDIX 1. Towards engineering structured, functional cardiac organoids

A1.1 Overview

One additional, nascent, area of study, based on our works highlighted in Chapter 4 regarding nanopatterned cell sheet culture on gelatin cylinders, is the investigation of engineering 3D cardiac organoid. Although engineering cardiac tissues in 3D with specific structures has yielded measurable differences in contractile function using video analysis of contractions, a direct measurement of tissue function is ideal, especially when addressing a working organic such as the heart. Towards this, we have begun preliminary investigations towards engineering fully 3D tissue structures or organoids, meaning tissues with depth and architecture within the tissue thickness as well as an additional structure or organization in 3D, which could allow for direct measurement of contractile forces, pressure generation and potentially biological mechanisms such as the Frank-Starling law. Our preliminary investigations have focused on utilizing a simplified organoid structure – a closed, hydrogel tube – and our developed platform and techniques to engineer contractile tissues wrapped around said tube. We hypothesize that our engineered tissues will be able to deform the closed hydrogel tube via muscle contractions, and this deformation, when in a closed-system, will generate pressure measurable with conventional instruments, such as pressure catheter. Towards this, we have begun preliminary results utilizing myoblast sheets and differentiating them into contractile muscle tissue as a surrogate for cardiac tissue. It is our hope that such an eventual developed organoid system could then be used for physiological structure-function investigations of overall cardiac tissue structure.

A1.2 Materials and Methods

A1.2.1 Production of aligned cellular tubes from fTNFS

Two days after fTNFS were seeded with C2C12 myoblasts, fTNFS cell sheets were rolled and casted into a tube format. Cell sheets were washed with DPBS to initiate a temperature change within the fTNFS scaffold and were observed for signs of cellular detachment using bright field microscopy; cell detachment was typically observed within 5-7 minutes after the temperature change. The fTNFS were then removed from the DPBS using forceps and excess liquid was dabbed off using a sterile tissue. Using forceps, the rectangular fTNFS (Fig. 34a) were rolled perpendicularly to their short axis so that the resulting cylinder was the length of the scaffolds' shortest side (1.25 cm). The cylinder was inserted into a tubular polystyrene mold (internal diameter = 2.81 mm) (Fig. 34b, iii) and the mold was attached to a custom base 3D printed from poly-lactic acid (PLA) (Fig. 34b, iv). Next, melted 10% gelatin wt/v in DMEM was mixed with a 10% transglutaminase solution in DPBS at a 1:1 ratio. TG is an enzyme that non-specifically crosslinks gelatin to create a thermostable hydrogel and was used to prevent the gelatin cell tubes from melting at culturing temperatures. 200 µl of the final gelatin-TG solution was pipetted into the lumen of the tubular mold containing the fTNFS and cell sheet. Immediately after, a custom printed cap was attached to the top of the mold (Fig. 34b, ii) and a glass capillary (Ø = 2mm) was inserted through the hollow cap and into the lumen of the gelatin filled mold. The glass capillary would allow for the formation of a lumen within the final cell laden tube. The entire mold was then chilled to 4°C from 1 hour to allow the gelatin to firm and crosslink, and cast the cell sheets onto its surface. After 1 hour at 4°C, the cap and capillary tube were carefully removed from the gelatin and mold. The base was then loosened from the mold and forceps were then used to gently push the fTNFS with the gelatin tube out of the mold. The fTNFS was then unwrapped from the cell tube and the tube was gently placed back onto its base with which it was casted. The base and

cell tube were then clipped into a custom stand (Fig. 34b, v) with the free end of the cell tube resting in the U-shaped slot as to hold the tube horizontally. Next, 15 µl of the melted gelatin-TG mixture was then added to the open end of the cell tube as to form a gelatin seal and a closed hollow lumen within the cell tube. This gelatin seal would later be punctured with a needle to take pressure measurements. Finally, the cell tube, base, and stand were then placed into a well of a 6-well plate, and warmed growth medium was added (DMEM, 10% FBS, 1% penicillin-streptomycin) (Fig. 34c).

A1.2.2. Cell tube culture and differentiation

The cell tubes were maintained in growth medium for up to 5 days or until full confluency around the entire tube was reached. Differentiation medium (DMEM, 2% horse serum, 1% penicillin-streptomycin) was added once confluency was reached. The cell tubes were differentiated and monitored with regular medium changes for 5-7 days or until myotubes were observed throughout the entire cell tube. Upon differentiation, a 6-well plate carbon-electrode insert (Ionoptix) was used to electrically stimulate the cell tubes (3V, 1Hz, 24 ms). The cell tubes were constantly stimulated for up to 7 days and single myotube contractions could be observed after 24 hours and uniform cell tube contractions after 48 hours. After uniform whole tube contractions were observed pressure measurement could be taken as described below.

A1.1.3. Cell tube pressure measurements

The cell tube, base, and stand were gently transferred to a 10 cm tissue culture dish and warmed Tyrode's solution was added until the cell tubes were completely submerged. The cell tubes were allowed to acclimate at 37°C without stimulation for 1 hour. The culture dish was then transported into a cell culture hood and a custom electrode holder was placed into the medium

surrounding the cell tube so that one carbon rod electrode was distanced 2 cm from the cell tube on either side. Platinum wires were used to connect the electrodes to alligator clips and adaptor cords that were plugged into the Ionoptix Myopacer system. A flexible catheter with a needle adaptor at its end was stabilized with clamps onto a movable stand so that the needle could be positioned to line up with the end of the cell tube submerged under the liquid. The stand could then be carefully moved forward until the tip of the needle punctured through the gelatin seal and into the air filled lumen of the cell tube. A baseline pressure without electrical stimulation and contraction could then be determined from the Lab Chart software. Finally, the tube could then be stimulated (3V, 1Hz, 24 ms) through the electrodes and the change in pressure within the lumen of the tube as a result of cellular contraction could be recorded.

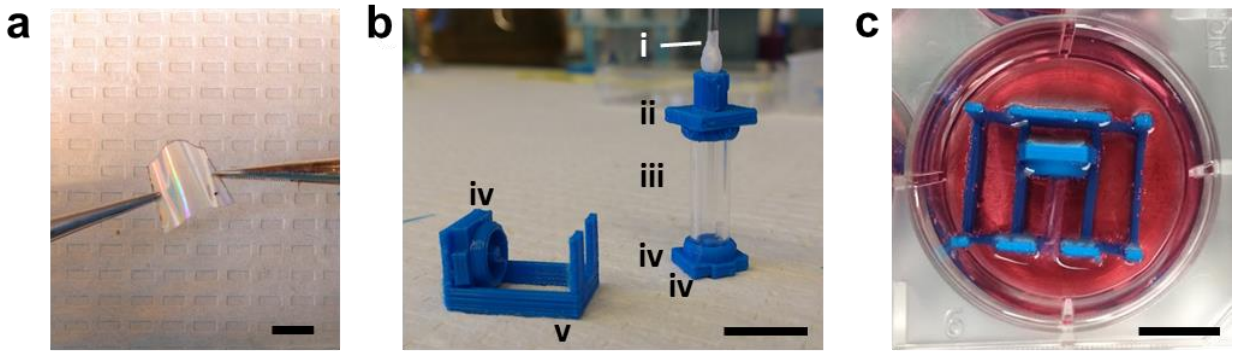

Figure 34. Methods for engineering hydrogel tubes for organoid engineering. (a) Photograph of an fTNFS scaffold to demonstrate flexibility and handling to wrap cell sheets into tubular shapes. Scale bar, 1cm. (b) Implements used to cast cell sheets into tubular shape (right) and housing platform for long-term culture (left). All parts were 3D-printed using PLA plastic. i. A glass capillary tube used to cast a hollow lumen down the center of the cellular tube. ii. A cap with hollow shaft to hold the glass capillary (i) in place during casting. iii. A hollow plastic cylinder where the fTNFS is inserted to create tubular tissues. iv. The cell tube base onto which the cellular tube is mounted. v. A stand which the tube base (iv) is snapped into in order to culture the cellular tube horizontally within a 6 well culture dish. Scale bar, 1cm. (c) Cell tube with housing platform in culture medium within the well of a 6 well culture dish.

APPENDIX 2. Detailed notes on TNFS-based cell sheet engineering

A2.1 Overview

The developed TNFS platform is a versatile, scalable platform that can allow for the engineering of many tissue types and is not limited simple to muscle tissues, as was presented in this dissertation. However, the TNFS platform has many variables which can affect the outcome of successful cell sheet formation, transfer, and stacking, which are each unique to the specific tissue being engineered, e.g., the incorporation of a stromal, ECM producing cell type for cardiac tissue engineering. As the inventor of this platform, I will provide a set of comprehensive notes into the variables and parameters affecting the TNFS platform. Through my many trials and experiments using the TNFS, I believe these to be factors which can affect tissue engineering success. Although many of these parameters may seem innocuous, they are all involved in some way towards successful TNFS-based cell sheet engineering and should be examined and tested empirically for new cell and tissues types, or re-evaluated in the event of troubleshooting.

A2.2 TNFS fabrication and material parameters

A2.2.1 Initial material selection

The polymer used in this dissertation was a mixture between NOA76 (Norland Optical) and glycidyl methacrylate (Sigma). NOA76 is a proprietary polymer and thus its chemical composition is unknown, but it is listed as a polyurethane acrylate by its supplier. For the immobilization of PNIPAM, epoxy groups must be present on the substrate surface. Additionally, the polymer must be compatible with capillary force lithography in order to engineer high-fidelity

nanostructures. I chose NOA76 due to its fast cure time and compatibility with a copolymer with protected epoxy groups. The curing of NOA76 uses UV light and therefore free radical polymerization, which then reacts with the acrylate groups of GMA and does not interact with the epoxy group. Other polymers and polymerization reactions could be used, in theory, should the end product yield high-fidelity nanostructures with epoxy functionalization. One unknown aspect about the materials chosen is the distribution of epoxy groups within the polymer. Although the polymer is mixed together vigorously before use, and used within 1 month of mixture, it is difficult to characterize the spatial organization of epoxy groups, and thus PNIPAM reaction sites, on the surface of the TNFS. Methods that can ensure consistent distribution and validation of epoxy groups on the TNFS surface would be a great improvement to the platform.

A2.2.2 PNIPAM molecular weight selection

In theory, based on the product number, the PNIPAM purchased was from Sigma with a listed molecular weight of 2,500 daltons. However, Sigma relabeled the molecular weight of the same product number twice – first, relabeled from 2,500 daltons to 4,500 daltons, and then relabeled back to 2,500 daltons. When contacted about this change, Sigma insisted that the methods to measure molecular weight had been improved (both times) such that the product was essentially the same with different labeling. However, I have found lot to lot variations coinciding with the changes in listed molecular weight. Molecular weight of the PNIPAM to be grafted has an important effect on the ability of the PNIPAM to undergo a thermoresponsive change in conformation. For the purposes of cell sheet engineering, PNIPAM thickness should be roughly 15-20μm, or the grafting density should be roughly 1.4ug/cm2. Changing the molecular weight of the PNIPAM affects the polymer length and subsequently thickness and density. This can be compensated by altering GMA percentage to change the free epoxy groups present for reaction.

My recommendation is to lot test PNIPAM with a cell type known to be responsive to a specific GMA percentage and culture condition before use with an unknown or valuable cell type.

A2.2.3 GMA concentration

Thus far, most cell types investigated have utilized a GMA percentage ranging between 0.5% to 5% wt/wt. In general, increasing GMA percentage should allow for more PNIPAM grafting and thus a more responsive substrate surface for the detachment of cell sheets. However, too densely grafted PNIPAM can also prohibit the initial adhesion of seeded cells, and over-responsive surfaces may cause spontaneous, uncontrolled detachment of cell sheets. Depending on culture length, it is thus important to initially test a range of GMA percentages (0.5%-5%) for the duration of the planned culture; prolonged culture and overconfluent sheets detach more readily, and therefore spontaneously, than sheets cultured for one to two days.

A2.2.4 Miscellaneous TNFS notes

I have noticed a difference between NOA76-GMA scaffolds which are dip coated immediately after polymerization versus scaffolds that have been cured overnight to finalize polymerization, with an overnight cure being preferred. Additionally, the number of uses the current PNIPAM solution has been utilized is also important – freshly made PNIPAM solutions will tend to graft more PNIPAM due to increased concentration. As the PNIPAM is slowly depleted, the concentration of the solution decreases, and thus the amount of PNIPAM grafted during each dip coat decreases. For a volume of 30ml DI H_2O, 1g of PNIPAM typically lasts me 4-5 whole volume uses. A method to easily characterize PNIPAM amount remaining in solution (PNIPAM can self-aggregate out of a solution if heated, but is difficult to quantify) or a detailed protocol investigating the concentration of PNIPAM over several rounds of dip coating with specific GMA

percentage and area scaffolds would allow for more reproducibility between scaffolds. Finally, polymerized scaffolds that have not been dip coated have an indefinite shelf life, but should be stored in a desiccator. Once dip-coated, the TNFS should be used within the week.

A2.3 Cell sheet parameters

A2.3.1 Initial cell selection

As extensively investigated in chapters 3 and 4, extracellular matrix deposited by the seeded cells is critical for successful cell sheet engineering. Attempts to pre-coat the TNFS with a matrix for cell sheet engineering have been unsuccessful. When investigating a new tissue type, preliminary background on cell ECM production is recommended. Should the cell investigated produce little to no ECM, a stromal cell population should be included to facility ECM deposition for cell sheet engineering. Additionally, due to this necessity of a cell-deposited sheet lamina, the TNFS has been unsuccessful in detaching single cell cardiomyocytes and myoblasts from the surface.

A2.3.2 Increasing cell attachment

Due to the polymeric nature of the TNFS, several cell types do not attach well to the TNFS without pre-treatment. In general, my pre-treatment solution of choice is fetal bovine serum – the nonspecific adsorption of inert proteins as well as abundant presence of adsorbed proteins which facilitate cell connections has generally been successful for more sensitive cell types. Additionally, FBS pre-treatment does not affect topographical cues. However, FBS is an undefined mixture of proteins and also an animal product, which may cause some concerns. As a result, the use of

fibronectin, gelatin, and matrigel have also been investigated, with varying levels of success dependent on cell type. In a head to head comparison of fibronectin with FBS for cardiac tissue engineering, cell sheets formed more confluent monolayers with pre-treatment of FBS over fibronectin, however this was in an impure cell population. Given the specific need to purify cardiomyocytes for cardiac tissue engineering, it is possible that there may be a more optimal ECM pre-treatment for TNFS-based cardiac tissue engineering work. However, all results in this dissertation used FBS pre-treatment to facilitate cell attachment for cardiac tissue engineering. Additionally, surface modifications, such as plasma or ozone treatment, should be avoided, as these destroy the grafted PNIPAM. Ozone and plasma pre-treatment prior to dip coating has been investigated, as well as the use of allylamine to react with non-reacted epoxy groups (theorized to potentially cause issues with cell detachments) as other pre-treatment protocols, but results were inconclusive.

A2.3.2 General cell sheet engineering notes

The process of detachment from the TNFS is an active cellular one, as is the process of attaching to other cell sheets. As a result, the wash buffer and wash buffer temperature, as well as incubation temperature, affects sheet detachment and sheet to sheet attachment. For instance, cold media will allow for faster sheet detachment than room temperature DPBS, however often this detachment is too quick for gel casting to be used. Additionally, as the sheet to sheet attachment is an active cellular process, appropriate time and environmental conditions may be specific to the cell type. Specifically, cardiomyocytes take longer to attach to one another in the form of cardiac sheets than C2C12 myoblasts. In general, for an unknown cell type it is better to err on the side of caution and allow for 2 hours+ for cell-cell connections to be formed and strong enough to hold cell sheets together and then optimized later. Finally, for particularly stuck cell

sheets which do not attach to one another but still spontaneously detach – such as, two sheets are stacked onto one another for two hours, then upon transfer, the sheets rip from one another and the bottom, TNFS contacting sheet still detaches and instead contracts into a small, condensed tissue – the edges of the cell sheet can be scraped around the periphery using a scalpel or micropipette tip and then immediately incubated with the gel-casted sheet to prevent bottom sheet detachment.

REFERENCES

1. SOBEL, B.E., et al., *Estimation of Infarct Size in Man and its Relation to Prognosis.* Circulation, 1972. **46**(4): p. 640-648.
2. Whelan, R.S., V. Kaplinskiy, and R.N. Kitsis, *Cell Death in the Pathogenesis of Heart Disease: Mechanisms and Significance.* Annual Review of Physiology, 2010. **72**(1): p. 19-44.
3. Olivetti, G., et al., *Cardiomyopathy of the aging human heart. Myocyte loss and reactive cellular hypertrophy.* Circulation Research, 1991. **68**(6): p. 1560-8.
4. Bergmann, O., et al., *Evidence for Cardiomyocyte Renewal in Humans.* Science, 2009. **324**(5923): p. 98-102.
5. Wollert, K.C. and H. Drexler, *Cell therapy for the treatment of coronary heart disease: a critical appraisal.* Nat Rev Cardiol, 2010. **7**(4): p. 204-215.
6. Laflamme, M.A., et al., *Cardiomyocytes derived from human embryonic stem cells in pro-survival factors enhance function of infarcted rat hearts.* Nat Biotech, 2007. **25**(9): p. 1015-1024.
7. Stevens, J.L. and T.K. Baker, *The future of drug safety testing: expanding the view and narrowing the focus.* Drug Discovery Today, 2009. **14**(3–4): p. 162-167.
8. Lundy, S.D., et al., *Structural and Functional Maturation of Cardiomyocytes Derived from Human Pluripotent Stem Cells.* Stem Cells and Development, 2013. **22**(14): p. 1991-2002.
9. Yang, X., L. Pabon, and C.E. Murry, *Engineering Adolescence: Maturation of Human Pluripotent Stem Cell–Derived Cardiomyocytes.* Circulation Research, 2014. **114**(3): p. 511-523.
10. Rodriguez, M.L., et al., *Measuring the Contractile Forces of Human Induced Pluripotent Stem Cell-Derived Cardiomyocytes With Arrays of Microposts.* Journal of Biomechanical Engineering, 2014. **136**(5): p. 051005-051005.
11. Neidlinger-Wilke, C., et al., *Cell alignment is induced by cyclic changes in cell length: studies of cells grown in cyclically stretched substrates.* Journal of Orthopaedic Research, 2001. **19**: p. 286-93.
12. Radisic, M., et al., *Functional assembly of engineered myocardium by electrical stimulation of cardiac myocytes cultured on scaffolds.* Proceedings of the National Academy of Sciences, 2004. **101**(52): p. 18129-18134.
13. Tulloch, N.L., et al., *Growth of Engineered Human Myocardium With Mechanical Loading and Vascular Coculture.* Circulation Research, 2011. **109**(1): p. 47-59.
14. Kawamura, M., et al., *Enhanced Survival of Transplanted Human Induced Pluripotent Stem Cell–Derived Cardiomyocytes by the Combination of Cell Sheets With the Pedicled Omental Flap Technique in a Porcine Heart.* Circulation, 2013. **128**(11 suppl 1): p. S87-S94.
15. Schaaf, S., et al., *Human Engineered Heart Tissue as a Versatile Tool in Basic Research and Preclinical Toxicology.* PLoS ONE, 2011. **6**(10): p. e26397.
16. Parker, K.K. and D.E. Ingber, *Extracellular matrix, mechanotransduction and structural hierarchies in heart tissue engineering.* Philosophical Transactions of the Royal Society B: Biological Sciences, 2007. **362**(1484): p. 1267-1279.
17. Bray, M.-A., S.P. Sheehy, and K.K. Parker, *Sarcomere Alignment is Regulated by Myocyte Shape.* Cell motility and the cytoskeleton, 2008. **65**(8): p. 641-651.

18. Palatinus, J.A., J.M. Rhett, and R.G. Gourdie, *The connexin43 carboxyl terminus and cardiac gap junction organization.* Biochimica et Biophysica Acta (BBA) - Biomembranes, 2012. **1818**(8): p. 1831-1843.
19. STREETER, D.D. and W.T. HANNA, *Engineering Mechanics for Successive States in Canine Left Ventricular Myocardium: II. Fiber Angle and Sarcomere Length.* Circulation Research, 1973. **33**(6): p. 656-664.
20. STREETER, D.D., et al., *Fiber Orientation in the Canine Left Ventricle during Diastole and Systole.* Circulation Research, 1969. **24**(3): p. 339-347.
21. Greenbaum, R.A., et al., *Left ventricular fibre architecture in man.* British Heart Journal, 1981. **45**(3): p. 248-263.
22. Sengupta, P.P., et al., *Left Ventricular Structure and FunctionBasic Science for Cardiac Imaging.* Journal of the American College of Cardiology, 2006. **48**(10): p. 1988-2001.
23. Sosnovik, D.E., et al., *Diffusion Spectrum MRI Tractography Reveals the Presence of a Complex Network of Residual Myofibers in Infarcted Myocardium / CLINICAL PERSPECTIVE.* Circulation: Cardiovascular Imaging, 2009. **2**(3): p. 206-212.
24. Roberts, D.E., L.T. Hersh, and A.M. Scher, *Influence of cardiac fiber orientation on wavefront voltage, conduction velocity, and tissue resistivity in the dog.* Circulation Research, 1979. **44**(5): p. 701-12.
25. Kanai, A. and G. Salama, *Optical Mapping Reveals That Repolarization Spreads Anisotropically and Is Guided by Fiber Orientation in Guinea Pig Hearts.* Circulation Research, 1995. **77**(4): p. 784-802.
26. Taccardi, B., et al., *Effect of myocardial fiber direction on epicardial potentials.* Circulation, 1994. **90**(6): p. 3076-90.
27. LeGrice, I.J., Y. Takayama, and J.W. Covell, *Transverse Shear Along Myocardial Cleavage Planes Provides a Mechanism for Normal Systolic Wall Thickening.* Circulation Research, 1995. **77**(1): p. 182-193.
28. Omens, J.H., K.D. May, and A.D. McCulloch, *Transmural distribution of three-dimensional strain in the isolated arrested canine left ventricle.* American Journal of Physiology - Heart and Circulatory Physiology, 1991. **261**(3): p. H918-H928.
29. Delhaas, T., et al., *Regional fibre stress-fibre strain area as an estimate of regional blood flow and oxygen demand in the canine heart.* The Journal of Physiology, 1994. **477**(Pt 3): p. 481-496.
30. Lorenz, C.H.P., John S.; Bundy, Jeffrey M., *Delineation of Normal Human Left Ventricular Twist Throughout Systole by Tagged Cine Magnetic Resonance Imaging.* Journal of Cardiovascular Magnetic Resonance, 2000. **2**(2): p. 97-108.
31. Russel, I., et al., *Regional assessment of left ventricular torsion by CMR tagging.* Journal of Cardiovascular Magnetic Resonance, 2008. **10**(1): p. 26.
32. Young, A. and B. Cowan, *Evaluation of left ventricular torsion by cardiovascular magnetic resonance.* Journal of Cardiovascular Magnetic Resonance, 2012. **14**(1): p. 49.
33. Buckberg, G.D., et al., *Active myocyte shortening during the 'isovolumetric relaxation' phase of diastole is responsible for ventricular suction; 'systolic ventricular filling'.* European Journal of Cardio-Thoracic Surgery, 2006. **29**(Supplement 1): p. S98-S106.
34. Gharib, M., et al., *Optimal vortex formation as an index of cardiac health.* Proceedings of the National Academy of Sciences, 2006. **103**(16): p. 6305-6308.
35. Chen, P.S., et al., *Effects of myocardial fiber orientation on the electrical induction of ventricular fibrillation.* American Journal of Physiology - Heart and Circulatory Physiology, 1993. **264**(6): p. H1760-H1773.

36. Tezuka, F., *Muscle Fiber Orientation in Normal and Hypertrophied Hearts.* The Tohoku Journal of Experimental Medicine, 1975. **117**(3): p. 289-297.
37. Wickline, S.A., et al., *Structural remodeling of human myocardial tissue after infarction. Quantification with ultrasonic backscatter.* Circulation, 1992. **85**(1): p. 259-68.
38. Stevens, K.R., et al., *Scaffold-Free Human Cardiac Tissue Patch Created from Embryonic Stem Cells.* Tissue Engineering Part A, 2008. **15**(6): p. 1211-1222.
39. Gerbin, K.A., et al., *Enhanced Electrical Integration of Engineered Human Myocardium via Intramyocardial versus Epicardial Delivery in Infarcted Rat Hearts.* PLoS ONE, 2015. **10**(7): p. e0131446.
40. Komae, H., et al., *Three-dimensional functional human myocardial tissues fabricated from induced pluripotent stem cells.* Journal of Tissue Engineering and Regenerative Medicine, 2015: p. n/a-n/a.
41. Sakaguchi, K., T. Shimizu, and T. Okano, *Construction of three-dimensional vascularized cardiac tissue with cell sheet engineering.* Journal of Controlled Release, 2015. **205**: p. 83-88.
42. Stevens, K.R., et al., *Physiological function and transplantation of scaffold-free and vascularized human cardiac muscle tissue.* Proceedings of the National Academy of Sciences, 2009. **106**(39): p. 16568-16573.
43. Shimizu, T., et al., *Polysurgery of cell sheet grafts overcomes diffusion limits to produce thick, vascularized myocardial tissues.* The FASEB Journal, 2006.
44. Zimmermann, W.-H., et al., *Tissue Engineering of a Differentiated Cardiac Muscle Construct.* Circulation Research, 2002. **90**(2): p. 223-230.
45. Zhang, D., et al., *Tissue-engineered cardiac patch for advanced functional maturation of human ESC-derived cardiomyocytes.* Biomaterials, 2013. **34**(23): p. 5813-5820.
46. Singelyn, J.M., et al., *Naturally derived myocardial matrix as an injectable scaffold for cardiac tissue engineering.* Biomaterials, 2009. **30**(29): p. 5409-5416.
47. Thavandiran, N., et al., *Design and formulation of functional pluripotent stem cell-derived cardiac microtissues.* Proceedings of the National Academy of Sciences, 2013. **110**(49): p. E4698-E4707.
48. Zimmermann, W.-H., et al., *Cardiac Grafting of Engineered Heart Tissue in Syngenic Rats.* Circulation, 2002. **106**(12 suppl 1): p. I-151-I-157.
49. Thomson, K.S., et al., *Proangiogenic microtemplated fibrin scaffolds containing aprotinin promote improved wound healing responses.* Angiogenesis, 2014. **17**(1): p. 195-205.
50. Colli Franzone, P., et al., *Spread of excitation in 3-D models of the anisotropic cardiac tissue. II. Effects of fiber architecture and ventricular geometry.* Mathematical Biosciences, 1998. **147**(2): p. 131-171.
51. Ashraf, M., et al., *Defining Left Ventricular Apex-to-Base Twist Mechanics Computed From High-Resolution 3D EchocardiographyValidation Against Sonomicrometry.* JACC: Cardiovascular Imaging, 2010. **3**(3): p. 227-234.
52. McDevitt, T.C., et al., *In vitro generation of differentiated cardiac myofibers on micropatterned laminin surfaces.* Journal of Biomedical Materials Research, 2002. **60**(3): p. 472-479.
53. Feinberg, A.W., et al., *Controlling the contractile strength of engineered cardiac muscle by hierarchal tissue architecture.* Biomaterials, 2012. **33**(23): p. 5732-5741.
54. Feinberg, A.W., et al., *Muscular Thin Films for Building Actuators and Powering Devices.* Science, 2007. **317**(5843): p. 1366-1370.

55. Annabi, N., et al., *Highly Elastic Micropatterned Hydrogel for Engineering Functional Cardiac Tissue.* Advanced functional materials, 2013. **23**(39): p. 10.1002/adfm.201300570.
56. Kim, D.-H., et al., *Nanoscale cues regulate the structure and function of macroscopic cardiac tissue constructs.* Proceedings of the National Academy of Sciences, 2010. **107**(2): p. 565-570.
57. Guyette, J.P., et al., *Bioengineering Human Myocardium on Native Extracellular Matrix.* Circulation Research, 2015.
58. Yildiran, T., et al., *Low Pulse Pressure as a Predictor of Death in Patients with Mild to Advanced Heart Failure.* Texas Heart Institute Journal, 2010. **37**(3): p. 284-290.
59. Pampaloni, F., E.G. Reynaud, and E.H.K. Stelzer, *The third dimension bridges the gap between cell culture and live tissue.* Nat Rev Mol Cell Biol, 2007. **8**(10): p. 839-845.
60. Griffith, L.G. and M.A. Swartz, *Capturing complex 3D tissue physiology in vitro.* Nat Rev Mol Cell Biol, 2006. **7**(3): p. 211-224.
61. Gauvin, R. and A. Khademhosseini, *Microscale Technologies and Modular Approaches for Tissue Engineering: Moving toward the Fabrication of Complex Functional Structures.* ACS Nano, 2011. **5**(6): p. 4258-4264.
62. Guerin, H.L. and D.M. Elliott, *Quantifying the contributions of structure to annulus fibrosus mechanical function using a nonlinear, anisotropic, hyperelastic model.* Journal of Orthopaedic Research, 2007. **25**(4): p. 508-516.
63. Lundon, K., *Structure and Function of the Lumbar Intervertebral Disk in Health, Aging, and Pathologic Conditions.* Journal of Orthopaedic & Sports Physical Therapy, 2001. **31**(6): p. 291-306.
64. Nikolaidou, T., et al., *Structure–Function Relationship in the Sinus and Atrioventricular Nodes.* Pediatric Cardiology, 2012. **33**(6): p. 890-899.
65. Aagaard, P., et al., *A mechanism for increased contractile strength of human pennate muscle in response to strength training: changes in muscle architecture.* The Journal of Physiology, 2001. **534**(2): p. 613-623.
66. Azizi, E., E.L. Brainerd, and T.J. Roberts, *Variable gearing in pennate muscles.* Proceedings of the National Academy of Sciences, 2008. **105**(5): p. 1745-1750.
67. Kanzaki, Y., et al., *Three-Dimensional Architecture of Cardiomyocytes and Connective Tissues in Hypertrophic Cardiomyopathy: A Scanning Electron Microscopic Observation.* Circulation, 2012. **125**(5): p. 738-739.
68. Fonseca, H., et al., *Bone Quality: The Determinants of Bone Strength and Fragility.* Sports Medicine, 2013: p. 1-17.
69. Kuo, P.-L., et al., *Myocyte Shape Regulates Lateral Registry of Sarcomeres and Contractility.* The American Journal of Pathology, 2012. **181**(6): p. 2030-2037.
70. Kada, K., et al., *Orientation change of cardiocytes induced by cyclic stretch stimulation: time dependency and involvement of protein kinases.* Journal of molecular and cellular cardiology, 1999. **31**: p. 247-59.
71. Neidlinger-Wilke, C., et al., *Cell alignment is induced by cyclic changes in cell length: studies of cells grown in cyclically stretched substrates.* Journal of orthopaedic research : official publication of the Orthopaedic Research Society, 2001. **19**: p. 286-93.
72. Salameh, A., et al., *Cyclic mechanical stretch induces cardiomyocyte orientation and polarization of the gap junction protein connexin43.* Circulation research, 2010. **106**: p. 1592-602.

73. Sato, M., et al., *Effects of B-Cell Lymphoma 2 Gene Transfer to Myoblast Cells on Skeletal Muscle Tissue Formation Using Magnetic Force-Based Tissue Engineering.* Tissue Engineering Part A, 2012. **19**(1-2): p. 307-315.
74. Coletti, D., et al., *Static magnetic fields enhance skeletal muscle differentiation in vitro by improving myoblast alignment.* Cytometry Part A, 2007. **71A**(10): p. 846-856.
75. Radisic, M., et al., *Functional assembly of engineered myocardium by electrical stimulation of cardiac myocytes cultured on scaffolds.* Proceedings of the National Academy of Sciences of the United States of America, 2004. **101**: p. 18129-34.
76. Tandon, N., et al., *Electrical stimulation systems for cardiac tissue engineering.* 2009. **4**: p. 155-173.
77. Gelain, F., et al., *BMHP1-Derived Self-Assembling Peptides: Hierarchically Assembled Structures with Self-Healing Propensity and Potential for Tissue Engineering Applications.* ACS Nano, 2011. **5**(3): p. 1845-1859.
78. Caldwell, D.J., R.R. Rao, and J.P. Stegemann, *Assembly of Discrete Collagen–Chitosan Microenvironments into Multiphase Tissue Constructs.* Advanced Healthcare Materials, 2013. **2**(5): p. 673-677.
79. Haraguchi, Y., et al., *Fabrication of functional three-dimensional tissues by stacking cell sheets in vitro.* Nat. Protocols, 2012. **7**(5): p. 850-858.
80. Takahashi, H., et al., *The use of anisotropic cell sheets to control orientation during the self-organization of 3D muscle tissue.* Biomaterials, 2013. **34**(30): p. 7372-7380.
81. Williams, C., et al., *Stacking of aligned cell sheets for layer-by-layer control of complex tissue structure.* Biomaterials, 2011. **32**(24): p. 5625-5632.
82. Xia, Y., et al., *Thermoresponsive microgel films for harvesting cells and cell sheets.* Biomacromolecules, 2013.
83. Radisic, M., et al., *Oxygen gradients correlate with cell density and cell viability in engineered cardiac tissue.* Biotechnology and bioengineering, 2006. **93**: p. 332-43.
84. Vunjak-Novakovic, G., et al., *Challenges in cardiac tissue engineering.* Tissue engineering. Part B, Reviews, 2010. **16**: p. 169-87.
85. Tatkiewicz, W.I., et al., *Two-Dimensional Microscale Engineering of Protein-Based Nanoparticles for Cell Guidance.* ACS Nano, 2013. **7**(6): p. 4774-4784.
86. Zan, X., et al., *Facile Method for Large Scale Alignment of One Dimensional Nanoparticles and Control over Myoblast Orientation and Differentiation.* ACS Nano, 2013. **7**(10): p. 8385-8396.
87. Namgung, S., et al., *Controlling the Growth and Differentiation of Human Mesenchymal Stem Cells by the Arrangement of Individual Carbon Nanotubes.* ACS Nano, 2011. **5**(9): p. 7383-7390.
88. Kim, H.N., et al., *Nanotopography-guided tissue engineering and regenerative medicine.* Advanced Drug Delivery Reviews, 2012.
89. Kim, D.-H., et al., *Guided Cell Migration on Microtextured Substrates with Variable Local Density and Anisotropy.* Advanced Functional Materials, 2009. **19**(10): p. 1579-1586.
90. Kim, D.-H., et al., *Mechanosensitivity of fibroblast cell shape and movement to anisotropic substratum topography gradients.* Biomaterials, 2009. **30**(29): p. 5433-5444.
91. Kim, P., et al., *Fabrication of nanostructures of polyethylene glycol for applications to protein adsorption and cell adhesion.* Nanotechnology, 2005. **16**(10): p. 2420-2426.
92. Nagase, K., et al., *Thermo-Responsive Polymer Brushes as Intelligent Biointerfaces: Preparation via ATRP and Characterization.* Macromolecular Bioscience, 2011. **11**(3): p. 400-409.

93. Mudera, V.C., et al., *Molecular responses of human dermal fibroblasts to dual cues: Contact guidance and mechanical load.* Cell Motility and the Cytoskeleton, 2000. **45**(1): p. 1-9.
94. Au, H.T.H., et al., *Interactive effects of surface topography and pulsatile electrical field stimulation on orientation and elongation of fibroblasts and cardiomyocytes.* Biomaterials, 2007. **28**(29): p. 4277-4293.
95. Goetsch, K.P., K.H. Myburgh, and C. Niesler, *In vitro myoblast motility models: investigating migration dynamics for the study of skeletal muscle repair.* Journal of Muscle Research and Cell Motility, 2013: p. 1-15.
96. Kino-oka, M., et al., *Evaluation of vertical cell fluidity in a multilayered sheet of skeletal myoblasts.* Journal of Bioscience and Bioengineering, 2012. **113**(1): p. 128-131.
97. Yang, H.-S.I., Nicholas; Tsui, Jonathan H; Kim, Hong Nam; Suh, Kahp-Yang; Reyes, Morayama; Kim, Deok-Ho, *Nanopatterned muscle cell patches for enhanced myogenesis and dystrophin expression in a mouse model of muscular dystrophy.* Biomaterials, 2013. **Accepted for publication**.
98. Huang, N.F., et al., *Myotube Assembly on Nanofibrous and Micropatterned Polymers.* Nano Letters, 2006. **6**(3): p. 537-542.
99. Ovsianikov, A., et al., *Laser printing of cells into 3D scaffolds.* Biofabrication, 2010. **2**(1): p. 014104.
100. Hosseini, V., et al., *Engineered Contractile Skeletal Muscle Tissue on a Microgrooved Methacrylated Gelatin Substrate.* Tissue Engineering Part A, 2012. **18**(23-24): p. 2453-2465.
101. Kim, H.N., et al., *Nanotopography-guided tissue engineering and regenerative medicine.* Advanced Drug Delivery Reviews, 2013. **65**(4): p. 536-558.
102. Tracy, L.E., R.A. Minasian, and E.J. Caterson, *Extracellular Matrix and Dermal Fibroblast Function in the Healing Wound.* Advances in Wound Care, 2016. **5**(3): p. 119-136.
103. Scavelli, K., A. Chatterjee, and D.J. Rhee, *Secreted Protein Acidic and Rich in Cysteine in Ocular Tissue.* Journal of Ocular Pharmacology and Therapeutics, 2015. **31**(7): p. 396-405.
104. Thery, M., et al., *The extracellular matrix guides the orientation of the cell division axis.* Nat Cell Biol, 2005. **7**(10): p. 947-953.
105. Yin, H., F. Price, and M.A. Rudnicki, *Satellite Cells and the Muscle Stem Cell Niche.* Physiological Reviews, 2013. **93**(1): p. 23-67.
106. Bischoff, R., *Interaction between satellite cells and skeletal muscle fibers.* Development, 1990. **109**(4): p. 943-952.
107. Grefte, S., et al., *Skeletal Muscle Development and Regeneration.* Stem Cells and Development, 2007. **16**(5): p. 857-868.
108. Ide, T., et al., *Structural characterization of bioengineered human corneal endothelial cell sheets fabricated on temperature-responsive culture dishes.* Biomaterials, 2006. **27**(4): p. 607-614.
109. Canavan, H.E., et al., *Surface Characterization of the Extracellular Matrix Remaining after Cell Detachment from a Thermoresponsive Polymer.* Langmuir, 2005. **21**(5): p. 1949-1955.
110. Shimizu, T., et al., *Fabrication of Pulsatile Cardiac Tissue Grafts Using a Novel 3-Dimensional Cell Sheet Manipulation Technique and Temperature-Responsive Cell Culture Surfaces.* Circulation Research, 2002. **90**(3): p. e40-e48.

111. Gillies, A.R. and R.L. Lieber, *Structure and Function of the Skeletal Muscle Extracellular Matrix.* Muscle & nerve, 2011. **44**(3): p. 318-331.
112. Jiao, A., et al., *Thermoresponsive Nanofabricated Substratum for the Engineering of Three-Dimensional Tissues with Layer-by-Layer Architectural Control.* ACS Nano, 2014. **8**(5): p. 4430-4439.
113. Wakelam, M.J., *The fusion of myoblasts.* Biochemical Journal, 1985. **228**(1): p. 1-12.
114. Wang, W., et al., *Matrix Metalloproteinase-1 Promotes Muscle Cell Migration and Differentiation.* The American Journal of Pathology. **174**(2): p. 541-549.
115. Zimowska, M., et al., *Distinct patterns of MMP-9 and MMP-2 activity in slow and fast twitch skeletal muscle regeneration in vivo.* Int J Dev Biol, 2008. **52**(2-3): p. 307-14.
116. Abmayr, S.M. and G.K. Pavlath, *Myoblast fusion: lessons from flies and mice.* Development (Cambridge, England), 2012. **139**(4): p. 641-656.
117. Klein-Ogus, C. and J.B. Harris, *Preliminary observations of satellite cells in undamaged fibres of the rat soleus muscle assaulted by a snake-venom toxin.* Cell and Tissue Research, 1983. **230**(3): p. 671-776.
118. Carlson, B.M., and Faulkner, John A., *The regeneration of skeletal muscle fibers following injury: a review.* Medicine and Science in Sports and Exercise, 1983. **15**(3): p. 187-198.
119. Ott, H.C., et al., *Perfusion-decellularized matrix: using nature's platform to engineer a bioartificial heart.* Nat Med, 2008. **14**(2): p. 213-221.
120. Kharaziha, M., et al., *Tough and flexible CNT–polymeric hybrid scaffolds for engineering cardiac constructs.* Biomaterials, 2014. **35**(26): p. 7346-7354.
121. Carson, D., et al., *Nanotopography-Induced Structural Anisotropy and Sarcomere Development in Human Cardiomyocytes Derived from Induced Pluripotent Stem Cells.* ACS Applied Materials & Interfaces, 2016.
122. Spotnitz, H.M., et al., *Cellular basis for volume related wall thickness changes in the rat left ventricle.* Journal of Molecular and Cellular Cardiology, 1974. **6**(4): p. 317-331.
123. Arts, T., et al., *Relating myocardial laminar architecture to shear strain and muscle fiber orientation.* American Journal of Physiology - Heart and Circulatory Physiology, 2001. **280**(5): p. H2222-H2229.
124. LeGrice, I.J., et al., *Laminar structure of the heart: ventricular myocyte arrangement and connective tissue architecture in the dog.* American Journal of Physiology - Heart and Circulatory Physiology, 1995. **269**(2): p. H571-H582.
125. Guan, X., et al., *Dystrophin-deficient cardiomyocytes derived from human urine: New biologic reagents for drug discovery.* Stem Cell Research, 2014. **12**(2): p. 467-480.
126. Tohyama, S., et al., *Distinct Metabolic Flow Enables Large-Scale Purification of Mouse and Human Pluripotent Stem Cell-Derived Cardiomyocytes.* Cell Stem Cell. **12**(1): p. 127-137.
127. Palpant, N.J., et al., *Inhibition of β-catenin signaling respecifies anterior-like endothelium into beating human cardiomyocytes.* Development, 2015. **142**(18): p. 3198-3209.
128. Cho, H., et al., *Self-Organization in High-Density Bacterial Colonies: Efficient Crowd Control.* PLoS Biol, 2007. **5**(11): p. e302.
129. Macadangdang, J., et al., *Nanopatterned Human iPSC-based Model of a Dystrophin-Null Cardiomyopathic Phenotype.* Cell Mol Bioeng, 2015. **8**(3): p. 320-332.
130. Rohr, S., *Role of gap junctions in the propagation of the cardiac action potential.* Cardiovascular Research, 2004. **62**(2): p. 309.
131. Tepass, U., et al., *Cadherins in embryonic and neural morphogenesis.* Nat Rev Mol Cell Biol, 2000. **1**(2): p. 91-100.

132. Leor, J., et al., *Bioengineered Cardiac Grafts.* Circulation, 2000. **102**(suppl 3): p. Iii-56.
133. Sekine, H., et al., *Cardiac Cell Sheet Transplantation Improves Damaged Heart Function via Superior Cell Survival in Comparison with Dissociated Cell Injection.* Tissue Engineering Part A, 2011. **17**(23-24): p. 2973-2980.
134. George, E.L., et al., *Defects in mesoderm, neural tube and vascular development in mouse embryos lacking fibronectin.* Development, 1993. **119**(4): p. 1079-1091.
135. Hirschy, A., et al., *Establishment of cardiac cytoarchitecture in the developing mouse heart.* Developmental Biology, 2006. **289**(2): p. 430-441.
136. Mekkaoui, C., et al., *Diffusion MRI Tractography of the Developing Human Fetal Heart.* PLoS ONE, 2013. **8**(8): p. e72795.
137. Kawel, N., et al., *Normal left ventricular myocardial thickness for middle aged and older subjects with SSFP cardiac MR: The Multi-Ethnic Study of Atherosclerosis.* Circulation. Cardiovascular imaging, 2012. **5**(4): p. 500-508.
138. Kaneko, N., et al., *Three-dimensional reconstruction of the human capillary network and the intramyocardial micronecrosis.* American Journal of Physiology - Heart and Circulatory Physiology, 2011. **300**(3): p. H754-H761.

Vita

Alex Jiao received his BS degree in Biomedical Engineering from Northwestern University in 2010. During his undergraduate education, he performed summer research in the lab of Dr. Jan Stegemann at the University of Michigan, focused on engineering mineralized biomaterials for bone tissue engineering, as well as research in the lab of Dr. Guillermo Ameer at Northwestern University, focused on biomaterials to adsorb amyloid beta peptides implicated in Alzheimer's progression. Under the guidance of Dr. Deok-Ho Kim, he is working towards his PhD degree in Bioengineering at the University of Washington. His current research areas include biomaterials, stem cell biology, and cardiac tissue engineering. He has authored and co-authored 8 peer-reviewed journal publications, presented 3 short talks, 5 poster presentations, and 1 book chapter. He has also filed 4 provisional patents related to his academic research as well as personal endeavors. While a graduate student, he received multiple student awards, including the ASME NanoEngineering in Medicine and Biology Student Paper Award, BMES Cellular and Molecular Bioengineer Student Travel Award, and the Annals of Biomedical Engineering Most Downloaded and Most Cited Review Article. He has also successfully received 2 NIH T32 training grants, an American Heart Association predoctoral fellowship and an NIH F31 National Research Service Award for his research projects.

Additionally, Alex has cofounded a biotechnology startup, miPS Labs, aimed at offering consumers affordable, pharmaceutical-grade cell cryopreservation. Alex has won multiple awards for miPS Labs, including prizes from the University of Washington Business Plan Competition, the UW Health Innovation Challenge, StartupUW's Bark Tank competition, and Social Venture Partner's Fast Pitch competition. Alex has successfully raised over $400,000 through prizes and private investments for miPS Labs, and miPS Labs will be joining the Techstars Seattle accelerator in the 2017 cohort to grow and establish miPS Labs in the Pacific Northwest.